Aalto University
School of Chemical
Technology

School of Chemical Technology
Degree Programme of Materials Science and Engineering

Minttu Pasanen

ELECTRODEPOSITION OF COPPER ON RESISTIVE CARBON NANOTUBE MATERIALS

Master's thesis for the degree of Master of Science in Technology submitted for inspection, Espoo, 19 October, 2015.

Supervisor Professor Olof Forsén

Instructors D.Sc. Jari Aromaa,
M.Sc. Pyry-Mikko Hannula

Aalto University
School of Chemical
Technology

Aalto University, P.O. BOX 11000, 00076 AALTO
www.aalto.fi

Abstract of master's thesis

Author Minttu Pasanen

Title of thesis Electrodeposition of copper on resistive carbon nanotube materials

Department Material Science and Engineering

Professorship Corrosion and hydrometallurgy **Code of professorship** MT-85

Thesis supervisor Professor Olof Forsén

Thesis advisors / Thesis examiners D.Sc. Jari Aromaa, M.Sc. Pyry-Mikko Hannula

Date 19.10.2015 **Number of pages** 98+1 **Language** English

The special properties of carbon nanotubes (CNTs), such as low density, high mechanical strength and particularly excellent electrical and thermal conductivity, have stimulated researchers to develop various CNT composites. Low density and significantly conductive Cu/CNT composites would revolutionize the field of technology and many different industry sectors with electrical wiring applications.

The production of Cu/CNT composites require a lot of research, because none of the produced Cu/CNT composites, reach better electrical conductivity than copper. Earlier research shows that the manufactured CNTs contain too much impurities and different wall structures, which decrease the electrical conductivity. In addition the bond between copper and CNT is too weak to conduct electricity. The conductivity and activity of CNT-materials may be improved by functionalizing and modifying the CNT structure. The aim of this research is to investigate the methods, which could be used to affect the potential distribution and current distribution, by improving the conductivity and electrochemical activity of CNT-substrates.

Surface properties of CNT substrates were investigated with electro-chemical impedance spectroscopy (EIS). Nucleation was estimated with galvanostatic deposition tests, scanning electron microscope (SEM) and optical microscope. The surface properties of CNT substrates were modified with heat treatment, Watts bath immersion, acetone, anodization, ethanol and different acid treatments. In addition secondary treatments such as copper deposition to Cu/CNT composite and resistance measurements were done to some samples. In copper deposition, the deposition rates before and after the modification treatments were compared. Part of Cu/CNT composites were post-treated with heat treatment using nitrogen gas atmosphere.

The results show that heat treatment, Watts bath immersion, anodization and boric acid immersion are the most effective methods for functionalizing and modifying the CNT structure and improved the electrical conductivity and electrochemical activity. The heat treatment affected strongly to electrochemical activity, but it seems to weaken the structure of the CNT samples. Immersion in Watts bath affects strongly in electrochemical activity and based on SEM-images, there isn't any agglomeration, weakening of the structure or special shape-changes. Acetone, sulfuric acid or nitric acid improved the electrochemical activity only slightly and ethanol addition provided no changes in the electrochemical activity. Watts bath immersion significantly affected the coating rate with lowest current, but more research is needed to confirm the effect.

Keywords: carbon nanotubes, conductivity, composite, electrochemical activity

Aalto-yliopisto
Kemian tekniikan
korkeakoulu

Aalto-yliopisto, PL 11000, 00076 AALTO
www.aalto.fi

Diplomityön tiivistelmä

Tekijä Minttu Pasanen

Työn nimi Kuparin sähkösaostus johtamattomille hiilinanoputki materiaaleille

Laitos Materiaalitekniikka

Professuuri Korroosio ja hydrometallurgia **Professuurikoodi** MT-85

Työn valvoja Professori Olof Forsén

Työn ohjaajat/Työn tarkastajat D.Sc. Jari Aromaa, M.Sc. Pyry-Mikko Hannula

Päivämäärä 19.10.2015 **Sivumäärä** 98+1 **Kieli** Englanti

Hiilinanoputkien (CNTs, *carbon nanotubes*) erityiset ominaisuudet, kuten pieni tiheys, suuri mekaaninen lujuus ja erityisen hyvä lämmön ja sähkönjohtokyky, ovat kannustaneet tutkijoita kehittämään erilaisia CNT -komposiitteja. Kevyt ja huomattavasti kuparia parempi Cu/CNT komposiitti voisi mullistaa johdin-teknologian monilla eri teollisuuden aloilla.

Cu/CNT komposiittien valmistus vaatii kuitenkin vielä paljon tutkimusta, sillä yksikään CNT-pohjainen komposiitti ei ole vielä ylittänyt kuparin sähkönjohtokykyä. Uusimmat tutkimukset osoittavat, että valmistetut hiilinanoputki-materiaalit sisältävät liian paljon epäpuhtauksia ja eri rakenteisia hiilinanoputkia, jotka vähentävät sähkönjohtavuutta. Lisäksi kuparin ja hiilinanoputken välinen sitoutuminen on liian heikko johtaakseen sähköä rajapinnassa. Hiilinanoputki-materiaalin sähkönjohtokykyä ja aktiivisuutta voidaan parantaa funktionalisoimalla ja muokkaamalla CNT:n rakennetta. Tämän diplomityön tarkoituksena on tutkia erilaisia menetelmiä, joiden avulla voidaan vaikuttaa potentiaali- ja virranjakaumiin, jotka parantavat CNT-substraatin sähkönjohtavuutta ja sähkökemiallista aktiivisuutta.

CNT-substraattien pinnan ominaisuuksia tutkittiin sähkökemiallisella impedanssispektroskopialla (EIS) ja kuparin ydintymistä CNT-substraattiin arvioitiin sähkösaostuksella, pyyhkäisyelektronimikroskoopilla (SEM, *scanning electron microscope*) sekä optisella mikroskoopilla. CNT-materiaalien pinnan ominaisuuksia modifioitiin lämpökäsittelyillä, Wattsin nikkelikylvyllä, asetonilla, anodisoinnilla, etanolilla ja erilaisilla happokäsittelyillä. Lisäksi osa näytteistä sähkösaostettiin kuparilla Cu/CNT komposiiteiksi ja mitattiin sähkövastuksen muutos tai kuparin saostumisen nopeutta verrattiin ennen näytteen käsittelyä ja käsittelyn jälkeen. Osa Cu/CNT komposiiteista jälkikäsiteltiin uunissa typpikaasun kanssa, hapettumisen estämiseksi.

Tulokset osoittavat, että lämpökäsittely, Wattsin kylpy, anodisointi ja boorihappo ovat tehokkaimmat funktionalisointi ja modifiointi keinot CNT:n sähkönjohtavuuden ja sähkökemiallisen aktiivisuuden parantamiseen. Lämpökäsittely vaikutti voimakkaasti sähkökemialliseen aktiivisuuteen, mutta vaikutti heikentävän CNT:n rakennetta. Wattsin kylpyyn upottaminen vaikutti voimakkaasti sähkökemialliseen aktiivisuuteen, ja SEM-kuvien perusteella upotus ei aiheuttanut agglomeroitumista, rakenteen heikkenemistä tai muodon muutoksia. Asetoni, rikkihappo ja typpihappo vaikuttivat sähkökemialliseen aktiivisuuteen vain hiukan ja etanolin lisäämisellä ei havaittu muutoksia aktiivisuudessa. Wattsin kylpy vaikuttaa selvästi pinnoituksen nopeuteen pienimmällä virralla, mutta vaikutuksen vahvistamiseksi tarvitaan lisää tutkimuksia.

Avainsanat: hiilinanoputket, johtokyky, komposiitti, sähkökemiallinen aktiivisuus

FOREWORD

This Master's thesis was carried out during 2015 at Aalto University School of Chemical Technology, department of Materials Science and Engineering at the Research Group of Corrosion and Hydrometallurgy. This thesis was a part of the European Union FP 7 UltraWire project for creating an ultraconductive copper composite.

First I would like to thank Professor Olof Forsén for giving me the interesting research subject and for the opportunity to work in the laboratory. I would also like to thank especially my thesis instructors, D.Sc. Jari Aromaa for sharing his extensive knowledge and giving practical advices for the electrochemical experiments and M.S.c Pyry-Mikko Hannula for supporting me and giving practical advices and ideas during the writing of this thesis. I wish to thank everyone involved in the UltraWire project.

Furthermore, I wish to thank the staff members of the Research Group of Corrosion and Hydrometallurgy for their help and support during this thesis. Finally, I would like to thank my fiancé Matti Junnila, my family and my friends for their support they have given me during my studies and the completion of this Master's thesis.

Espoo, 19th of October 2015

Minttu Pasanen

TABLE OF CONTENTS

1 INTRODUCTION

Carbon nanotubes (CNTs) were discovered in 1991. Since then it has been theoretically and experimentally proven, that this material has exceptional properties, such as high mechanical strength and particularly good electrical and thermal conductivity.[1][2][3] These properties, as well as their stiffness, large elastic strain, high aspect ratio and low density, stimulated researchers to incorporate carbon nanotubes e.g. into polymers or ceramics for the development of multifunctional CNT-based composites.[2] This interesting material could revolutionize the field of technology and many different industry sectors with electrical wiring applications.[4][5][6] Therefore CNT-based conductor materials could have a major impact on both technology and economy.[7]

The manufacturing- and processing methods of CNTs require still a lot of research, before industrially obtained CNT-based conductor materials and completely working Cu/CNT composites can be published. There are no commercially manufactured Cu/CNT composite that reach better electrical conductivity than copper. Today's research shows that the manufactured CNTs contain too many impurities, which decrease the electrical conductivity. Single walled metallic nanotubes would have best properties as conductors, but they are the most difficult to manufacture. All methods also produce semiconducting CNTs in large concentrations. The conductivity may be improved by functionalizing and modifying the CNT surfaces. Functionalizing and modifying the interface contributes to the bond between copper and CNTs, because the number of bonds and their respective strength is changed. In addition, they affect the activity of the CNT.

The aim of this Master's thesis is investigate the methods, which can be used to affect the potential and current distribution for electrochemical composite production. These distributions are affected by the conductivity and electrochemical activity of carbon nanotube substrates. The focus was in the effects of surface properties of CNTs and on the growth of nucleation of copper. The ultimate target is a copper-based conductor wire with improved electrical conductivity and significantly enhanced physical properties compared to copper. Surface properties of CNT substrates were measured and characterized by different methods like electrochemical impedance spectroscopy (EIS) and nucleation was estimated with galvanostatic deposition tests, scanning electron microscope *(*SEM) and optical microscopy. The experiments aimed to find correlations between surface modification and nucleation. The surface properties of CNT substrates were modified with heat treatment, Watts nickel bath, acetone, anodization, ethanol and different acid treatments.

2 CARBON NANOTUBE

Copper and aluminum are the commonly used conductor materials because they have good electrical conductivity and low weight. Also silver has been used in some applications; because of its resistivity is 5 % lower than copper. However, silver is a more expensive material and, therefore, the price limits its use considerably. CNTs could provide entirely new system solutions and better properties than copper and aluminum because copper and aluminum have poor mechanical performance, weight, creep, resistive losses, electromigration and limitations in current carrying capacity.[6][7] Benefits of nanocomposite materials have recently attracted much research, because a large number of ohmic losses could be avoided with low-resistivity CNTs and this creates an opportunity for many diverse applications[2][7][8].

CNTs have many interesting properties such as high mechanical strength and good electrical and thermal conduction. These properties are caused by the unique structure of CNT. Depending on the geometry of CNTs, they can act like metallic or semiconducting materials.[6][7] Individual carbon nanotubes combine excellent electrical and mechanical properties and very low weight. The main focus in this thesis is on improving the activity of the CNT surface.

2.1 CNT surface morphology and structures

Carbon nanotubes are seamless structures based on graphene sheets. They are described as a hexagonal lattice of carbon atoms rolled to a tube form[9]. CNTs are divided to two sub-categories; SWCNTs (single-walled carbon nanotubes) and MWCNTs (multi-walled carbon nanotubes). SWCNTs are formed from a single layer and MWCNTs from multiple (usually 10 to 30) layers of graphene structures.[10][11] Figure 1 shows MWCNT's overlapping graphene layers. The distance between the cylinders is approximately 0.34 nm and between atoms and graphite plane 0.14 nm[10].

The diameter of the SWCNTs are usually between 0.5 - 10.0 nm and MWCNTs from 4 - 400 nm[10][11][12]. The length varies from hundreds of micrometers up to a few centimeters, for SWCNT and MWCNTs[11][13][14]. Smallest diameter reported with CNTs is 0.4 nm and this is believed to be the smallest possible based on the bending force with the atoms in the graphene lattice[10]. The ends of MWCNTs can be open or closed. In general, large diameter nanotubes have flatter end than small diameter nanotubes. Figure 1 shows three typical closed models: symmetric, asymmetric and flat.[13]

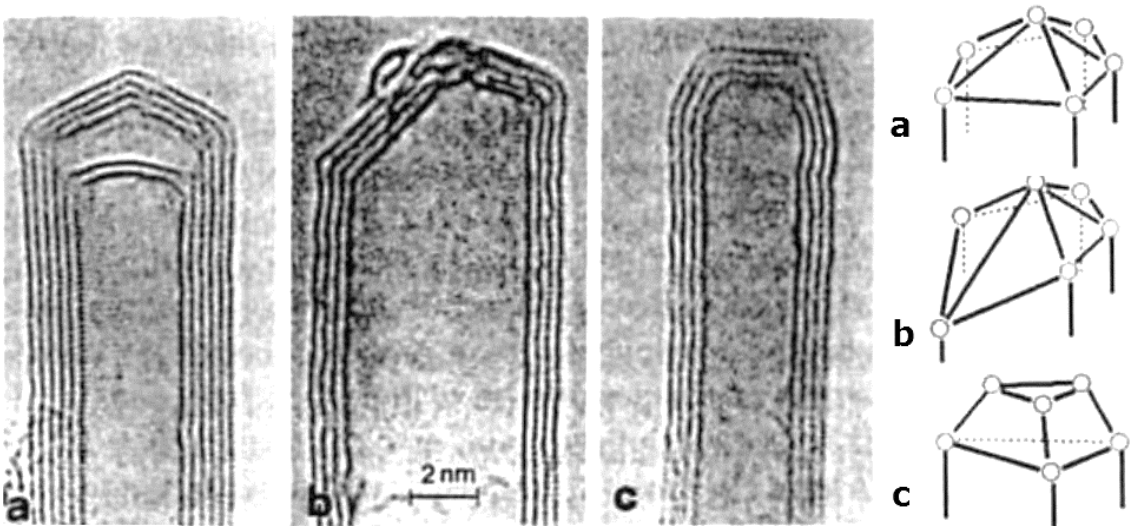

Figure 1. Three different MWCNTs end: a) symmetrical, b) asymmetric and c) flat and MWCNT's overlapping graphene cylinders, modified after[13].

SWCNTs are generally classified into three different categories depending on how the graphene walls are wrapped up into a tube form.[14] The mirror images of achiral carbon nanotubes are identical with the original nanotubes unlike the mirror images of the chiral nanotubes. Achiral nanotubes occur only in two kinds of structures: armchair and zigzag (Figures 2a and 2b) while there is a wide variety of possible structures of chiral nanotubes (an example in Figure 2c).[13]

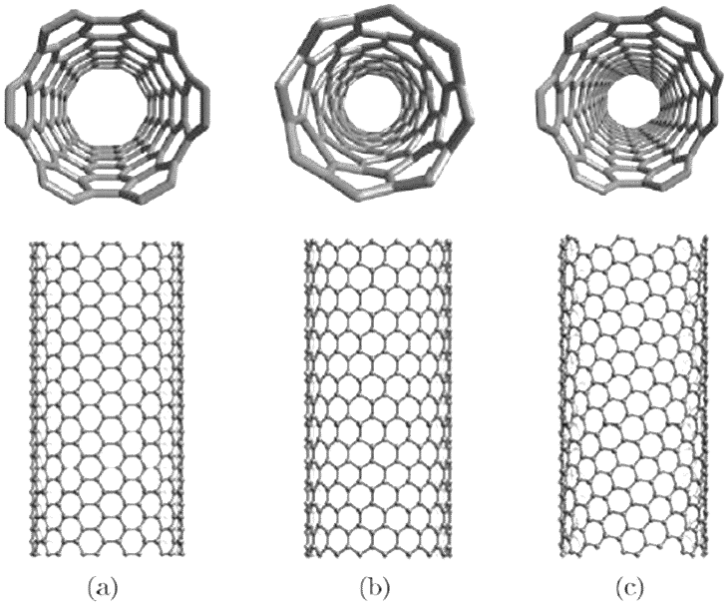

Figure 2: Carbon nanotubes wall structures a) armchair b) zigzag c) chiral, modified after[10][13].

The determining factor of the carbon nanotube structure is the direction of hexagonal carbon rings compared to the nanotube axis in the honeycomb structure. The primitive translation vectors a_1 and a_2 form a base to a hexagonal lattice plane. Figure 3 shows

that the hexagonal carbon rings may be occasionally twisted in the honeycomb lattice. This allows a variety of nanotube structures without breaking the cylindrical nanotube form. Single-walled nanotube structure is defined with chirality vector C_h that corresponds with a cross section of the tube that is perpendicular against the tube axis (in Figure 3: vector OA). Chiral vector Ch can be present with unit vectors a_1 and a_2 (Formula 1).[15][16]

$$Ch = na_1 + ma_2 \equiv (n, m), \quad (1)$$

where n and m are integers, $0 \leq |m| \leq n$.

Translation vector T (In Figure 3: vector OB), shows longitudinal axis direction of the nanotube and is perpendicular to the chiral vector Ch. The carbon nanotube can be modeled, when the lattice is rotated to a cylinder and when the points: O, A and B, B' are combined.[15] Chirality angle θ stands for the angle between the vectors C_h and a1 that represent the angle of the hexagons compared to the nanotube axis and defines the helical-symmetry. When θ = 0 °, m = 0, i.e. Ch = (n,0), the structure stands for the zigzag (9,0) nanotube and when θ = 30°, n = m, i.e. Ch = (n,n), the nanotube has armchair (5,5) structure. The structure is called chiral (10,5) if the chirality angle gets any other values than the previous.[15]

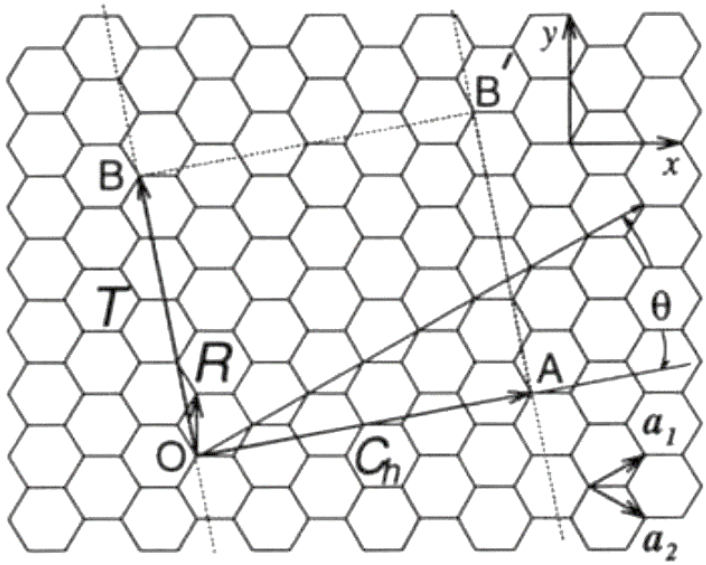

Figure 3. The honeycomb lattice, which forms a nanotube when turned into a cylinder. There is also the chirality vector (C_h) and the translation vector (T), modified after[13].

The wrapping direction of the graphite layer, as well as other structural characteristics, affect the electrical conductivity of the nanotubes and based on these properties they can be divided into metal or semi-conductive carbon nanotubes[10][11][17]. A produced SWCNT network consists of approximately two of thirds of semiconductors and one-third

of conductors. All armchair structures having carbon nanotubes are conducting. Zigzag structure including carbon nanotubes can be conducting if the conditions in Formula (2) are fulfilled.[14]

$$\frac{n-m}{3} = an\ integer \tag{2}$$

The best conductance of nanotubes can be achieved only if small diameter single-walled tubes have same chirality or they both are either the armchair or metallic zigzag. The conductance of the armchair/zigzag contact is however much lower than the armchair/armchair contact, even if the zigzag nanotubes could be metallic.[18]

2.2 Production method

The formation-method of nanotubes is not yet known exactly and their growth mechanisms seem to be influenced by many factors at the same time[19]. CNT manufacturing processes that are currently in use utilize the thermal decomposition of available carbon sources[14]. Carbon nanotubes are generally produced by three main competing techniques; chemical vapor deposition (CVD), arc-discharge and laser-ablation, but specific established and economical production method is not found[19]. All methods can be divided into more than one sub-category depending what kind of nanotubes are needed[19][20]. CVD method options are growth in the gas phase, use of alcohol as a carbon source, water-assisted manufacturing, and using a high-pressure carbon monoxide (high-pressure CO, HiPCO)[20]. Arc-discharge methods generally produce a high amount of impure materials but have the highest quality transport properties[7][19]. Laser-ablation can produce only small amounts of pure nanotubes. Chemical vapor deposition is generally used to produce MWCNTs or poor quality SWCNTs because controlling of SWCNTs can be difficult. Despite this, there are positive aspects with CVD e.g. the suitability for mass production.[19] There is an ongoing search to find the cheaper and more suitable methods to produce high-quality nanotubes with easily controllable properties[19][20].

Quantity, structure and properties of CNTs vary depending on the manufacturing process and production parameters. Differences are found mainly in the number of layers, chirality, defect areas and electrical conductivity. Strictly controlled CVD method enables an economical way to manufacture large amounts of SWCNT and MWCNT. On the other hand, the tubes are not homogeneous, they often have a many structural defects and their properties are difficult to control. Sharma et al. (2007), and Eklund et al. (2002) investigated the temperature and the flow rate of gas containing carbon, and found that a higher temperature and a slower flow produced smaller tubes and enabled the growth

of SWCNTs.[7][19][20][21][22] SWCNTs are expected grow only over 500 °C, but despite this, Cantoro et al. (2006) succeeded preparing SWCNTs at 350 °C[23]. Usually when carbon nanotubes grow at low temperatures, the problem is a non-homogeneous product and the large size of the tubes. Moreover MWCNTs and SWCNTs are mixed in the same product.[20] Sharma et al. (2007) reported that low-temperature and high-pressure caused more damage in tubes and produced large curvature MWCNTs. They presented that a number of walls of CNT remained uniform in the growth process.[7][19][20][21] In 1993 Joce-Yacaman et al. found that the reaction time affected especially the length of the nanotubes with CVD method[20][24] and the thickness of the tubes could be determined with optimization of production method[25]. Strict formation mechanisms of nanotubes are still unknown, so the final manufacturing method requires a lot of research before it can be implemented[7][14]. Moreover a new cleaning treatment method for high-quality CNTs should be developed[7].

The production of CNTs with batch CVD-method can be divided into two parts: preparation of catalyst and actual growing of tubes. At the first stage a metal-nanoparticle catalyst is spread on the substrate and heated in a closed chamber to the decomposition temperature of the catalyst. After this, the catalyst begins to form small groups. Iron, cobalt and nickel are the most used catalysts, but Takagi et al.(2006) managed to grow SWCNTs with gold, silver and copper catalysts.[26] At the second stage, the substrate is placed into a heated reactor, where the flow of carbon-containing gas and process gas are led. Carbon sources are usually carbon monoxide or hydrocarbon gases like methane and as process gas nitrogen or hydrogen is used. The carbon-containing gas absorbs energy from heat or plasma leading to carbon atoms to detach and transported to the substrate.[20] After that, the carbon atoms are attached to the edges of the catalyst and the growth of CNTs on begins on the substrate surface.[14][20] Growth-temperatures are usually 500 - 1000 °C and depend on the method[11][14][25]. Controlling the deposition of the catalyst particles may also affect the locations of the carbon nanotubes. However, the CVD process has major advantages compared to other manufacturing methods. The tubes can grow directly to the desired substrate and desired shaped areas. The process is also easily scalable to industrial-scale production. Because of this the CVD is currently the most potential method for manufacturing carbon nanotubes commercial applications.[6][7][11][20][25] Figure 4 shows a schematic drawing of batch CVD devices. The preparation of the catalyst and the actual growth of carbon nanotubes can be performed in the same reactor[20].

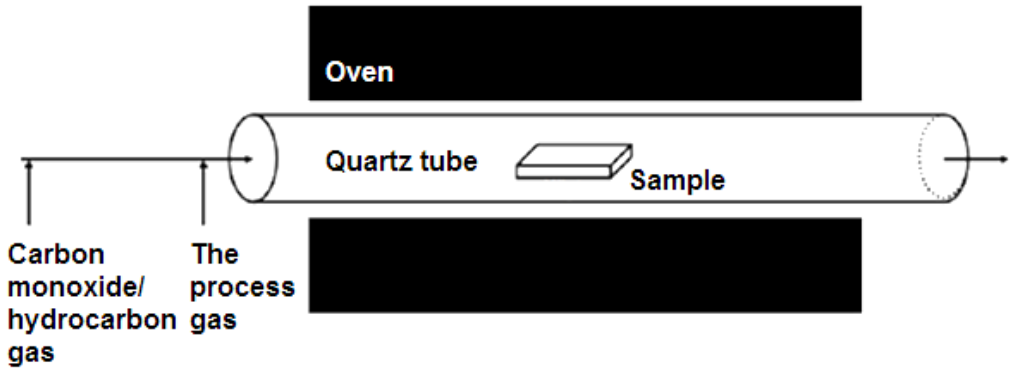

Figure 4. The schematic drawing of batch CVD devices, modified after[20].

One-step spinning of CNTs out of a CVD-method is probably the easiest and fastest production method. Figure 5 shows the schematic drawing of continuous CVD devices. Synthesis takes a few seconds and the product can be spun out of the reactor 100 meters per minute continuously.[11] A kilogram of synthetic amorphous carbon costs approximately 1 USD so, CNT fibers may become competitive with regard to metal wires because CNTs are several times lighter than aluminum and copper.[11] Unfortunately, at present a gram of high-quality carbon nanotubes cost about 500 USD and that is about three times too expensive for commercial applications[7].

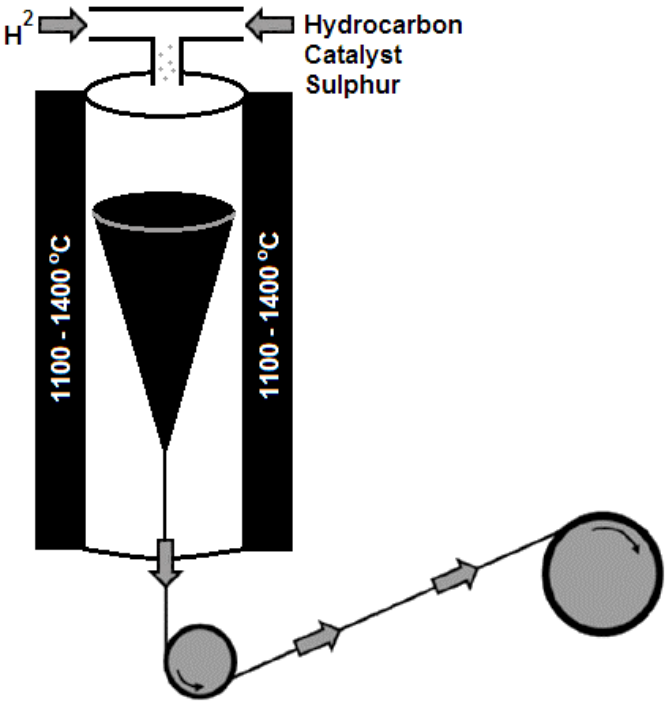

Figure 5. The schematic drawing of continuous CVD devices, modified after[11].

Carbon nanotubes are often used in the manufacturing process of electronic components. The semiconductor industry can utilize CVD-method manufactured CNTs, only if the tubes are of consistent quality.[20] The nanotubes need to be thin, long, and straight.

It is also important that the nanotubes are free of impurities and defects that would interfere with the functioning of components. After the production an abundance of nanotubes are found on the substrates that are difficult to use in the manufacturing process because of their quality. Moreover, large particles are difficult in characterization of nanotubes e.g. with an atomic force microscope (AFM) and amorphous carbon from deposition can form a short circuit between the manufactured electrodes.[25]

2.3 CNT network electrical conductivity

Führer et al. (2000) shows that the resistance of SWCNT-samples with metallic / metallic contact is about 100 - 400 kΩ, but for semi-conductive / metallic contact can be up to two times higher[27]. The use of armchair CNTs will ensure the highest possible conductivity because armchairs are truly metallic regardless of their diameter. The small diameter nanotubes are convenient to pack and allow for a minimal wire.[11] In addition, CNTs are mostly empty space, therefore CNT fibers are specifically low weight when compared with other metallic conductors. The density of SWCNT is about 1.3 g/cm^3 and copper density is 8.98 g/cm^3. Figure 6 shows SEM images of 10 µm and 34 µm CNT fibers produced by water-assisted CVD. The larger yarn has more outer fibers and is less tightly bound; therefore the properties are less effective than with the small diameter nanotubes.[28]

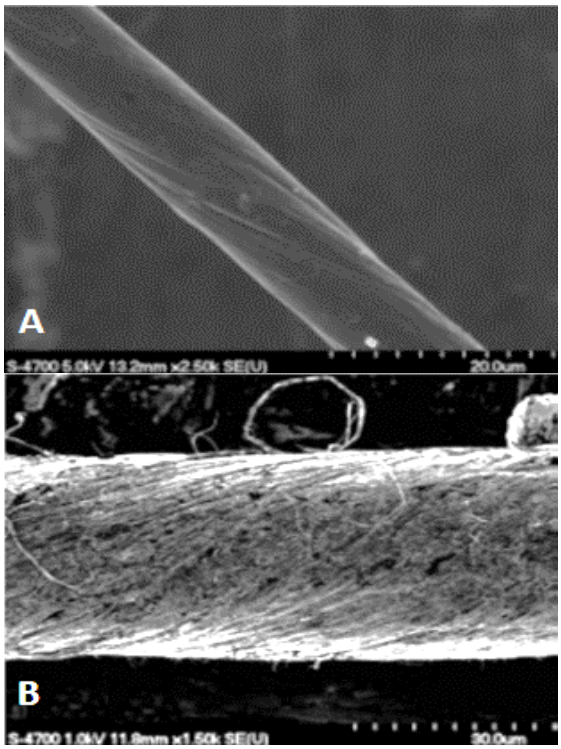

Figure 6. A) SEM image of 10 µm diameter CNT yarn, B) SEM image of 34 µm diameter CNT yarn, modified after[28].

Other structural characteristics that affect the electrical conductivity of CNT networks are e.g. single- or multi-walled structure, length, diameter defects like lattice vacancies, added atoms, bends, twists and collapses, impurities like amorphous carbon, aromatic hydrocarbons and other chemical compounds produced during synthesis, chemical doping, alignment of the CNT bundles and degree of condensation on the fiber. The best electrical achievement of the CNTs would be received if the CNT was metallic, long, SWCNT-structure without any defects and impurities. At present it is known, that electrons can travel ballistically in an individual CNT and the problem is to get the electricity to run between the individual nanotubes. A similar effect may result if CNT bundles are too far from each other and electron hopping is disrupted. In addition, Bourlon et al. (2004) reported that only two outermost shells of the MWCNT participated in the electrical conductivity[29]. The rest of shells only added weight to the system, and therefore it would be optimal to have only SWCNTs or DWCNTs (double-walled CNTs) in the fiber.[6][30] Figure 7 shows transmission electron microscopy (TEM) image of the bundle of armchair SWCNTs.

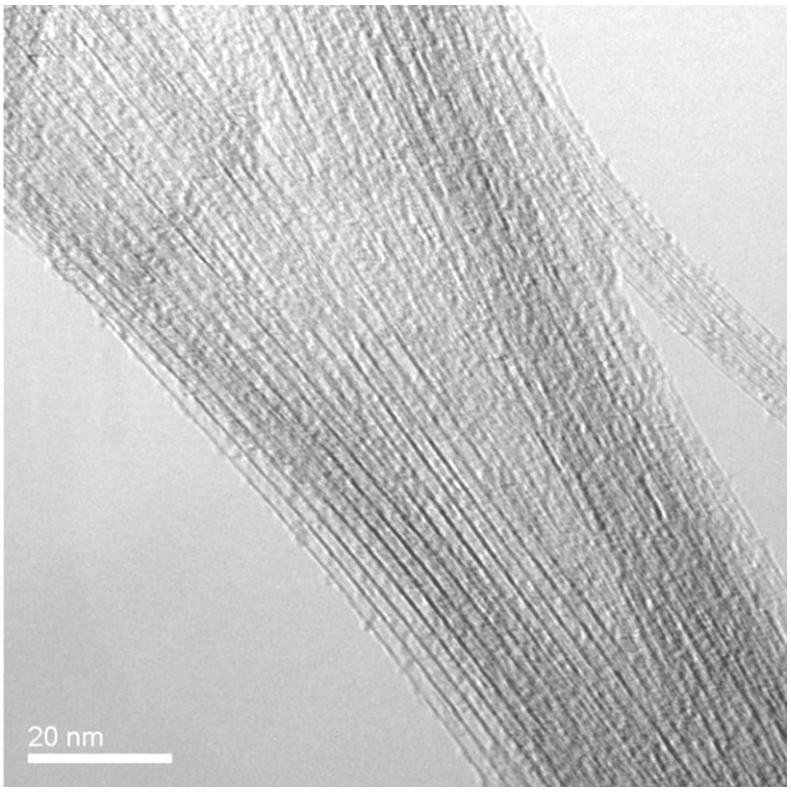

Figure 7. TEM image of the bundle of armchair SWCNTs[11].

Metallic carbon nanotubes may be electrically conductive up to a thousand times better than copper by theoretical estimations[31][32]. Deng (2009) revealed that the axial electrical conductivity of metallic CNTs can be in the order of 10^6 S/m while copper conductivity is

$5.96 \cdot 10^7$ S/m.[33]. In addition, carbon nanotubes have a very high thermal conductivity.[11][32][34] Berber et al. (2000) predicted theoretically that the thermal conductivity of SWCNT at room temperatures should be 6600 W/m K and Kim et al. (2001) measured the conductivity of 3000W/m K for multi-walled carbon nanotubes at room temperature[35][36]. Thermal conductivity of copper is 400 W-W/m·K.[20][33] Lekawa-Raus et al. (2014) showed that thermal conductivities of SWCNT and MWCNT are measured experimentally in the axial direction at 3500 and 3000 W/-m·K[11].

Carbon nanotubes have been found to work as ballistic conductors. When the conductor is shorter than the mean free path of the conductor, the motion of electrons is ballistic. Because of that, resistance does not depend on the length of the conductor.[20] The electron mean free path is the average distance that an electron travels before it collides and changes direction. The conducting of energy is depending directly of the length of the electron mean free path.[18][37] The electron mean free path is 39 nm for copper and 38 nm for gold at room temperature[38].The electron mean free path for CNT can be at least ten times higher than copper and the calculated theoretical electron free path of CNT is about 1 μm[39]. Long and structurally perfect tubes should conduct particularly well in theory, but these kinds of tubes are very difficult to achieve[18][37]. Yang Chai et al. (2010) investigated and experimentally validated the relationship between the diameter and the mean free path of the CNT. Their research shows that the mean free path of the CNT (the average diameter of 12 nm) is around 315 nm. Figure 8 shows the mean free path research results from Yang Chai et all. (2010).[40]

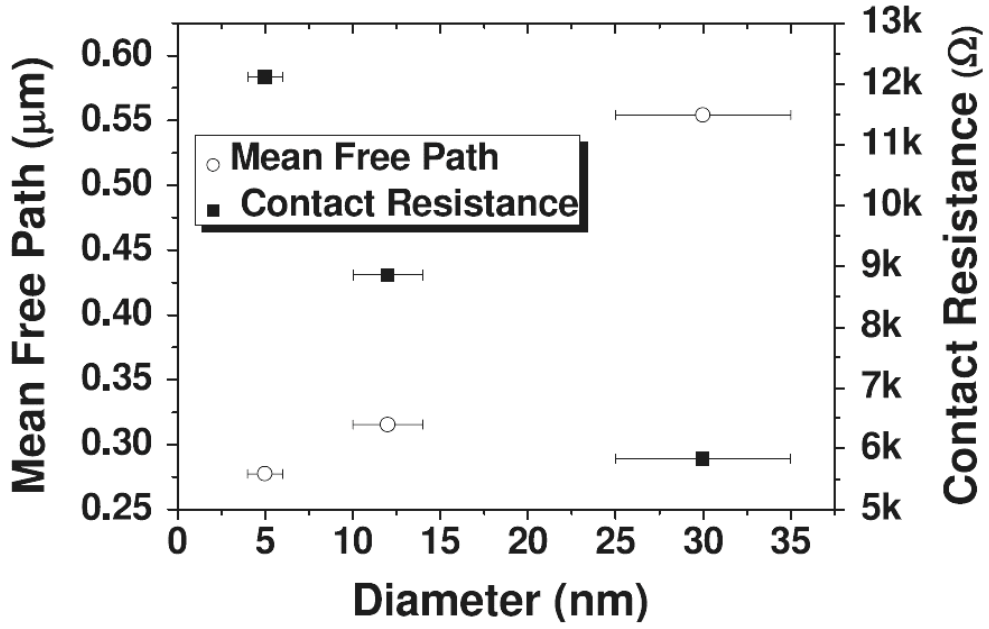

Figure 8. The mean free path and contact resistance of the CNT as a function of the CNT diameter, modified after[40].

Carbon nanotubes are called sometimes unidimensional conductors because current can conduct only in the direction of the axis in the tubes. In a perpendicular direction of the axis they are insulators. SWCNTs are supposed to work also as quantum conductors, where electrons energies are quantized in the tube. Chico et al. (1996) and Frank et al. (1998) investigated the effects of damages in tube structure with impacts on conductivity. They found that even a single defect in the structure of tubes significantly affects the electrical conductivity.[41][42] Zhen Yao et al. (1999) measured that individual SWCNTs can maintain a significant high current density of more than 10^9 A/cm^2, that is about 300 times higher than copper ($3.1 \cdot 10^6$ A/cm^2)[43].

MWCNTs pass a very high current density from 10^6 to $2.43 \cdot 10^8$ A/cm^2 without adverse effects. Way et al. (2001) measured that MWCNTs withstood a high current density of more than 10^9 A/cm^2 and one of the tubes more than 10^{10} A/cm^2[44]. Table 1 shows the summary of Way et al. (2001) measurements on two nanotubes, Table 2 shows summary of the properties of carbon nanotubes and bulk copper and Table 3 shows summary of the properties of Cu/CNT composites.[44]

Table 1. Summary of measurements on two nanotubes, modified after[44].

Nanotube	**I**	**II**
Diameter [nm]	8.6	15.3
Length between the appropriate electrodes [μm]	2.6	2.5
Measuring method	Constant voltage, 2-terminal	Constant current, 4-terminal
Resistance [kΩ]	2.4	1.7
Current density [A/cm^2]	$1.8 \cdot 10^{10}$	$5.4 \cdot 10^9$

Table 2. Summary of the properties of carbon nanotubes and bulk copper[11][20][28][43][44][45][46].

Property	**SWCNT**	**MWCNT**	**Copper**
Density [g/cm^3]	~1.3	~2.6	8.98
Young's modulus [GPa]	~1000	~1000	110 - 128
Tensile strength [GPa]	~50	~100	0.209
Yield strength [GPa]	45	-	0.075
Max. current [A/cm^2]	~10^9	~10^{10}	10^6
Thermal conductivity [W/(mK)]	~6000	~3000	400

Table 3. Summary of the properties of Cu/CNT composites produced by spark plasma sintering[47][48].

Property	**Cu/CNT** 5 vol.%	**Cu/CNT** 10 vol.%	**Cu/CNT** 15 vol.%	**Cu/CNT** 20 vol.%
Relative density [%]	98.5 - 99.7	98.1 - 99.1	97.1	96,51
Young's modulus [GPa]	80	137	100	106
Yield strength [GPa]	*0.37	*0.589	0.341	0.22
Electrical Conductivity [%]	80 IACS	78 IACS	76 IACS	50 IACS

*Estimated with shear-lag model. Measured values are 0.149 GPa (5 vol.%) and 0.197 GPa (10 vol.%).[47]

Van der Waals forces attach the individual carbon nanotubes combining them into a network with a distance of 0.4 nm from each other. A large CNT network is difficult to produce in such a way that the properties of individual CNTs remain unchanged because e.g. the chirality, impurities and different diameters and lengths degrade the properties of the network. Densification of CNTs is researched to improve electrical conductivity. In this way, the structure is less porous when the contact between the tubes is better. In addition, the densification affects mechanical strength of the CNT material.[37][49] Koziol (2007) published the densification method of CNTs with acetone. Acetone wetted CNT fibers, and volatile acetone pulled the CNTs closer to each other.[49] Figure 9 shows spun CNT fibers before and after densification with acetone. Another method, for modified CNTs contacts, is twisting. With the twisting of yarns, longer yarns can be produced from short CNTs and also the contact area between the tubes and mechanical strength is increased. However, too large twisting angles reduced the mechanical strength of CNT yarns. Figure 10 shows various examples of twisted CNT yarns.[9]

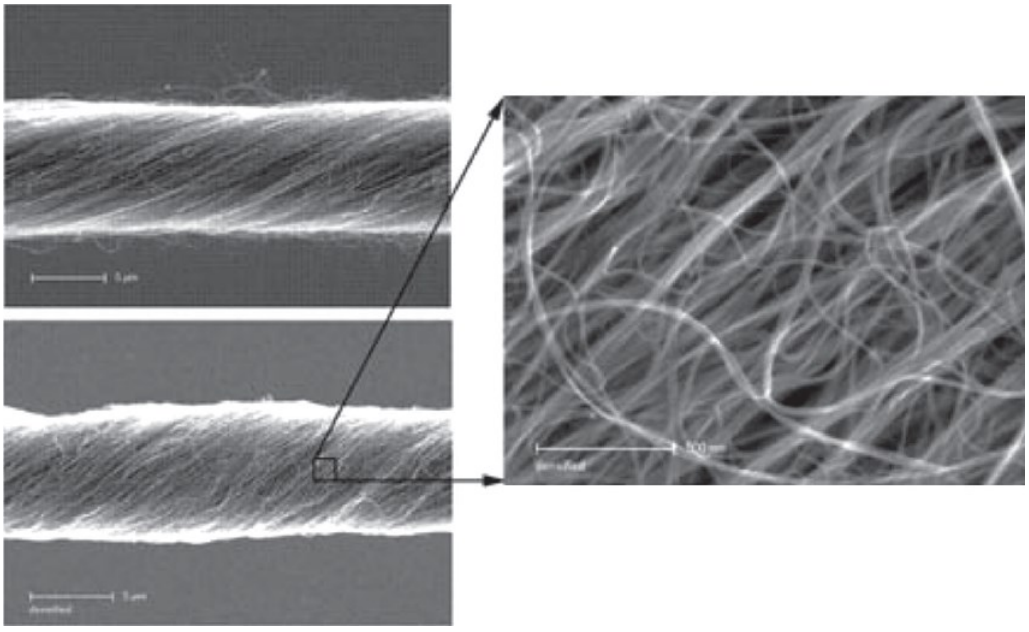

Figure 9. CNT fibers before and after densification with acetone, modified after[9].

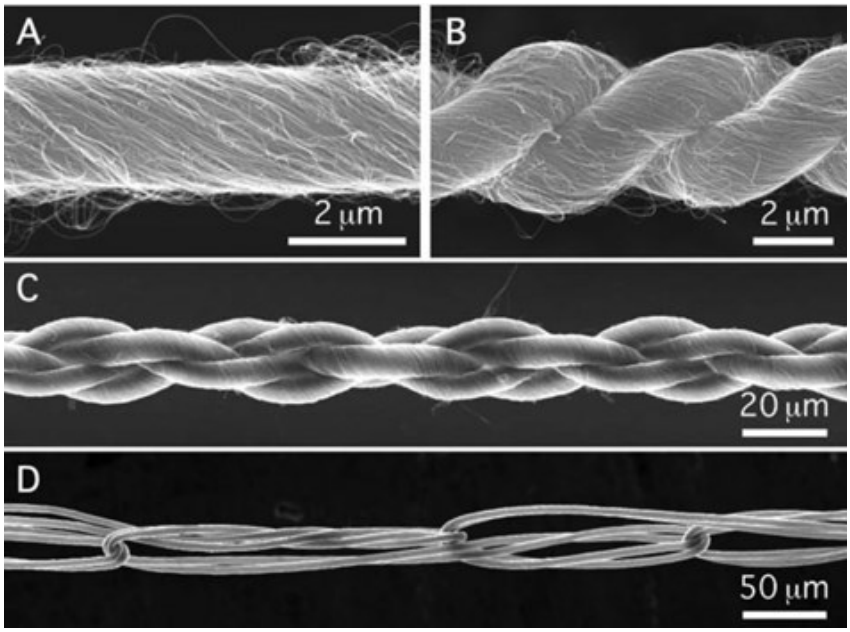

Figure 10. SEM images of A) single, B) two-layer, C) four-layer, and D) knotted MWCNT yarns[9].

2.4 Purifying and functionalization of CNT

All the manufacturing processes of carbon nanotubes generate additional reaction by-products like soot, wrapped graphite strips, amorphous carbons, metal catalysts, carbon nanoparticles (e.g. small fullerenes) and other unwanted particles. In water dispersions, the purification is done in two stages. First, the nanotubes are separated from the soot, and second, different size tubes are sieved. The finished product should be as homogeneous as possible.[10][15][32]

The most common purification methods for CNT are:

- Oxidizing treatment:
  - Removes carbon impurities, but may also damage the nanotubes.
  - The temperature and the time of oxidizing must be strictly controlled.
  - The oxidizing treatment is the most suitable for the MWCNT structures.[10] [32][50]
  - The used metal catalyst may be removed, but initially the surface should be cleaned by oxidizing or ultrasonic.
  - E.g. HNO_3 does not affect the carbon-structures, but removes the metals[10]
- Annealing:
  - The material is heated to high temperature in a vacuum, wherein the carbon nanotubes are oriented again and structural defects reduced.
  - The annealing also removes graphite and fullerenes, as well as it melts metals.[10]

- Ultrasonication:
    - The material is placed in a solution (e.g. in alcohol) that is oscillating in ultrasonic frequency.
    - Separation of particles depends highly on the solution.
    - Too long time of sonication causes destruction of nanotubes.
- Magnetic cleaning:
    - Inorganic nanoparticles are added in an individual carbon nanotube solution.
    - A permanent magnet is connected with the used test tube, which collects ferromagnetic particles on the solution surface during sonication.
    - This purification method works well in small laboratory systems.[10]
- Microfiltration:
    - Removes small fullerenes and metal particles.
    - The SWCNT materials are mixed with carbon-disulfide solution, which is pressurized to flow through the membrane.
    - The impurities which are longer than the nanotubes remain in a sieve.[10]

The separation can be facilitated by functionalization, where the solubility of nanotubes is improved compared to the solubility of impurities. After this the filtering of impurities becomes easier. Sieving different sizes of carbon nanotubes are often used in chromatography, wherein nanotube-solution is pressurized through the porous material. The most effective purification methods of additional reaction products are ultrasonication, functionalization and micro-filtration.[10]

Functionalization is a procedure that aims to modify the carbon nanotubes with attaching reactive chemical groups to the surface of carbon nanotubes[51][52]. The functionalization of CNTs is quite common, either through direct chemical modification or through chemical bonding[53]. The general methods are covalent bonding of chemical groups and attaching functional molecules with non-covalent methods. This has effect with the chemical nature of CNTs but also with their electrical properties. Functionalization may seem similar to the doping of carbon nanotubes, but the aim of doping is only to change the electrical properties by adding a foreign molecule or an atom to the carbon nanotube structure without changing the hexagonal lattice structure. The purpose differs with these methods and so does the bonding energy between the substitute atoms and carbon atoms. Adding a covalent bond between a foreign atom and the carbon atom in a defect area on the surface requires more energy to form.[51][52]

Functionalized carbon nanotubes are expected to have a major role with research focused in fields of material science in the future. Carbon nanotubes have great solubility

and with increasing functionalization possibilities, they will have plenty of utilization targets with different nanomaterials.[30] Unprocessed carbon nanotubes do not usually contain many active functional groups but their structure provides interesting possibilities through functionalization[53]. The research of CNTs is much more complicated than other macro-molecule materials because carbon nanotubes are aggregated easily into bundles. The probability of finding two identical SWCNTs is minimal.[54]

There are two basic ways to perform functionalization with carbon nanotubes. First way is to attach functional groups directly to graphite surface and the second way is to use carboxylic acids, which are bound to the surface of nanotube acting as an anchors for further functionalizing groups. This functionalization has increasing effect on the aforementioned solubility of carbon nanotubes when performed.[30] The attachment of molecules, take typically place in the defect areas that are displayed in Figure 11. A) Carbon structures can be altered by five- or seven membered carbon rings leading to bending of the carbon nanotubes. B) Sp3-hybridization in defects. C) Oxidative conditions can cause damage in the carbon framework leaving apertures. D) Open end of the SWCNT is terminated with COOH- NO-, OH- or O-groups.[54]

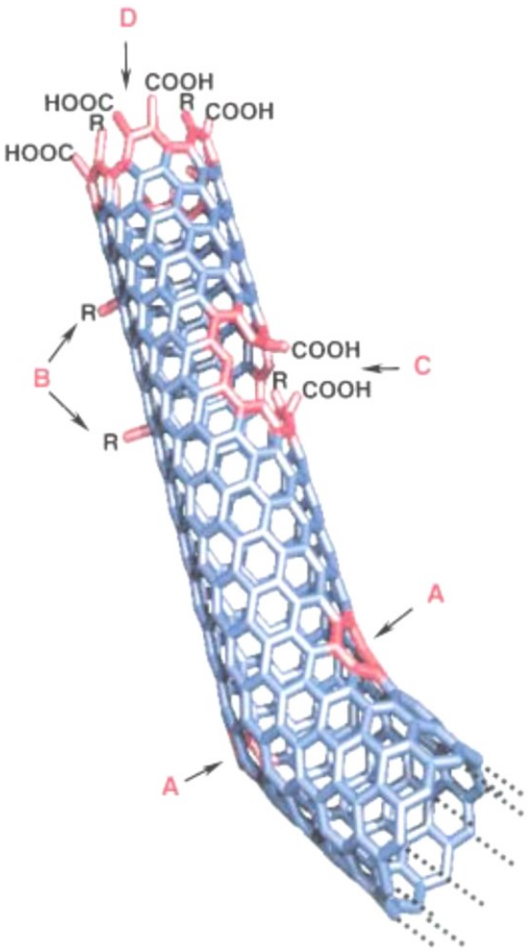

Figure 11. The attachment of molecules take typically place in the defect areas[54].

Molecular and supramolecular chemistry ways include defect functionalization, covalent functionalization of the side surfaces, non-covalent of additional atoms, ions, or clusters attached to the outside of the nanotube shell with surface-active agent, e.g. formation of supramolecular adducts with surface-active agent or polymers, and functionalization with additional atoms, ions, or clusters enclosed within their inner spheres. In Figure 12 there are different kinds of functionalization methods for nanotubes. A) Functionalization of structural defects for nanotubes. B) Covalent functionalization of the side surface. C) Non-covalent functionalization (of additional atoms, ions, or clusters attached to the outside of the nanotube shell) with surface-active agent. D) Non-covalent functionalization (of additional atoms, ions, or clusters attached to the outside of the nanotube shell). E) Functionalization with (additional atoms, ions, or clusters enclosed within) their inner spheres, for example C60. The tubes of methods B – E are drawn in the ideal way, but defects are found in the actual situation.[54]

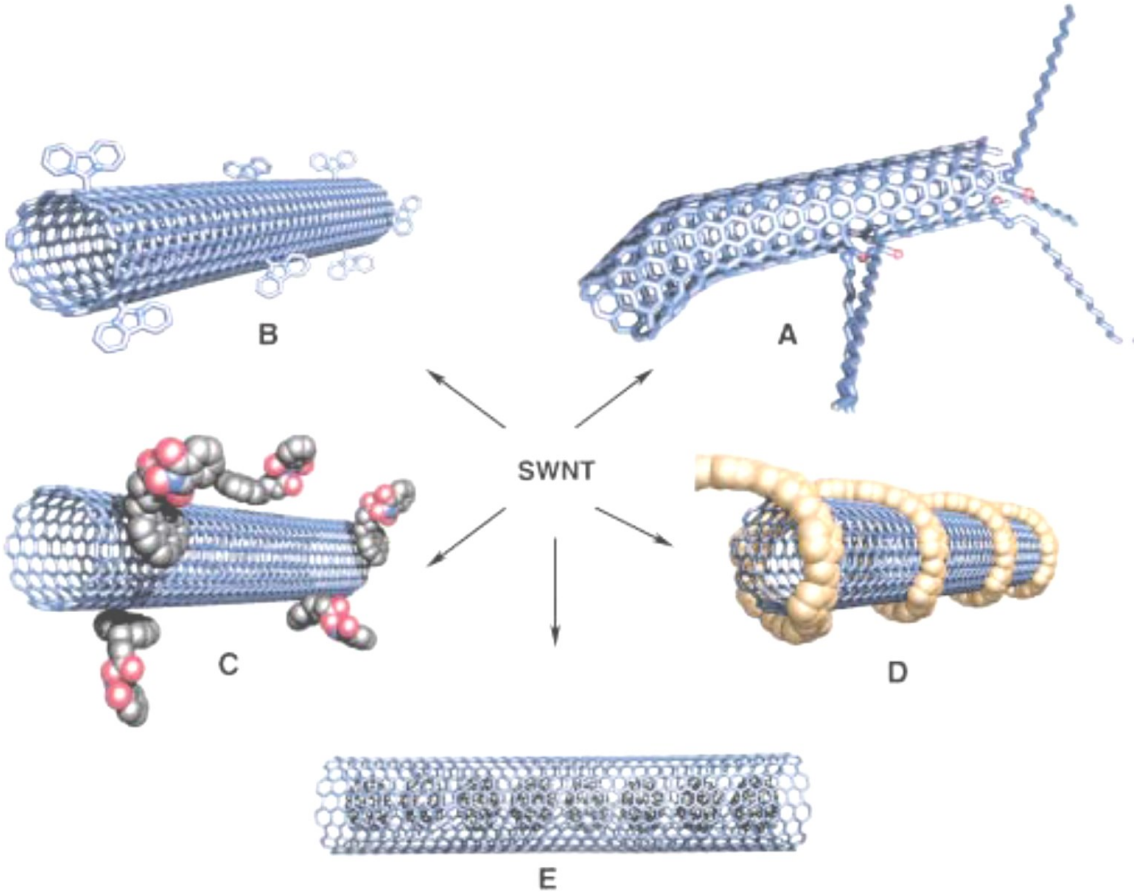

Figure 12. Variety of possibilities for functionalization of single-walled carbon nanotubes[54].

In covalent functionalization, desired groups attached to surface of CNTs, such as carboxylic acid, epoxy and hydroxyl groups of graphene-oxides. A specific reagent may react with a number of different groups. The selectivity of reactions may be difficult to demonstrate because CNT structure is very complex to characterize.[30][55] Most covalent functionalization requires the addition of carbonyl and carboxyl groups with aggressive treatment as mixture of HNO_3/H_2SO_4 or by plasma etching.[52]

Geng Xu et al. (2011) investigated anodized CNTs reporting a new method to prepare Cu/CNT composites. The method combines continuously fiber spinning, CNT anodization and metal deposition. The anodized CNT surfaces contribute a stronger bonding with the deposited copper compared to un-anodized surfaces. When the anodized CNT fiber was coated with 1 μm Cu, it resulted the strength of ~800 MPa and without the anodization 611 MPa. Additionally the conductivity of anodized CNT composite was almost four times higher. Research showed that when increasing the Cu thickness to 3 μm, the strength of anodized fiber remained in ~600 MPa but its conductivity increased rapidly 4.5 times.[56]

3 ELECTROPLATING THEORY

In electrodeposition of copper, the sample is immersed in an electrolyte bath. The bath may contain metal salts, acids, bases, complexing agents and additives. The growth of coating is controlled with the placement of the anode and cathode, current density and additives. The structure of final coated surface should generally be fine-grained and homogenous but is dependent on the application. The coated sample acts as cathode and dissolvable or inert type of metal as anode. A dissolvable anode supplies power into the bath and dissolves in the process. The concentration of dissolvable metal needs to be controlled in the bath. An inert anode supplies current to the bath while launching oxygen evolution. The Cu^{2+} ions are deposited as Cu atoms onto cathode surface during electrolysis.[57] Figure 13 shows the electrolytic cell and the mechanism of electrochemical deposition when the plated electrode e.g. CNT sample is the cathode and dissolvable or inert type of metal is the anode.

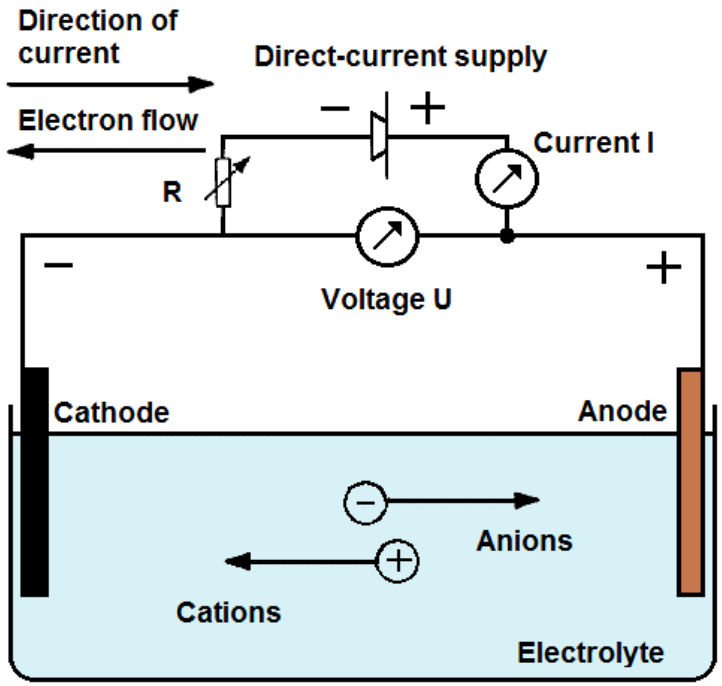

Figure 13. Electrolytic cell where the anode dissolves and the cathode is deposited.

Deposition of metal may include side reactions like hydrogen formation at the cathode. This leads to inefficiency and causes the cell to use only a part of the total current in the metal deposition. The efficiency of electrolysis is an important parameter in electrodepositing process and is calculated using the Formula (3):

$$\eta_e = \frac{I_{me}}{I} \tag{3}$$

where I_{me} is the amount of current used in the metal deposition and I is the total current in the cell [A].

The mass of the deposited metal on the cathode depends on the amount of used electricity and it follows Faraday's law Formula (4):

$$m = \frac{I \cdot t \cdot M}{z \cdot F} \cdot \eta_e \tag{4}$$

where I is the total current in the cell [A], t is the deposition time [s], M is the molar mass [g/mol], z is the number of electrons and F is the Faraday constant [96488 C/mol or As/mol]. The deposit thickness d [cm] can be solved from Formula (5):

$$d = m/\rho A \tag{5}$$

where ρ is the density of the metal [g/cm^3] and A is the area of deposition [cm^2].[58]

The electrode surface is a complicated system. Near the electrode surfaces, there are narrow film like areas that are called anode- and cathode films. The properties in these areas differ from the properties of the bulk solution. The films are a combination of the electronic double-layer (Helmholtz), diffusion layer and the flow layer. Nearest to the surface of the electrodes there are two layers of adsorbed ions and molecules, farther out is diffusion layer and the outermost is flow layer. In diffusion layer the concentration of reactant changes. The stronger concentration, the higher the rate of reactions that occur. In order for the cathode to be deposited, the cation needs to traverse at first to the cathode in the electrolyte and then through the cathode-film (the diffusion layer). The thickness of the diffusion layer is 10 - 100 µm and the cations move in it due to the differences in concentrations. When a hydrated metal ion approaches the metal surface, the combined water molecules begin to polarize and leave. On the metal surface the strength of electric field is already so high, that all water molecules are detached and the metal ion is ready to be reduced to metal. The ion is then adsorbed to the surface of the

sample and transferred to a suitable growth place by surface diffusion. Figure 14 shows the migration and deposition of metal ion in aqueous acid bath.[59]

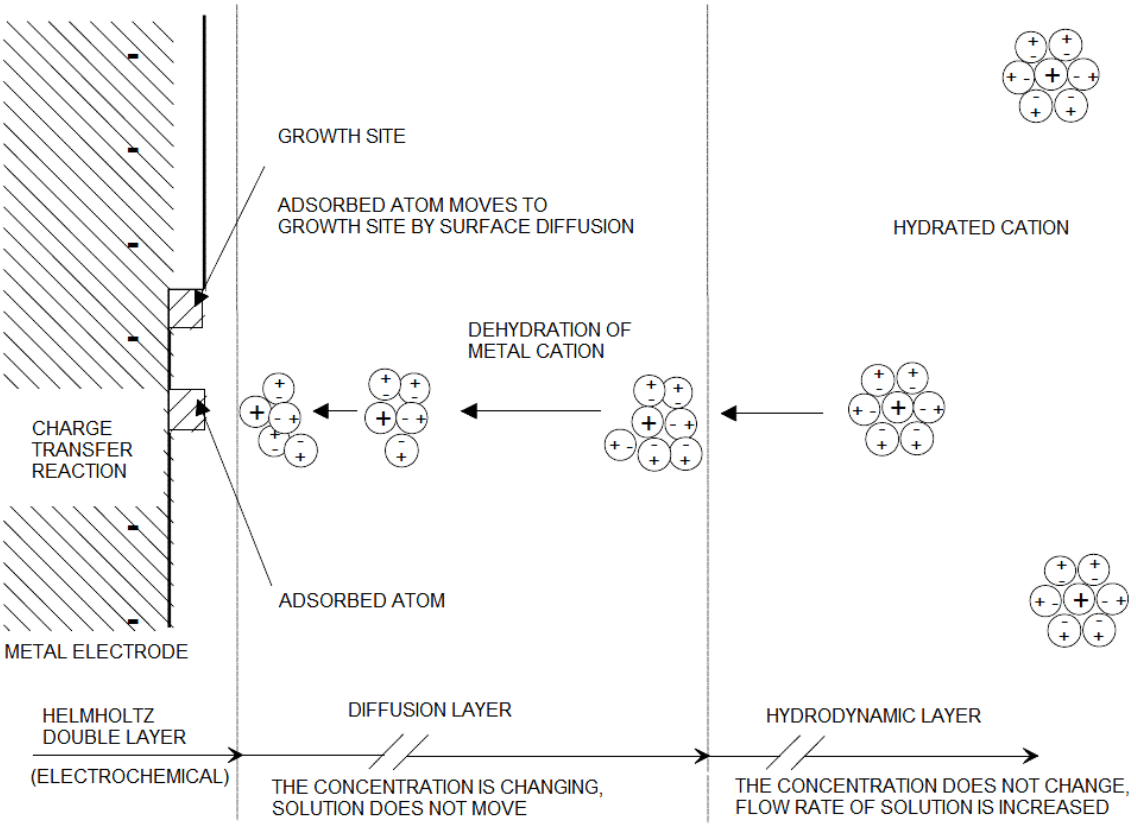

Figure 14. Surface layers of an electrode during the cathodic deposition of metal, modified after[57].

3.1 Electrolyte baths

In copper electrodeposition, the electrolyte generally consists mainly of sulfuric acid and copper sulfate. These kind of baths are easy to use, have a high current efficiency, and are relatively cheap.[60] In addition baths may contain chlorides, additives and impurities dissolved from the anode[57]. The composition of copper sulfate electrolyte is generally 150 - 250 g/l $CuSO_4 \cdot 5H_2O$, 30 - 75 g/l H_2SO_4 (96 - 98 %) and 30 - 150 mg/l NaCl. The optimal temperature is 20 - 45 °C and cathode current density is 100 - 2000 A/m^2.[60]

The electrolyte contains many compounds that all have specific functions. Some compounds have a positive effect and others have harmful effects. The electrolyte component types and their roles are listed in Table 4.[57]

Table 4. Electrolyte components of interest in electrodeposition[57].

Component	Role
Metal ion	Source of metal
Anion	Maximize solubility
	Provide anode reaction
	Conductivity
	pH-control
Auxiliary salt	Ionic strength and conductivity
	Buffering and pH control
Impurities	By-product for recovery
	Detrimental to efficiency or purity
Inorganic additives	Assist anode life
	Impurity removal
Organic additives	Cathode leveling
	Impurity control and improved efficiency
	Grain refiner
	Mist suppressor
Water	Solvent
Suspended solids	Incorporation into cathode or remove as cell sludge

Higher concentrations and higher temperatures allow work with higher current density. Lower copper concentration and higher sulfuric acid concentration will increase the throwing power and improve metal distribution, but they decrease the cathodic current efficiency i.e. the deposition rate is low when the copper concentration is low. If higher deposition rate is desired, more concentrated baths should be used.[59][60] If the amount of sulfuric acid is too low, there is a risk of a sponge-like copper formation at the surface and the reduction of copper (I) oxide that decreases the current efficiency. Also the amount of chloride has a high impact and it should be kept within limits. Normal gloss-copper bath contains typically 20 - 100 mg/l chloride. If the concentration is too low, the deposition layer is striped and uneven and if the amount of chloride is over 100 mg/l, the deposition layer is dim and produces a veil-like surface. Copper sulfate bath works at a large area of current densities, where the concentration of bath, moving and temperature determine the limits.[60]

Sulfate-baths require phosphorus-alloyed and very clean anode materials. The anode copper may contain impurities such arsenic, bismuth, iron, nickel, lead, antimony, selenium, tellurium and noble metals. Impurities can be divided into three types depending on their behavior and equilibrium potential in the electrochemical series; The impurities that are more noble than copper do not dissolve into the electrolyte, the impurities that are less noble than copper dissolve in the electrolyte and other soluble impurities such as nickel and bismuth become more concentrated during the process and can cause

contamination of cathodes.[57] Metallic impurities were found to cause decreases of conductivity and formability of copper even at very low concentrations[60][61]. Even 0.001 % of phosphorus, arsenic and nickel decreases electrical conductivity but sulfur, selenium, and bismuth affect only mainly the mechanical strength of copper deposit[60].

Slight concentrations of additives are usually important to be added into the electrolyte and they become more crucial with increasing current density[57]. Brightener additive allows the coating to be stiffer and it provides usually high quality. Brighteners are usually formed from combination of organic materials, where part of them work as base-gloss and others as cover-gloss. Preferred brighteners ingredients are e.g. butyne-1.4-diol, propargyl alcohol, phenol, ethanol and sulfur-containing agents. Also, a low power efficiency leads to stiffer coating.[60] The additives can be used to achieve a flat, dense and pure copper layer on the cathode surface. Especially the formation of nodules can be avoided with the use of organic additives such as thiourea, glue (gelatin) and avitone. These and chloride work also as grain refiner agents.[57] Normally also surfactants e.g. polyglycol ethers have to be added to provide good wetting and to prevent porosity caused by hydrogen gas[60].

Gloss and smoother coating can be also improved if the copper is driven with pulse electroplating, e.g. 10 - 45 s with cathode and 2 - 15 s with anode or 10 s with cathode and 1 s without power. During the anodic phase, the copper layer dissolves while the original anodes deposited. The longer the deposited material acts as anode, the higher effect it has on smoothness and polishing of the surface. Pulse electroplating provides also following advantages: Better covering power, fine-grained surface, the higher current density and therefore a shorter processing time, improved anode dissolution, lower porosity and more high-tensile deposited layer. The disadvantage is the higher equipment cost and complexity of treatment, nevertheless pulse electroplating has a beneficial impact to layer growth and the deposition rate.[60]

The electrolyte affects energy consumption, mass and heat transfer in the cell. In addition the properties of electrolyte can be desirable electrodeposition operations. E.g. high electrical conductivity decreases the power consumption and low viscosity and density increase the transport properties. The diffusion coefficient of Cu^{2+} in copper electrolyte is also an important factor because it determines the current density during electrolysis.[61] Subbaiah (1989) has investigated densities, electrical conductivities and viscosities of sulfuric acid and copper sulfate solutions. It seems that the conductivity is affected especially by the sulfuric acid concentration, which is due to the effect of hydrogen ions in the solution. Also increasing the temperature increases the conductivity but if the copper

concentration is increased above 40 g/l, the conductivity decreases. Cu^{2+} and H_2SO_4 concentrations and temperature have an influence on viscosity. The increase in concentration increases viscosity whereas increase of temperature decreases viscosity.[61]

3.2 The wetting ability of electrolyte

The chemical inertness of CNT surfaces and interactions that cause adhesion between surfaces and particles appear to have a significant impact on the manufacturing of Cu/CNT composites. Moisture has also effect directly on the bonding of the particles, thus these two issues are closely linked. There are many type of bonding that can take part in a number of different chemical and electrical interactions. Most notable of these are the van der Waals-based molecular interactions, as well as the adhesion of the fluid caused by condensation.[25]

The hydrophobicity and hydrophilicity are terms used to describe how the material takes contact with water. Contact angle θ is used to measure the hydrophobic effect between a water drop and the measured surface. The contact angle is the angle that is formed between the curved edge of the droplet and the surface. In the general case, the contact angle is not completely same at the edges of the droplet but its value depends also of the local properties of the surface. It is sufficient to determine two positions of θ, typically in the cross-section of the front and back parts. Contact angle of the ideal hydrophilic surface is 0°, and increasing contact angle indicates increasing of hydrophobic properties. On an ideal hydrophilic surface, water does not form any drops, and basically any amount of water can wet throughout the surface. In practice, this situation can't be detected and the water spreads on an indefinable area in the hydrophilic surface and the contact angle is close to zero. Surfaces that contact with the water with an angle of 90° or more are generally considered as hydrophobic. There are also super-hydrophobic surfaces with contact angle up to 150°.[25][62] Figure 15 shows hydrophobic and hydrophilic contact angles.

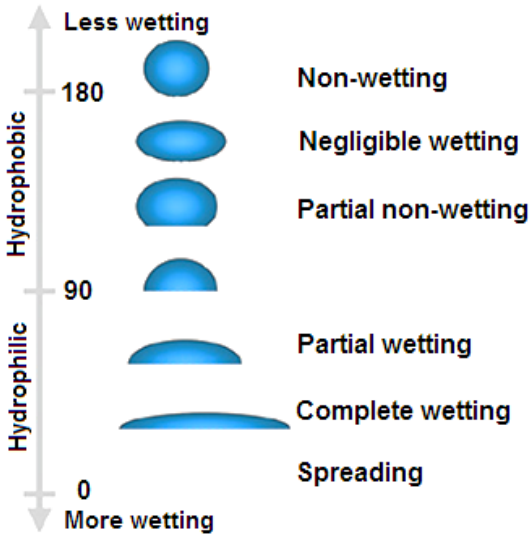

Figure 15: Hydrophobic and hydrophilic contact angles, modified after[63].

Interactions between solids are usually attractive[64]. For this reason, the loose impurities that are placed on the surfaces, remain often attached to them. The forces that cause bonding of particles in surfaces, depend on the particles and the substrates. Electrically charged or chemically active material pairs have electrostatic interactions or chemical acid / base interactions that are significant to them.[25]

Van der Waals interactions

Van der Waals forces i.e. dispersion forces are weak forces between the molecules, that are expressed when the molecules are up to 0.3 - 0.4 nm from each other. Van der Waals forces are caused due to the polarization of molecules turning them to dipoles. The internal electron density of the atoms and molecules are not stable, and varies randomly from side to side. This creates spontaneous electric dipoles which induce the opposite field adjacent molecules causing the attraction. Van der Waals forces occur in all materials, but they are weakest forces between molecules and can't break the stronger forces, such as tension of water. A material that is bound together with Van der Waals cohesive forces is not miscible with water, because water hydrogen bonding force is stronger. E.g a drop of water on a waxed surface appears as a drop due to this. Water's surface tension is stronger than van der Waals force of wax.

The effective range of the van der Waals -forces is only few nanometers, and the strength of it in different materials is characterized with the Hamaker constant A_1. The constant describes the situation where the same materials are interacting with each other. If the materials are not same, the constant is formed as Formula (6).

$$A_{12} = \sqrt{A_1 + A_2}, \quad (6)$$

where A_1 and A_2 are the Hamaker constants for each material. If the interaction is still associated with a third medium, constant can be calculate with Formula (7).

$$A_{123} = A_{12} + A_3 - A_{13} - A_{23} \quad (7)$$

For the calculation of the constants numerical values there are two main theories: London's van der Waals theory and Lifshitz's macroscopic theory. London's theory is based on the sum of individual atoms and their interactions with nearby pieces. Lifshitz's theory is based on two macroscopic pieces interaction in a third medium. London's van der Waals theory is considered more rough and inaccurate, because it gives the completely right results only with distances less than 10 nm and additionally the sum of interactions in behaving linearly is questionable.[64]

The numerical values of Hamaker -constants are very small, typically 10^{-12}. However, the forces caused by the van der Waals interaction are usually significant in micro- and nano-level or with other interactions. The form of the force generated by van der Waals interaction depends essentially on the geometry of the situation. In Figure 16 relevant parameters of spherical and tubular particles in van der Waals interaction are shown. Major parameters are the distance between pieces Z_0 and dimensions of pieces. The pieces are never quite stuck together in atomic-level and experimental determination of Hamaker-constants is therefore difficult. The distance of Z_0 is very small and it can't typically be measured, therefore in practice it is assumed to be between 4Å < Z_0 < 10Å.[25][64]

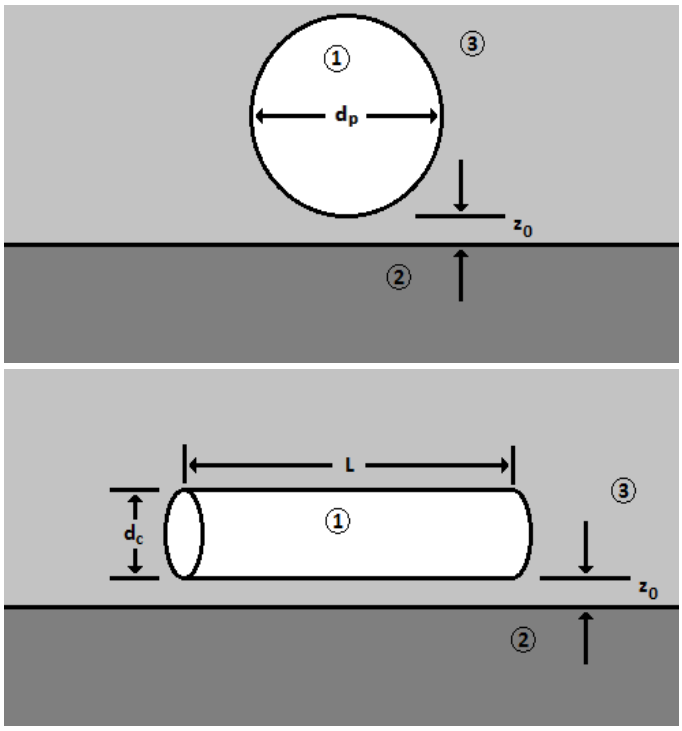

Figure 16. Relevant parameters of spherical and tubular particles in van der Waals interaction[25].

The adhesion force with spherical particles is in form of Formula (8):

$$F_{ad} = \frac{A_{123} d_p}{12 Z_0^2} \tag{8}$$

And in tubular particles are in form of Formula (9).[64]

$$\frac{F_{ad}}{L} = \frac{A_{123} d_p^{1/2}}{16 Z_0^{3/2}} \tag{9}$$

In purity and purification of the surfaces should be noted that with spherical impurities (Figure 16) intensity of van der Waals attraction is directly proportional to the particle diameter d_p. This linear dependence causes that the force decreases slowly when the size of particles are decreases. Therefore van der Waals attraction becomes the dominant interaction for very small particles. The amount of mechanical forces that are used to clean the surfaces is instead proportional to the mass of the particle. Therefore, the efficiency of the cleaning is scaled in third potency of particle size. Because of this removing small particles from surfaces requires very high accelerations.[64]

Another factor for strength of van der Waals interaction is roughness of the surface. The roughness that is smaller than particle size, typically weaken the attraction, because the effective distance of force is shorter. When the effective distance is shorter, the actual contact area is smaller and only a small fraction of the mass of the particle access the effective distance from the surface. If the roughness is same size than particles or larger, the contact area can grow because of their interaction. Therefore, the attraction of small particles can improved with uneven surfaces.[64]

Capillary interactions

Attraction caused by wetting is second significant interaction for particles and substrates and it is caused by moisture between surface and particles. Typically attraction follows from condensation of moisture into the atomic level in gap between surface and particle. The shape has effect in the condensation area. If the shape is curved in the contact area, this contributes to condensation and therefore, condensation can occur at significantly low relative humidity. It has been shown that the adhesion in particles surfaces increases highly when relative humidity is 50 %. Generally 60 - 70 % is the limit, and after that the condensation from the air begins to form bridges between the surface and particles.[64]

If the surface is previously immersed in the liquid, the moisture on the surface after drying may also contribute bonding of particles to the surface. In this case, the capillary adhesion can become a major factor in a very dry environment.[64] This type of residue layer can be difficult to remove. Bhattacharyan & Mittal (1987) showed that even twenty four hours long sintering has not significantly reduced the adhesive force of particles[65]. In Figure 17 the capillary interaction between the spherical impurity and surface are shown. The fluid-filled gap between the surface and the spherical impurity causes two attractive interactions: the surface tension (F_{LV}) and Laplaces pressure or capillary pressure Fp, which follows the decrease of internal pressure of the fluid.[64] Contact angle θ of droplet for to surface and surface tension of the liquid γ_{LV} are important variables besides the parameters of the Figure 17.[25]

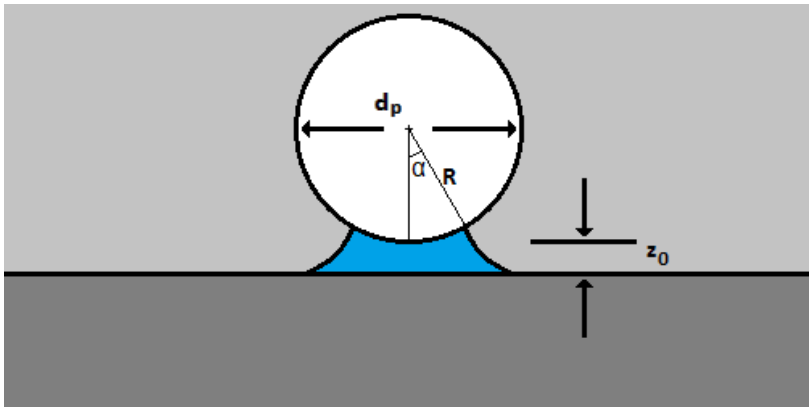

Figure 17. The capillary interaction between the spherical impurity and surface[25].

3.3 Nucleation and growth of nuclei

Electrodeposited metal consists of crystals, which are initiated as nucleus. The nucleated metal deposition will grow into a macroscopic crystalline product. Formation of new crystals begin with the adsorption of a single ion from electrolyte. This adatom is lightly committed to the surface and can dissolve again, form a new nucleus or grow into a crystal. The adatoms move by surface diffusion, and if surface diffusion is prevented or compounds blocked at the growth places, the adatom concentrations grow up and then new nucleation and growth sites are formed. A crystallization (nuclei growth) of electrodeposition occurs in several places at the same time and growth ends when boundaries between of the two adjoining grains growth meet. When adatoms encounter each other, they become more stable and form larger clusters. Clusters become a nucleus, when they achieve a certain critical size and will not dissolve anymore. Crystallization of nuclei at the same area form a regularly oriented structure. The nucleation begins when overpotential is high enough. The larger the overpotential, the more nuclei are formed. Growth of nuclei requires adsorbed atoms to transfer to suitable locations for nucleation.

Usually this takes place in a corner or a tip of sample. The structure of coating depends on the relative differences between formation rates of adsorbed atoms and surface diffusion rates. Low deposition current density means low polarization leading to low formation rate of atoms if surface diffusion is relatively fast and the deposit is growing locally. When the formation rate of atoms is fast, a lot small grain size nuclei are grown. Figure 18 shows three steps of nucleation: nucleation, growth of nuclei and the three-dimensional growth of crystals and Figure 19 shows SEM pictures of nucleation from different locations of a CNT sample.[57][59]

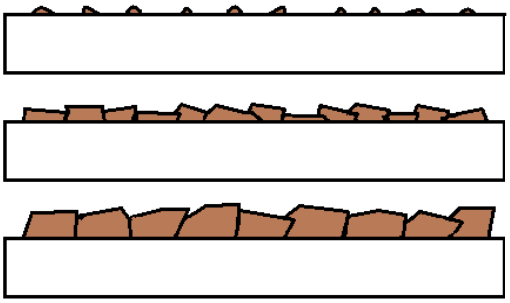

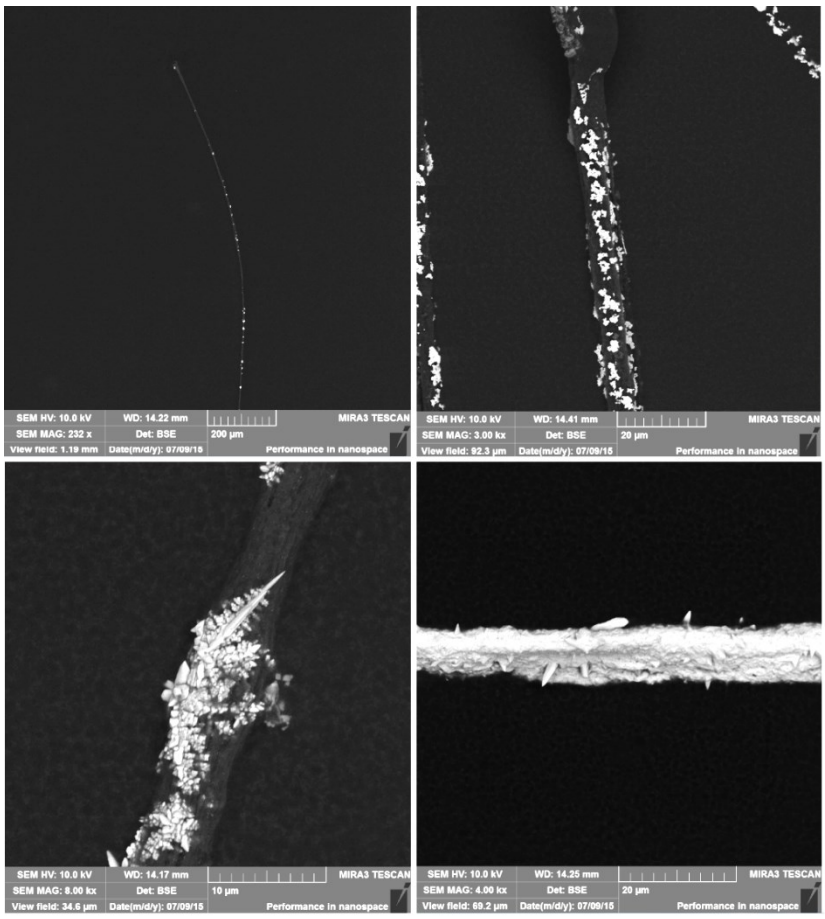

Figure 19. SEM pictures of nucleation (sample is deposited with -0,1 mA current 120 s).

3.4 Morphology of deposit

The quality of the deposition is affected by e.g. current density, concentration of the electrolysis, stir, temperature, pH, the activity of metal ions, activity of other cations and anions, complex structure, inhibitors and material. Grujicic (2002) has shown, that when pH and copper concentration increase, the nuclei size increases but the nuclei population density decreases. In addition, an increase in deposition potential creates smaller nuclei and higher nuclei population density. The morphology of deposited copper depends of the temperature. The optimal current density for most coating baths is a 100 - 500 A/m^2. The current density does not indicate how the coating is formed on the profiled surface. Moreover the current efficiency varies along the micro profile of the surface.[66]

Growing habit and direction of nuclei are different and deposit becomes polycrystalline. There are five most typical deposit morphologies for polycrystalline deposit: Field orientated isolated crystal type (FI), Basis-orientated reproduction type (BR), Twinning intermediate type (Z), Field orientated texture type (FT) and Unorientated dispersion type (UD).[67] Field orientated isolated crystal type, basis-orientated reproduction type, twinning intermediate type and field orientated texture type are seen with two-dimensional nucleation, but unorientated dispersion type requires three-dimensional nucleation[57]. Figure 20 shows the most typical deposit morphologies, unless the twinning intermediate type Z.

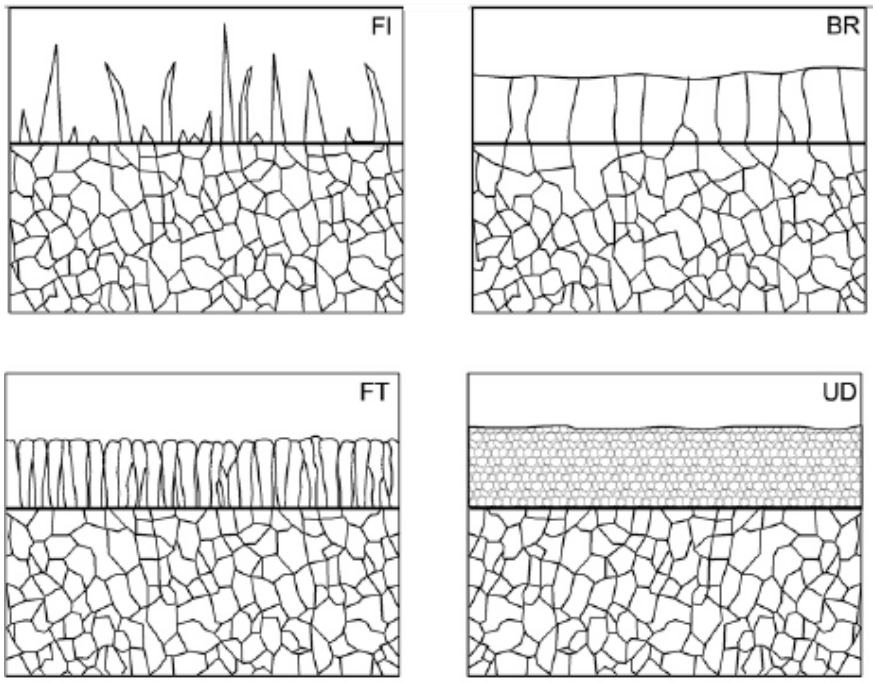

Figure 20. Most typical deposit morphologies[67].

The FI-type crystals occur usually at low inhibition. Increasing current density turns deposited whiskers to prismatic crystals, leading to dendrites and finally to powder deposits. The BR-type structure occur at moderate inhibition levels and the current densities. The deposition follows the base material and has sufficient time for lateral growth and when the deposit is sufficient thick, the surface roughness of BR results in FI-type deposition. FT-type is noticed with increasing amounts of inhibitors or high current densities. The UD-type is noticed with the strongest inhibition and if the current density is too high, the deposit will change to a powder form.

The morphology of deposition can be modified by using inhibitors. The nucleation increases and the grain size decreases when the inhibitor is added to the electrolyte or the ratio of current density and metal ion concentration is increased. Inhibitors are usually organic substances that slow down the deposition reaction. Adding a strong inhibitor prevents crystal growth and therefore increases the nucleation of crystals. When a weak organic inhibitor is added, only two-dimensional nucleation and growth of nuclei occurs. The crystal growth is slowed, when the inhibitor concentration increases. Edges of the crystal are rounded if there is high concentration of weak inhibitor or the inhibitor is strong. When the electrolyte concentration of the inhibitor is added, the deposit structure is changed: BR becomes at the first in the Z, and then the FT and finally in the UD.[59] Figure 21 shows different types of polycrystalline electrodeposition and inhibition intensity.

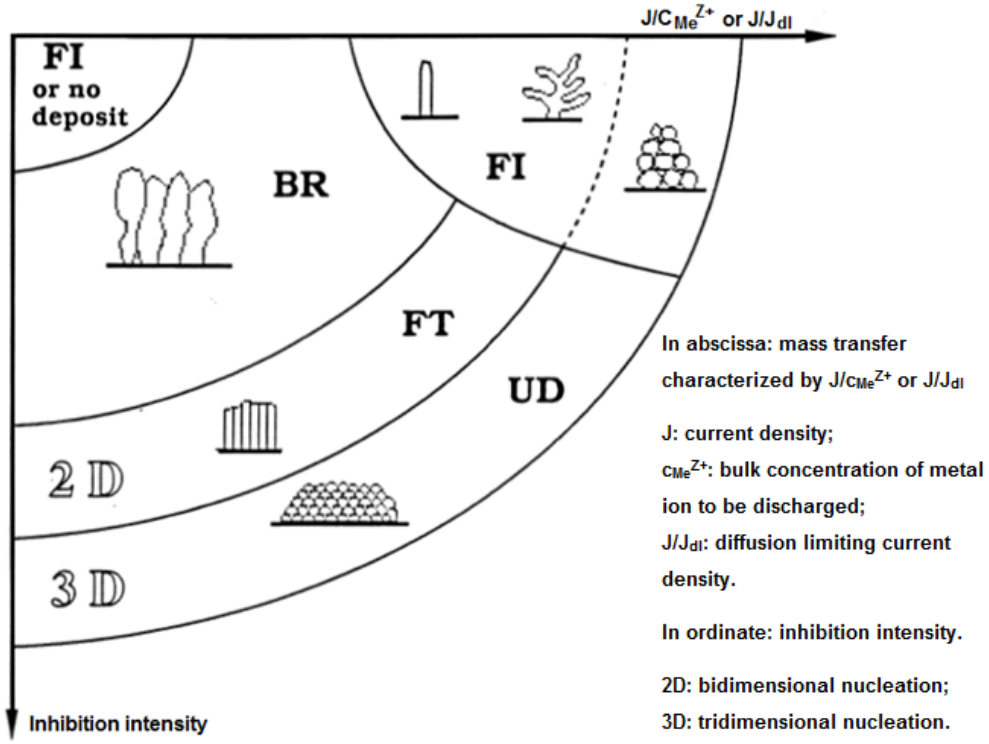

Figure 21. Different types of polycrystalline electrodeposition and inhibition intensity, modified after[68].

3.5 Polarization

Electrochemical phenomena are based on the reactions at the surface of materials, controlling the thermodynamic unit, the Gibbs free energy change ΔG [J/mol]. Gibbs free energy change can be used to assess the probability of a reaction. The higher the change in free energy is with the reaction (i.e. how negative the change is), the more likely the reaction takes place. The kinetics determine the rate of the reaction and the electrochemical reaction rate is described the magnitude of the electric current. Usually the chemical reactions occur in several subsequent steps and the reaction rate of the electrochemical reaction can be for example controlled by charge transfer, mass transfer or electrical resistance of the electrolyte.[66]

When the electrode is polarized, potential is not determined with the Gibbs energy change or Nernst equation. The electrode is not at equilibrium. The reactions are so fast in ideally polarized electrode that its potential does not change when the current passes though the electrode. Perfectly polarized electrode maintains the potential value, which is adjusted with external power supply. When the metal electrode is immersed in metal-ion containing solution, there is a dynamic equilibrium between the electrode and the solution. The electrode is positioned at reversible equilibrium potential E^o, of which value depends on the thermodynamics of the reactants and electrode can diverge in either direction caused by external disturbance. Usually, if the potential equilibrium of the electrode is high, the reaction proceeds to direction of the cathodic reaction and if the potential equilibrium with electrode is low, the reaction proceeds to the direction of anodic reaction.[58] The deviation of the electrode potential referred to reversible equilibrium value is called overpotential i.e. overvoltage η. (Formula 10).

$$\eta = E - E^o \tag{10}$$

where E^o is a thermodynamic equilibrium potential of electrode, E is potential of the polarized electrode and η is the overpotential. Overpotential has positive values for anodes ($E > E^o$) and negative values for cathodes ($E < E^o$).[59]

The net current can pass through only in polarized electrodes. The electron transfer can occur only if the reactant material can arrive at phase boundary of electrolyte and solid electrode and if the reaction products can be removed. The transfer of reactants forms a part of the overall reaction and in the case of deposition on the electrode, may the formation of crystal lattice unite to overall reaction. The overall reaction can also be associated with reactions such as adsorption processes and reactions in the solution phase (e.g. dissociation, association and acid-base reactions). The overall reaction mechanism

can hold in multiple steps, where the slowest step determines the rate of overall reaction.[59] Depending on which is the slowest step, the overpotential (polarization form) can be divided into five format: The activation potential η_a, the diffusion overpotential η_d, the reaction overpotential η_r, the crystallization overpotential η_k and the resistance overpotential η_Ω. The most important forms of overpotential are the activation potential, diffusion overpotential and especially in electrolysis process the resistance overpotential. Diffusion overpotential means mass from bulk solution to the electrode surface and vice versa.[69] The resistance overpotential is not a kinetic factor, and it caused by a specific resistance between the electrodes and the electrolyte.

The electrode reaction includes mass transport, adsorption/desorption and charge transfer steps. In the charge transfer step, the charge transfers between solid phase's electron and solution phase's ion over the boundary surface. A graph between the electrode overpotential and current density is polarization diagram that can be used to estimate the reaction rate with different potentials.[59] The higher the current density, the higher the reaction rate[58].

The exchange current density i_0 describes reaction rate in a dynamic equilibrium. The exchange current density is the current per unit area used in the reaction (Formula 11).[59]

$$i_0 = l_a/A = -l_c/A \tag{11}$$

where l_a is the anodic current and l_c cathodic current.

The system, which has a high exchange current density, is polarized slowly and the potential does not change a lot, when high current is driven through. The system, which has a low exchange current density, is polarized easily and the potential changes significantly, when current is driven through.[57] When the exchange current density approaches zero, the reaction rate at surface of the electrode approaches zero. This may be caused by two reasons: the reactions don't have sufficient high driving force (change of Gibbs energy and reaction rate constant approach to zero) or concentration of one of the reactant approaches zero. When the exchange current density is $i_0 \approx 1$ mA/cm^2, the electrode is polarized slowly, and when $i_0 \approx 10^{-3}$ mA/cm^2 it corresponds to fairly quickly polarizing electrode. When the exchange current density is $i_0 \approx 10^{-6}$ mA/cm^2 the electrode is polarized easily. The exchange current density depends on the reactants and their concentrations. When the source material or product is solid, the activity is high and i_0 depends only of the concentration of the component in solution. The exchange current density between metals and metal-ions vary between 10 - 10^{-15} mA/cm^2 depending on metal and the solution.[59]

If the potential of the electrode is changed to the negative direction, the strength of cathodic partial reaction increases compared to the anodic reaction. Then a cathodic net reaction occurs at the surface of electrode. A deviation to the positive direction induces the anodic net reaction, which can be detected as a positive current. Butler-Volmer equation describes the connection between overpotential and current density. According to this equation the current density of anodic or cathodic partial reactions depends exponentially of the overpotential, (Formula 12).[59]

$$i = i^+ + i^- = i_0 \cdot \left[\exp\left[\frac{\alpha \cdot z \cdot F}{R \cdot T} \cdot \eta \right] - \exp\left[-\frac{(1-\alpha) \cdot z \cdot F}{R \cdot T} \cdot \eta \right] \right] \quad (12)$$

where i_0 is exchange current density, η is overpotential and α is charge transfer factor. The charge transfer factor value is between 0 - 1. When the charge transfer factor is over 0.5, the anodic partial reaction is strengthened faster than cathodic reaction increasing the overpotential. When the charge transfer factor is less than 0.5, cathodic partial reaction is strengthened faster. The anodic and cathodic partial reactions are therefore not usually identical and the polarization curves have different shapes. Butler-Volmer equation is used when only the charge transfer step is studied.[59]

The polarization phenomena are summating, and the overall polarization of electrode is the sum of all slowing factors of overall potential reaction at a particular current density. The overall polarization is usually calculated by the sum of the individual polarization phenomena, which are functions of the current and current density, such as for example the in Formulas (13), (14) and (15).[59]

$$\eta_a = a + b \cdot \log(i) \quad (13)$$

$$\eta_c = \frac{RT}{zF} \cdot \ln\left(1 - \frac{i}{i_L}\right) \quad (14)$$

$$\eta_\Omega = I \cdot R_\Omega \quad (15)$$

On a logarithmic current density scale, the activation polarization occurs as a straight line in Butler-Volmer equation in the whole current density area. The mass transport- and ohmic polarization are hardly affected in low current density area, but with high current densities they have a strong effect. All other factors affecting the overall polarization are harmful because they distort the graph of activation polarization. The effect of mass transfer phenomena must be removed or it must be compensated, e.g. with rotating electrode. The solution resistance is reduced to minimum so that its disturbing effect can be

eliminated. Different polarizations can be recognized for example as follows: The activation polarization η_a describes the charge transfer. η_a increases significantly when polarization current is increased and decreases when current is reduced. The size of activation polarization depends on the physical and chemical structure of electrode material. The diffusion polarization η_d increases and decreases slowly, when the current is turned on or off. The change of η_d depends on the diffusion coefficient of substance. The diffusion polarization is the only form of overpotentials, which can affected with stirring and it does not affect the nature of the electrode surface. The ohmic polarization η_R appears or disappears when the polarized circuit is connected or disconnected.[59]

Hydrogen evolution may start, because the deposition requires the polarization in the cathodic direction. Strong hydrogen formation may prevent the deposition of metal and destroy the quality of the coating. Hydrogen formation depends on used current density and hydrogen over voltage of metal. Hydrogen over voltage depends on the exchange current of hydrogen evolution at the surface of metal. The lower the exchange current is, the higher hydrogen formation becomes and this decreases hydrogen formation. In coating purposes this is a desirable situation. All side reactions affect to the quality of coating. The hydrogen evolution produces hydrogen bubbles on the electrode surface, and when the bubbles attach to the surface, the coating cannot deposit under the bubble.[59]

On a resistive electrode such as carbon nanotube material the polarization and local reaction rate is highest near the current feed point and decreases with distance along the substrate. The consequence is that the charge transfer overpotential decreases and the resistance of the wire consume the applied potential as a function of distance from the current feed point leads to non-uniform charge transfer overpotential along the surface. This effect is known as the terminal effect.[70] Also the current density is highest near the current feed point in the beginning of deposition and causes a higher local deposit thickness. The depositing metal provides more conductivity with time and the conductance of the cathode improves. After this, a more uniform current distribution is achieved and the deposit covers the substrate surface leading to a uniform current distribution for the system.[71]

3.6 Current distribution

The thickness distribution of electrodeposits depend on the current distribution covering the cathode determining the local current density at the surface[57]. Composition, growth rate, microstructure and the properties of the deposited metal are depending on the current distribution and potential at the electrode. The local current density is varying on the

electrode surface causing differing deposit morphology. Different surface points are operating at different parts of the polarization curve.[72] The current distribution is determined by many factors e.g. the electrode surface polarization, the mass transfer in the electrolyte and the geometrical characteristics of the electrodes and the cell[57]. The current density itself can't provide information how even the deposition will be. There are several affecting factors that have effect on the current distribution e.g. the system geometry, conductivity of electrodes and electrolyte, the diffusion and activation overpotential and the hydrodynamic factors in the system. In microprofile there are three types of current distribution; primary, secondary and tertiary current distribution.[73] All the three are involved in different degrees[57].

The primary current distribution depends mainly on current and conductivity of the electrolyte, but it is also affected by the distance between the anode and cathode (ohmic resistance), shape of the cathode and the placement of anode around the cathode. The reaction overpotential (activation overpotential) and the concentration overpotential (diffusion overpotential) are ignored.[57][59] On rough surface, the current density is higher at the top of the peaks and therefore the rate of polarization is higher due to primary current distribution. Smooth primary current distribution is achieved in two different geometries: parallel similar size plates or with nested cylinders. The current flows in the electrolyte through the shortest route and therefore more metal is deposited on a point closer the anode compared to a further point.[57][59]

The secondary current distribution depends on the resistance of the electrolyte, the activation overpotential and the mass transfer polarization phenomenon. It flattens the primary current distributions on the surface of cathode and is always more uniform compared to the primary current distribution.[57][59][73] When the current density increases, the activation polarization on the peaks increase. The growth of the polarization causes resistance in the current flow in the peaks of the cathode forcing the current to access the recesses in the surface. If the activation polarization is slowing the reaction more than the solution resistance, the mass transfers to the cathode surface bottoms. Increases the secondary current distribution leads the metal into the recesses on the profile. Organic additives modify the growth of the deposits and increase the polarization resistance and the effect of secondary current distribution.[57][59]

The tertiary current distribution depends on the ion transportation between the electrode and solution through the diffusion layer and the mass transfer rate. It also flattens the secondary current distribution. It begins to affect when the deposition rate is high enough,

causing variations in the concentration gradient on the surface. The surface concentration depends on the diffusion coefficient and the thickness of the diffusion layer.[57][59] The effect of the concentration polarization is defined by the ratio of surface concentration to bulk electrolyte concentration. The surface concentration is affected by a local mass transfer coefficient. The effect of the tertiary current distribution is dependent on how large is the irregulaties of the surface compared to thickness of the diffusion layer.[59][73] The irregularities on a surface can be divided into a macro- and micro profile. The deposit surface on a macro profile is rough, when their characteristic length is higher than the diffusion layer thickness. The tertiary current distribution will follow the surface profile. If the characteristic length is smaller than the diffusion layer thickness, the metal will deposit more the peaks of the micro profile because the diffusion length from the electrolyte to the peak is smaller and the tertiary current distribution will work against the levelling effect of secondary current distribution.[73]

Uneven current distributions are caused by diffusion and ohmic resistance and therefore, the current density is higher at peaks compared to recesses, if the process is mass transport controlled. To achieve a leveled surface, the process is required to change to activation control, thus the result is either a uniform current density (levels the surface after sufficient time) or a nonuniform current density (by leveling agents, which increase the current in the pores).[58] The higher the current density is, the faster deposit is grown on the surface of the sample. On the other hand, the current efficiency decreases with increasing current density, which slows down the deposition. The current density does not indicate how the coating is distributed on the profiled surface meaning that the current efficiency of the changes is also unknown. The electric field is stronger in points where the corners and tips of electrodes are sharper. At the peaks the current density would be infinitely large, if other factors than the geometry of object and the conductivity of the solution would not affect the deposition. The metal concentration is high on the peaks, the diffusion layer is thin and activation polarization is controlled by deposition. In the recessess, the metal concentration is low, the diffusion layer is thick and mass transfer polarization is controlled by deposition.[59]

Deposition of the coating can be controlled by suitable anode system, because if the electrode system is poorly designed, primary current distribution is uneven. In this case, the coating will deposit unevenly on the sample e.g. thicker coating agglomerate in the corners of the sample and near the anode areas because local current density is large. At the same time only thin layer is deposited in pits and recessions. Uneven deposition can also cause tensions which distort the coating sample or the shape and dimensional errors. The coating deposits uniformly throughout the sample when the deposition is controlled by an auxiliary anode or a shape anode. The auxiliary anode is an additional small anode, which is placed e.g. inside the recess. Shape anode is a special anode, which follow the shape of the sample as closely as possible. The auxiliary anode and shape anode affect the primary current density because they decrease the distance between the electrodes in flat surface or under the recess compared to the ridge and under the corner. Figure 22 shows uneven deposition and different auxiliary anodes.[59]

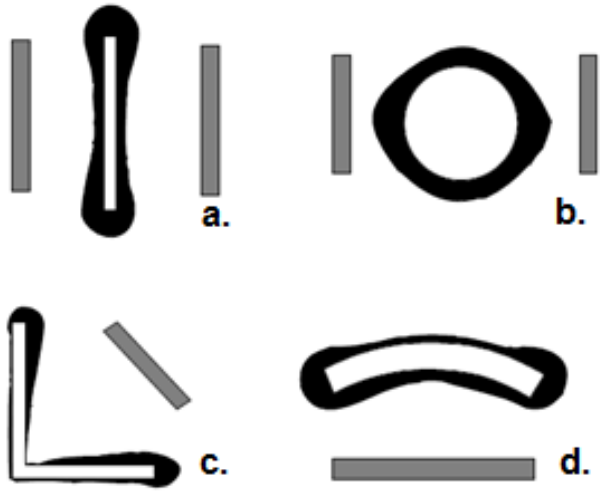

Figure 22. Uneven primary current distribution causes uneven deposition. a) Thicker coating agglomerate in the ends of the sample compared to the center, b) a circular piece doesn't plate round shape, c) an angled piece is not deposited with desired thickness, d) the other side of the piece has a thicker coating, modified after[59].

Different baths modify the surface profile in electrodeposition. Covering power refers to the extent that plating bath is able to cover at the sample surface[58]. It also describes the limit of current density suffice to start the deposition process and how much the surface is plated with a metal at the beginning of deposition. It could be estimated by searching the lowest current density area, where coating exists. The lower the current density for deposition to begin, the better covering power is achieved. Other factors affecting the covering power are the substrate surface, the composition of electrolyte, temperature and viscosity.[58] The covering power depends on the electrodeposited metal and the activation polarization of the base metal. It describes e.g. how the coating is electrodeposited at a small dimension recess and where the local current density is low. Covering

power affect only the beginning of the deposition process. The covering power improves when the startup current density required is increased i.e. activation polarization is high. In uneven surfaces the spread of the coating is adjusted with activation polarization.[59]

Throwing power describes the ability to form an even coating on a surface of a complex component by the depositing bath. All of the factors that increase the polarization, improve the throwing power. Usually this is achieved by reducing the metal concentration, increasing the current density and reducing the stirring. Impact of the elements depends on the used electrolyte: in acid baths, the temperature and stirring weren't significantly affected because metal-ion concentrations are high. The cathode film will be thin, when the metal ion concentration is high. The throwing power is high in baths, where the metal concentration is low. When the cathode film is thick, the concentration polarization increases strongly because of the current density is increased. The polarization of sample depends mainly from the activation polarization. The throwing power is low in a bath, where concentration polarization high. The coating can grow faster in concentrated baths because high concentration causes higher limiting current density and used current density can be higher in deposition. Usually dilute baths are used in producing even surfaces and concentrated baths in fast growing coating.[59]

The throwing power can be divided to macro- and micro throwing powers. The macro throwing power is related to evening larger grooves and micro throwing power to smaller surface imperfections.[58] Macro throwing power describes the relationship of thickness between the thinnest and thickest coating. Micro throwing power describes e.g. how the coating is divided over deviations when the primary current distribution on the surface is even.[59] The thickness of the diffusion layer in macro profile is constant. Macro throwing power is poor in acid electrolytes, where the deposited metal ions are hydrated. The cathode film is thin and the activation and concentration polarizations are in the same magnitude. The macro throwing power is good with electrolytes, where the concentration of deposited metal complex is low. The cathode film is thick and concentration polarization becomes large easily when current density increases. The effective current density describes how the used current density is divided in the cathode. The peaks in the surface are polarized strongly because of primary current. Secondary current transfers the metal-ions to the bottoms of pits.[59] Macro- and micro throwing powers are related to each other inversely; the factors which increase the concentration polarization improve the macro throwing power, but reduce the micro throwing power[58][59]. The micro throwing power can be improved by increasing the concentration of metal ions, temperature or stirring[59].

Distribution of metals over the micro-profile is divided to three categories depending of coating division. Coating can uniformly be distributed to peaks and recessions (good micro throwing power ability), only to recessions (good leveling power ability) or only to the peaks (poor micro throwing power ability). In the last case the current density increases and causes the mass transfer polarization become higher than the activation polarization. The leveling power is special case of micro throwing power, which describes the ability of the bath to deposit efficiently the coating on the recessions of the micro-profile and level it out. Leveling power describes the ability of depositions to level out the micro profile. A bath which has good leveling power deposits coating effectively to the recessed microstructure.[59] The leveling power can be improved by reducing the limiting current density, increasing the concentration of metal ions, increasing temperature or increasing stirring. In addition, it can be influenced by additives such as brighteners, suppressors, accelerators and levelers. The brighteners are adsorbed onto the protrusions of the micro-profile. This contributes the deposition making it available to cover the pores. The suppressors are inhibiting the copper deposition and enhance deposition properties. Accelerators are affecting the suppressors and make it possible to deposit the features. The levelers prevent redundant plating keeping the surface uniform.[58]

When the sample used in electrodeposition is a resistive substrate, the potential drop on the surface causes uneven current density distribution. This is known as terminal effect. Armini et al. (2010) researched plating onto silicon wafer and found, that terminal effect leads to higher deposition rate at the edge of the wafer than in the center. In electrodeposition it is important that resistive substrate receives the same current density in each part of the sample because filling of the smallest features is completed in the first few seconds. The same current density can be achieved with low current, configuration of segmented anode or low conductivity electrolyte. In addition to low acidity electrolyte, a porous resistive element between the cathode and anode, position of sample and the sample distance from the anode can promote a high solution resistance. When the effect of the increased substrate resistance on the potential drop is counteracted with promoting a high solution resistance, the overpotential becomes same across the sample. However, these procedures are applicable only in case where a sufficient plating overpotential is over the whole surface of sample.[74] Potential drop along the cathode surface is caused by the resistance of thin conducting substrate and the current is higher near the current collector corner. Figure 23 shows the current flow through the cell.[71]

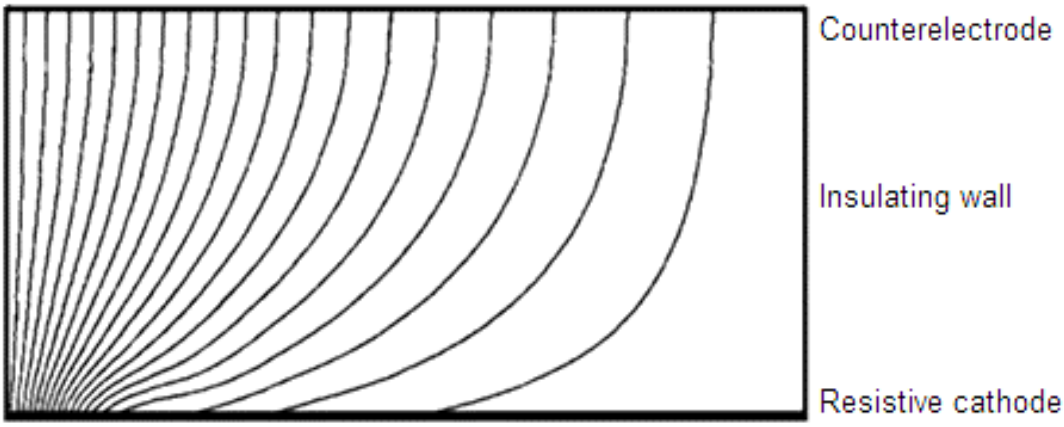

Figure 23. Current flow through the electrolyte phase during deposition onto a resistive cathode, modified after[71].

Alkire and Varjian (1974) showed that wire resistance, electrolyte resistance and charge transfer reaction resistance act to consume the applied potential. The importance of these effects is indicated by two dimensionless parameters (Formula 16 and Formula 17). The Formula (16) is proportional to the exchange current density divided by the metal conductivity and Formula (17) contains information about the electrolytic solution.[70]

$$\varepsilon = \frac{2nFL^2 i_0}{\sigma r_i RT} \tag{16}$$

$$\psi = \frac{r_{i^2\sigma}}{L^{2k}} \tag{17}$$

where ε is dimensionless reaction velocity parameter, n is the number of electrons in electrode reaction, F is Faraday's constant, L is length of wire electrode [cm], i_0 is exchange current density [A/cm^2], σ is electrode conductivity, [(ohm-cm)$^{-1}$], r_i is radius of wire electrode [cm], R is gas constant, T is temperature [°K] and κ is electrolyte conductivity [(ohm-cm)$^{-1}$].[70]

A large value if the Formula (17) corresponds to a reversible reaction on an electrode of low conductivity. The potential of this system is consumed primarily by the electrode resistance and not by charge transfer overpotential. The electrochemical reaction occurs primarily near the electrical contact end of the wire. The large values of ε and the ohmic resistance of the wire cause an uneven current distribution.

High solution conductance or low electrode conductance, i.e. ψ has a small value, the used potential is consumed more by ohmic losses in the phase of electrode than by ohmic losses in the phase of electrolytic solution. Formula (18) and Formula (19) define the geometric configuration of the cell.[70]

$$p_0 = \frac{r_o}{r_1} \tag{18}$$

$$\gamma = \frac{r_1}{L} \tag{19}$$

where p_0 is dimensionless geometric parameter, $r_o$is radius of outer cylinder [cm], r_i is radius of wire electrode [cm], γ is dimensionless geometric parameter and L is length of wire electrode [cm].[70]

Figure 24 shows how the three overpotentials (ohmic solution overpotential η_S, activation overpotential η_A and ohmic wire overpotential η_W) vary with along the wire electrode distances. The sum of the overpotentials is always a constant. If distance along the sample ξ = 0, the used potential of the electrical contact at the end of the electrode is distributed between the charge transfer overpotential and the ohmic loss in the electrolyte. The metals ohmic resistance acts by consuming an increased proportion of the applied potential when moving further down the wire. In this case the charge transfer overpotential decreases with distance along the wire.[70]

In Figure 24 the variation of charge transfer overpotential along the wire leads to uneven current distribution. The reaction rate is highest at the contact end of the wire and it decreases with distance along the wire. If the value of ψ is low (and the charge transfer and wire resistance affect), the resistance of the electrolyte is low. If the value of ξ is high, the ohmic loss in the metal is high, the current distribution is uneven and if the value of ξ is low, the charge transfer overpotential is dominant and the current distribution is uniform. Figure 25 shows that if ohmic resistance of the solution is increased, because ψ is increased it causes the reaction rate distribution to become flatter. The reaction distribution can be uniform even if the value of ξ is high caused by the resistance of the electrolyte solution.[70]

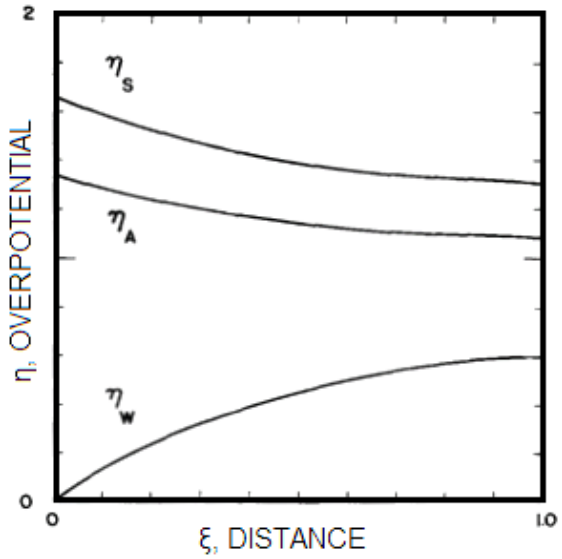

Figure 24. Overpotential distributions along a resistive wire electrode, modified after[70].

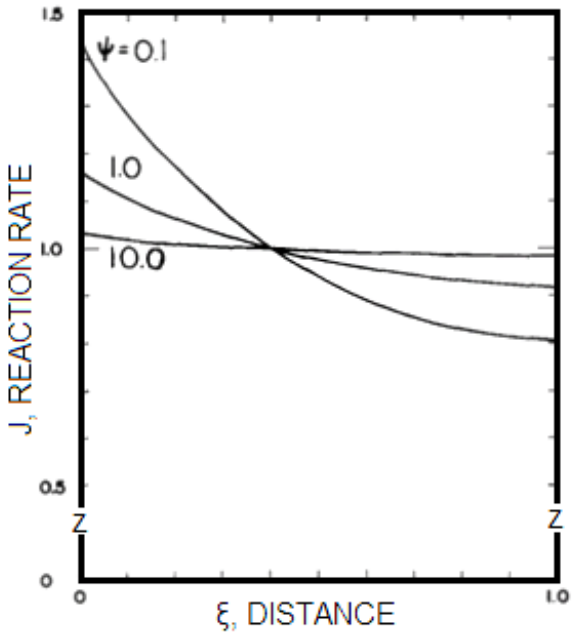

Figure 25. Effect of electrolyte conductivity on current, modified after[70].

3.7 Adhesion

Adhesion is a micro phenomenon where there is an attraction between two different materials. It occurs at randomly independent points on the surface of material. The adhesion causes e.g. the capillary phenomenon and it is significant for electrodeposition between different materials.[75] The adhesion of deposit on a cathode can be measured experimentally in terms of forces, when the force of the adhesion is defined as the maximum force per unit area exerted, when two materials are separated. Another experimentally

measured method is to measure work or energy of adhesion defined as the work done in separating or detaching two materials.[76] Adhesive bonding for plated coating have three different forms: Chemical bonding, undirected homopolar bonding and mechanical bonding. Chemical bonding occurs when the coating surface is cleaned and activated. The incoming metal atoms can crystallize on the substrate. If the bonding breaks by an external force, the fracture occurs in the crystal lattice of the weaker metal. Undirected homopolar bonding occurs when the coating surface is prepared to a lesser degree and the incoming atoms are attached to the surface with this type of bonding. This bond is similar to cohesive bonding between molecules of liquid and there is no interchange of electrons. Undirected homopolar bond is weaker than chemical bond, but still strong enough for the fracture to occur within the weaker metal in the failure. Mechanical bonding occurs when the incoming metal atoms are deposited within the interstices of a roughened surface. It forms an interlocking bond between the deposited metal and the substrate. This kind of bond is obtained e.g. on a sandblasted surface because roughening increases the surface area for bonding. Mechanical bond is the weakest bond of these three forms but it is not supplemented by other bonding types. In forming bonds all of these require the substrate to be properly wetted by the deposition solution. Therefore the surface is in intimate contact with the source of metal atoms.[75]

Proper adhesion is critical in maintaining appearance, device integrity or electrical continuity in all engineering applications when depositing metal on the substrate. The adherence is believed to be dependent on the nucleation of metal, when forming metal clusters of metal atoms acting as adhesion points. Seah et al. (2001) researched that increase in nucleus density promotes adhesion. An increase of deposition voltage or current density is applied, it increases the delamination force with the copper and the surface.[77] Prentice et al. (1998) have researched that the substrate adhesion increases with current density. They used the Hull cell and focused on determining the relationship between applied current density used to electrodeposit copper and the adhesion of the metal to a polyimide substrate. The result showed that higher number of nuclei resulted in a stronger adhesion. Figure 26 shows that the adhesion is highest near the left side of the cathode, because the left side is nearest the counter electrode and the current density is also highest.[78]

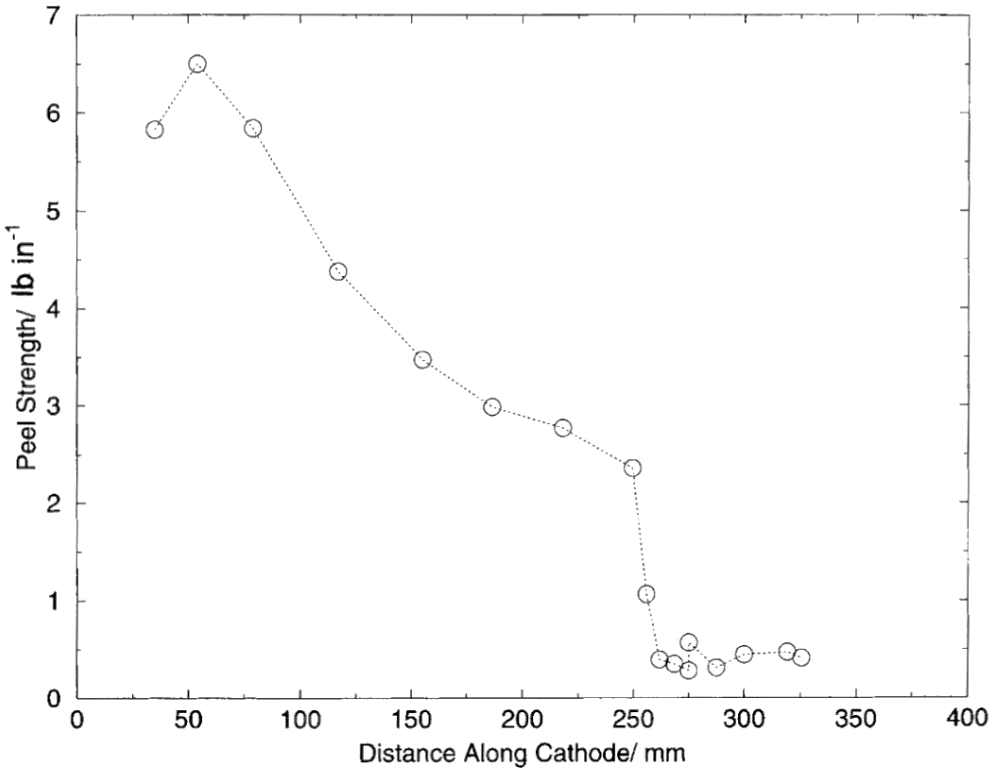

Figure 26. Peel strength against distance along the cathode. The current density is highest at the left side of the cathode[78].

In the high current density area, the adhesion is around 6 lb in^{-1} and in the lowest current density area, the adhesion is less than 1 lb in^{-1}, which is unacceptable in most technical applications. Adhesive failure was observed at the copper/catalytic layer interface at low values on peel strength, less than 1 lb in^{-1}, and at high values of peel strength are observed a cohesive failure with the catalyst layer. Prentice et al. (1998) found that oxygen has strong adhesion on the peeled side of the copper strips on samples. This result refers to that copper oxide and other similar compounds are formed at the interface with good adhesion. A possible cause of the correlation between adhesion and current density is that the additional generated heating caused by increased current promotes further curing of the metal-polymer bond[78]. Baumgartner and Scott (1995) presented that heating samples for 2 h at 200 °C increased adhesion significantly compared to room temperature samples.[79] However, adhesion decreases rapidly at higher temperatures, thus further studies are needed to elucidate the mechanisms that are responsible for the increase in adhesive strength with increasing current density.[78]

Baumgartner (1992) and Scott and Baumgartner (1995) researched that adhesion can be improved with mechanical or chemical surface modification and that moisture at the metal-polymer interface adversely affects adhesion. Modification of surface of the polymeric substrate is usually promoting adhesion.[79][80] Krause and Speckhard (1991) found

that if significant moisture was present at the interface, adhesion could decrease an order of magnitude. It is advantageous to operate at high current densities to maximize the production rate of plated parts, but the effect of local current density on adhesion has not been analyzed quantitatively.[78][81] Rosa et al. (2009) researched copper deposition on titanium. They found that only current density had a significant effect. When the current density was increased, it increased adhesion force. Increases in copper concentration, sulfuric acid concentration and deposit thickness had decreasing effect on adhesion.[82] The other mechanism believed to affect adhesion of electrodeposition is keying action i.e. provided by growth of depositing metal cluster inside grooves, ditches and pits on the surface. The number of nuclei grows with mechanical polishing of cathode because it produces many defects and small scratches on the surface. The size of the defects may affect the adhesion mechanism. Small defects are furthering nucleation and larger defects improve the keying action.[83]

If the plating environment and the used substrate favor epitaxial growth, this may promote good adhesion. In electroless deposition using nonmetallic substrates, the adhesion may occur in crevices on the surface of the substrate that are generally made with etching. In these situations, the keying action is primarily behind the adhesion.[84] As showed in Section 3.4, there are five most typical deposit morphologies for polycrystalline deposit (FI, BR, Z, FT and UD). Fischer noted that adhesion depends on the substrate microstructure to the deposit microstructure. If the microstructure of deposit adapts to the microstructure of the base metal, the adhesion will be good. This means that good adhesion is achieved with the base-oriented reproduction type (BR).[67]

Lahiri et al. (2010) researched the selection of Ti and Ni as diffusion barrier layer and catalyst layer. The main focus in the research was the conductivity of the chosen materials and adhesion of CNTs to the substrate. Ti and Ni seemed to be the best choices for barrier and catalyst materials because deposition of highly conductive metals as diffusion barrier layer and catalyst layer ensured a lower contact barrier. Poor adherence of CNTs to the substrate is affecting field emission under an intense local electric field and that often leading to its fault. Lowering contact resistance and a high sustained emission current results good adhesion strength.[85] Calderón-Colón et al. (2009) investigated the effects of morphological parameters on the field emission properties of macroscopic CNT films. They showed that CNT cathodes with long-term stability under high current and high voltage conditions can be manufactured by optimizing the surface orientation and density of the CNTs and improving the adhesion. Adhesion of the CNTs to the substrate surface also plays a significant role in the emission stability, especially under high voltage.[86]

Wei (2006) researched the adhesion behaviors such as interfacial shear stress and bond breaking at large strains, reinforcements in elastic modulus, and their temperature dependence in a polymeric CNT composite, through molecular dynamics simulation method. When determining the efficiency of CNTs used as nanofibers and the structural stabilities of CNT composites, it is crucial to determine the adhesion behavior and reinforcing properties. While adhesion is usually achieved through covalent bonding, there are non-covalent van der Waals interactions present. They have been verified to have an important role in the interface of molecule structures and reinforcement in the CNT composites.[87]

Moon et al. (2006) presented the significance of adhesion between nanotube emitter and the substrate, to achieve an acceptable operating time of the CNT emitters[88]. Lahiri et al. (2010) showed results that field emission investigations indicating indirectly the good adhesion between the substrate and the CNTs[85]. Yang et al. (2008) researched adhesion between SWCNTs and the Cu matrix with transmission electron microscopy (TEM). The activated defect sites of acid-treated SWCNT surfaces have many functional groups: carbonyl groups, oxygen-hydrogen bonds and C-O bonds. Functional groups promote a lot of the combinations between SWCNTs and Cu, and with the help of ultrasonic vibrations, induce the formation of a wettable SWCNT/Cu interface. Figure 27 show the typical sites of Cu deposition on SWCNTs and that the interface between SWCNTs and Cu matrix is wettable and in good adhesion. Cu is deposited at the end and on the activated outer surface of SWCNTs, which is similar to that found in the depositions of nickel and multi-walled carbon nanotubes (MWCNTs).[89]

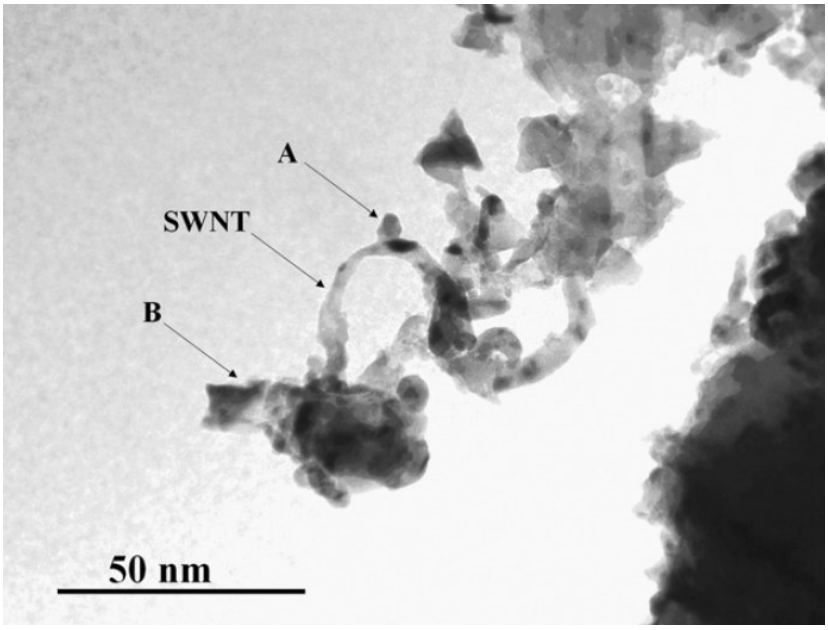

Figure 27. TEM micrograph of Cu/SWCNT showing the two typical sites for copper nucleation: A) at the end, and B) on the outer surface of a SWCNT[89].

4 EXPERIMENTAL

The purpose of the experiments was to research the methods, which can be used to affect the potential distribution and the current distribution. These methods improve the conductivity and electrochemical activity of carbon nanotube substrates. The focus was in the effects of surface properties in CNTs and on the growth of nucleation. Surface properties of CNT substrates were measured and characterized by different methods like electrochemical impedance spectroscopy (EIS) and nucleation was estimated by galvanostatic deposition tests and with scanning electron microscope (SEM) and optical microscopy. The aim of the experiments was to found correlations between surface modification and nucleation. The surface properties of CNT substrates have been modified with heat treatment, Watts nickel bath, acetone, anodization, ethanol (C_2H_5O), boric acid (H_3BO_3), sulfuric acid (H_2SO_4) and nitric acid (HNO_3).

In addition couple of the samples have secondary treatments like copper deposition to form Cu/CNT composite and characterized by 4-wire resistance measurements. In copper deposition, the deposition rates between before and after modification treatments were compared. Part of Cu/CNT composites were modified with heat treatment in nitrogen gas atmosphere.

4.1 Samples

In research different lengths (3 - 7 cm) of fibers and yarns (in average diameter 10, 20, 30 and 200 µm) were used. The samples consist mainly of MWCNT and present some percentages of SWCNT. The CNT samples are produced by dry spinning directly from a CVD reactor in the University of Cambridge and the materials are unfunctionalized and contain unknown amounts of carbonaceous impurities and catalyst metals.

In developing and processing CNT material for example impurities, defects and the weakness of the CNT materials should be considered. Different types of functionalization treatments are needed and because lightweight CNT material will float and break very easily, a rigid sample holders are needed and this limits the methods in sample preparation. The tests were done with two different sample holder materials: the PVC holder and glass-plate. The PVC sample holders are made by gluing a copper wire to the holder with a standard glue and the glass-plate sample holders are made by Foil shielding Tape no. 1183 (resistance 0.005 Ω) manufactured by 3M. In PVC sample holders the contact to CNT sample is made by gluing the upper end of the CNT to the copper wire with conductive Alfa Aesar silver adhesive paste 42469 (sheet resistance <0.025 Ω) and

lower end to the PVC holder with a standard glue. In glass-plate sample holders the contact to the CNT sample is made by gluing the upper end of the CNT to the Foil shielding Tape with conductive Alfa Aesar silver adhesive paste 42469 (sheet resistance <0.025 Ω) and lower end to the glass plate with a standard glue. PVC sample holders were made for sample lengths of 20 - 70 mm and glass-plate sample holders were made for sample lengths of 3 - 30 mm. The two different sample holder setups with glued CNT samples are shown in Figure 28.

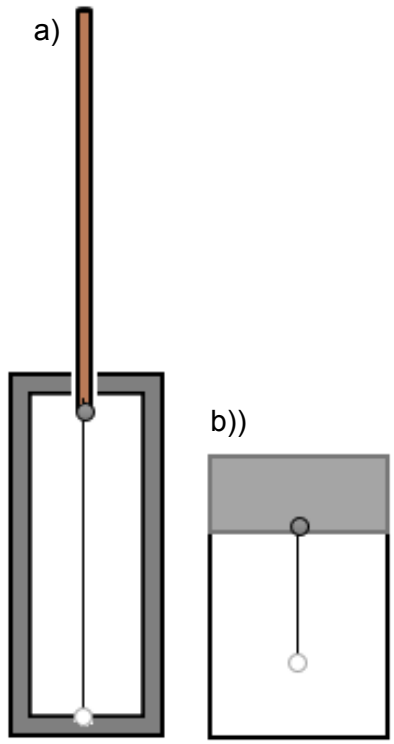

Figure 28. The two different sample holder setups a) PVC and b) glass-plate.

4.2 Test equipment

Electrochemical tests were done using ACM Instruments Gill AC potentiostat with programs AC Impedance, long term LPR sweep, potentiostatic and galvanostatic with Gill AC Sequencer software. The electrochemical tests were done using standard three-electrode arrangement, where the carbon nanotube material is the working electrode (cathode) and a copper on both side of the sample as the anode. The reference electrode was a calomel electrode (KCl, SCE) and was placed as close to the CNT sample as possible using a protective Schott tube with Pt frit. In addition, the reference electrode and sample should be placed in the center of the cell. A sketch of the setup in electrochemical testing is shown in Figure 29 with the reference electrode and the PVC sample holder. The used setup of electrochemical tests is shown in Figure 30.

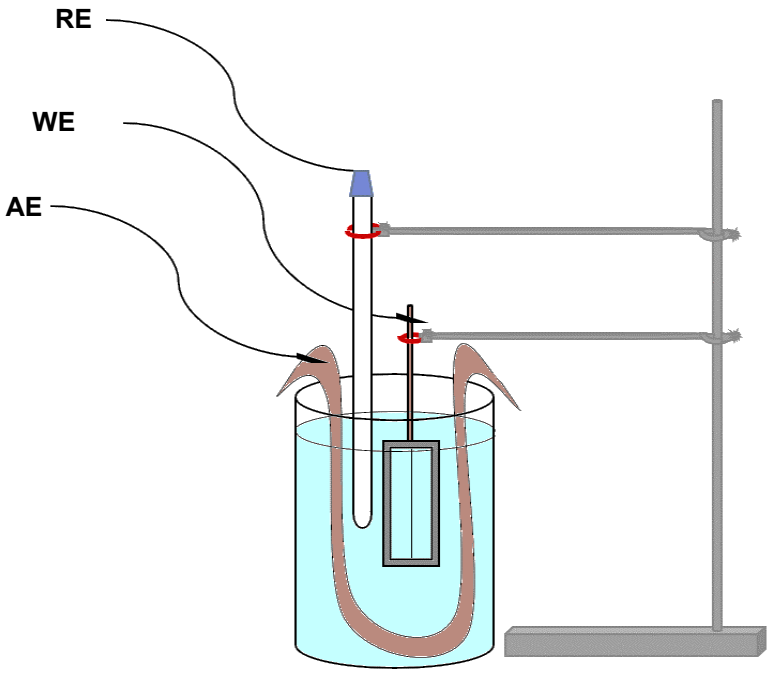

Figure 29. Electrochemical cell, reference electrode and PVC sample holder.

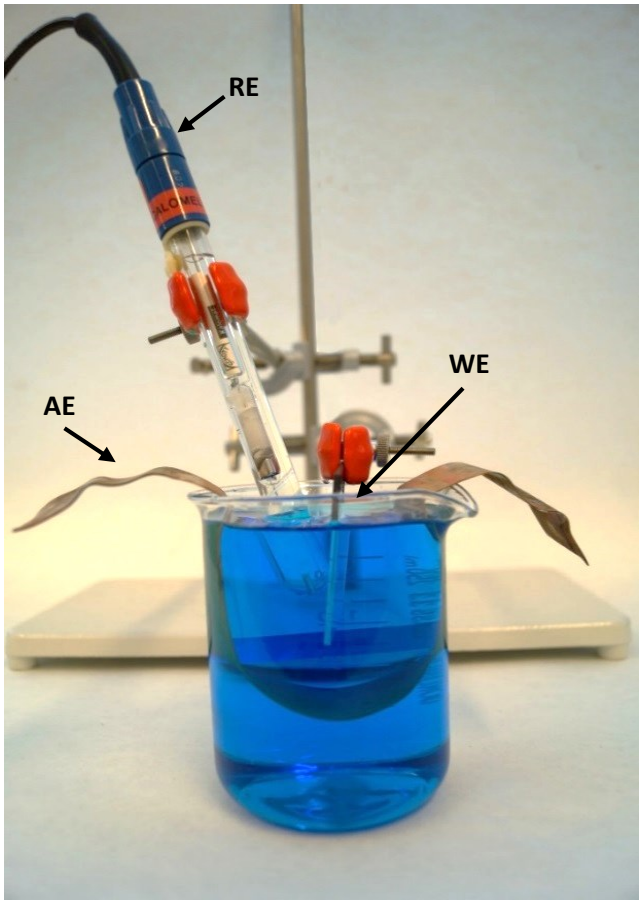

Figure 30. Actual setup of electrochemical cell, reference electrode and glass-plate sample holder.

4.3 The electrolytes

The baths used in research were the compositions shown in Table 5. Bath 1 is a base electrolyte used for electrochemical tests and nucleation tests and it is highly conductive. It contained 150 g/l $CuSO_4 \cdot 5H_2O$, 40.8 ml/l H_2SO_4 (96 - 98 %) and 5.04 mg/l NaCl, where copper sulfate and sulfuric acid are forming the ionized species in solution. The electrolyte bath 1 has a quite high copper concentration and low acid concentration. It is a composition that is used for general purposes when high deposition rates are needed. If the electrolyte has low copper and high acid concentrations such as 50 g/l $CuSO_4 \cdot 5H_2O$ and 240 g/l H_2SO_4, it is preferred to use with high throwing power. Bath 2 is a Watts bath used for nickel deposition and it contained 310 g/l $NiSO_4 \cdot 6H_2O$, 50 g/l $NiCl_2 \cdot 6H_2O$ and 40 g/l H_3BO_3. Watts nickel bath was used to modify surface properties of samples with different immersion times. The electrolytes were made with Pro Analysis grade chemicals and distilled water.

Table 5. Used electrolyte compositions.

Bath	Composition	
Bath 1	$CuSO_4 \cdot 5H_2O$	150 g/l
	H_2SO_4 (96 - 98 %)	40.8 ml/l
	$NaCl$	5.04 mg/l
Bath 2, Watts bath	$NiSO_4 \cdot 6H_2O$	310 g/l
	$NiCl_2 \cdot 6H_2O$	50 g/l
	H_3BO_3	40 g/l

4.4 EIS theory

Electrochemical impedance spectroscopy tests (EIS) are based on a small alternating voltage and alternating current signal disturbing the electrochemical reactions in the surface of electrode. The changes in the impedance of the electrode are obtained through fitting the EIS results. EIS measurements provide insight into the change of corrosion film characteristic and the corrosion process occurring at the interface. EIS tests can usually measure several values of parameters at the same time, such as polarization and the double layer capacitance that indicates the surface activity and electrical conductivity of the sample.[90][91]

The effect of different factors for impedance spectra in electrochemical process and typical aqueous solution can be studied with different frequency ranges:

- More than 10 kHz, solution and corrosion product resistance
- About 1 kHz, the double layer capacitance
- 1 - 100 Hz, charge transfer processes
- F <1 Hz, diffusion- and adsorption processes
- F → 0 Hz, direct current measurement comparable of polarization resistance

For example resistances of electrolytes and charge transfers, double-layer capacitance of electrodes and impedance caused by the mass transfer (Warburg impedance) can be extrapolated from EIS-spectrum.[92]

The analysis of impedance measurement is based on different time constants of electrochemical reactions. Thus their responses appear on different frequency ranges. Potential and current of a stationary state and frequency of alternating voltage describe the impedance. The stationary states are maintained with potentiostat or galvanostat. Changed frequency of alternating voltage signal may disturb it. The higher the frequency of the signal, the faster it can be measured. When the signal frequency decreases, the measurement will slow down, because the measurement of impedance at each frequency requires at least one full cycle (1 Hz requires one second, 10 mHz for a hundred seconds). Usually accurate measurements can't be done during a one cycle, but with one frequency number of cycles can be measured and the impedance can be calculated.[90]

When the frequency is low or high enough that only the resistance components of the resistor affects, the phase angle has the value 0°. The value -90 ° is achieved, when only the capacitive components are affected. The frequency of maximum phase angle decrease when the capacitance of double layer increases. The effect of the double layer capacitance is showed in the Figure 31 as a declining line, which angular coefficient is theoretically -1, but it may become as well low gradient. The higher the capacitance value is, the lower frequency range the effect occurs.[90]

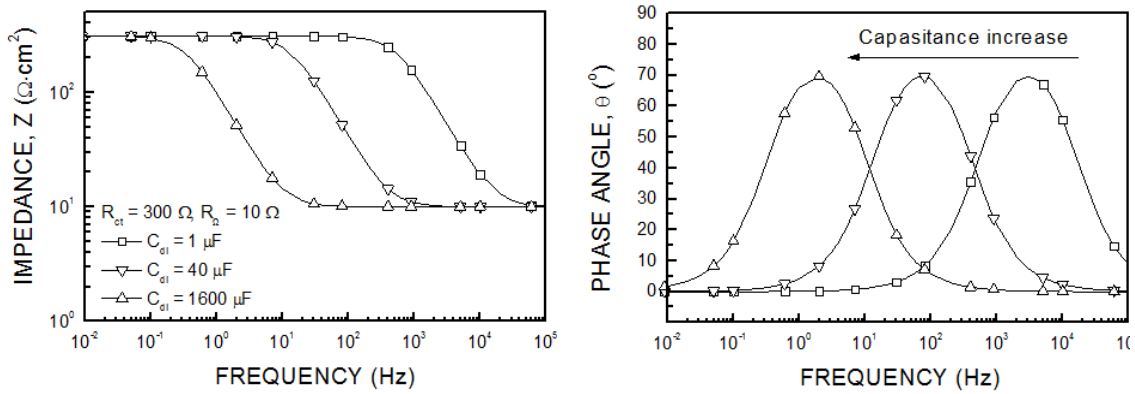

Figure 31. The effect of the double layer capacitance[90].

The simplest equivalent circuit, which describe the surface of electrode, is Randles equivalent circuit. Randels equivalent circuit is taking into account the solutions resistance, charge transfer resistance and electrical double layer capacitance. The solution resistance describes resistance of solution and in some cases also resistance of corrosion products. The parallel connection of the charge transfer resistance and capacitance of the electrical double layer describe the reactive interface.[90]

The higher the resistance value is, the higher is the value of impedance. The higher the value of the capacitance, the lower frequency range its effects appear. When the charge transfer resistance increases, the low frequencies limit (R_{ct}+R_{Ω}) of impedance increases and capacitive area becomes more visible. This displays as higher and wider peaks in the phase angle in the graph. When the ratio of charge transfer resistance and the resistance of the solution are increased, the central part of capacitive area shows more clearly the capacitive phenomena.[90]

At high frequencies, like usually 1 kHz, the capacitance conduct easily and current flows through it. In this case, the part of charge transfers and resistance remains minimal but the part of solution resistance stands. Then the horizontal part of the impedance display the magnitude of the solution resistance. When the signal of frequency decreases, the double layer capacitance conducts easily and impedance increases. In Figure 32, the capacitive area is shown as declining line. If assumed that the mass transfer phenomena doesn't affect the impedance spectrum, at high frequencies (like a few tens kHz) the measured impedance describes the ohmic resistance of the system. It contains an uncompensated solution resistance, equipment contact resistances and layers of non-reacted reaction products. At low frequencies, the capacitance does not conduct, but the flow passes through the charge transfer resistance. Then the horizontal part of the impedance displays as the sum of solution resistance and charge transfer resistance. At low frequencies, when the frequency approaches to zero, the measured impedance describes the sum of all resistances in the system. In the simplest case, the limit of the low frequencies is the sum of the charge transfer and ohmic resistance.[90]

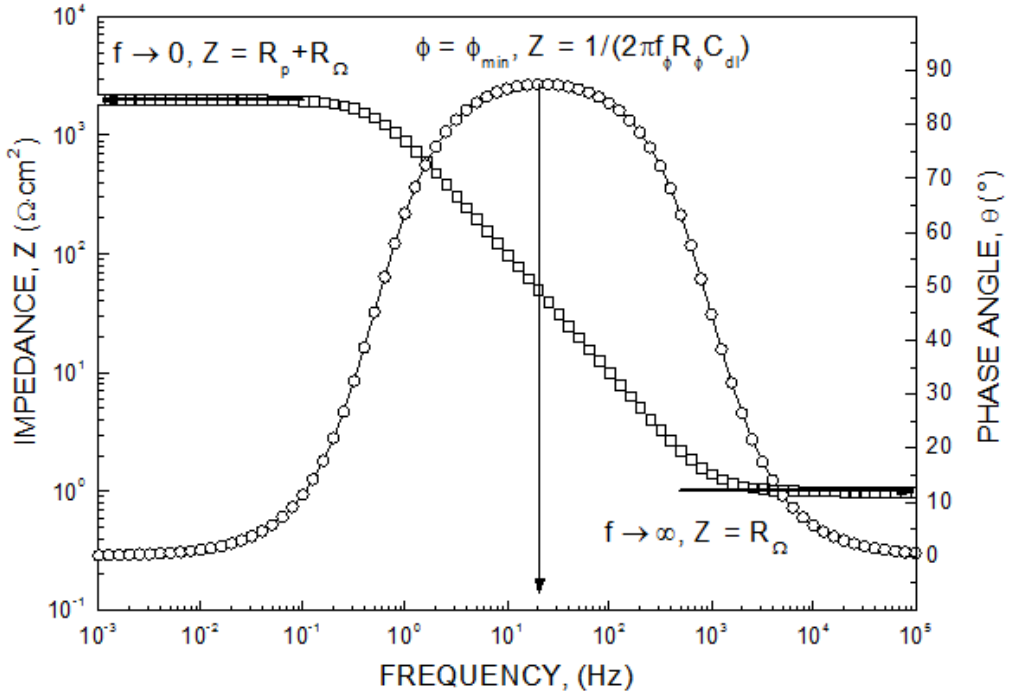

Figure 32. The impedance of Randles-type equivalent circuit[90].

EIS tests

Electrochemical impedance spectroscopy experiments were carried out in various solution conditions: in copper sulfate (bath 1), copper sulfate + C_2H_5O, Watts bath (bath 2) and H_2SO_4. In addition the immersion times and surface treatments varied. The CNT sample acts as cathode and dissolvable or inert type of metal as anode. When the used electrolyte is copper sulfate based (bath 1), the used anode is copper and in other baths the anode is inert. The measurements were made at room temperature and using 60 readings per test. In H_2SO_4 -measurements, the additional DC offset was varying between 0 - 400 mV, but in all other measurements, the additional DC offset was 0 mV. The impedance values are taken with finish frequency 0.01 Hz, start frequency 100000 Hz, amplitude 10 mV/RMS and cell settle time 10 s. An example of the electrochemical impedance spectrum is shown in Figure 33. The impedance is drawn with the black circles and phase angle with white triangles. R_Ω is solution resistance, R_{ct} is a charges transfer resistance, R_p is polarization resistance and C_{dl} is capacitance.

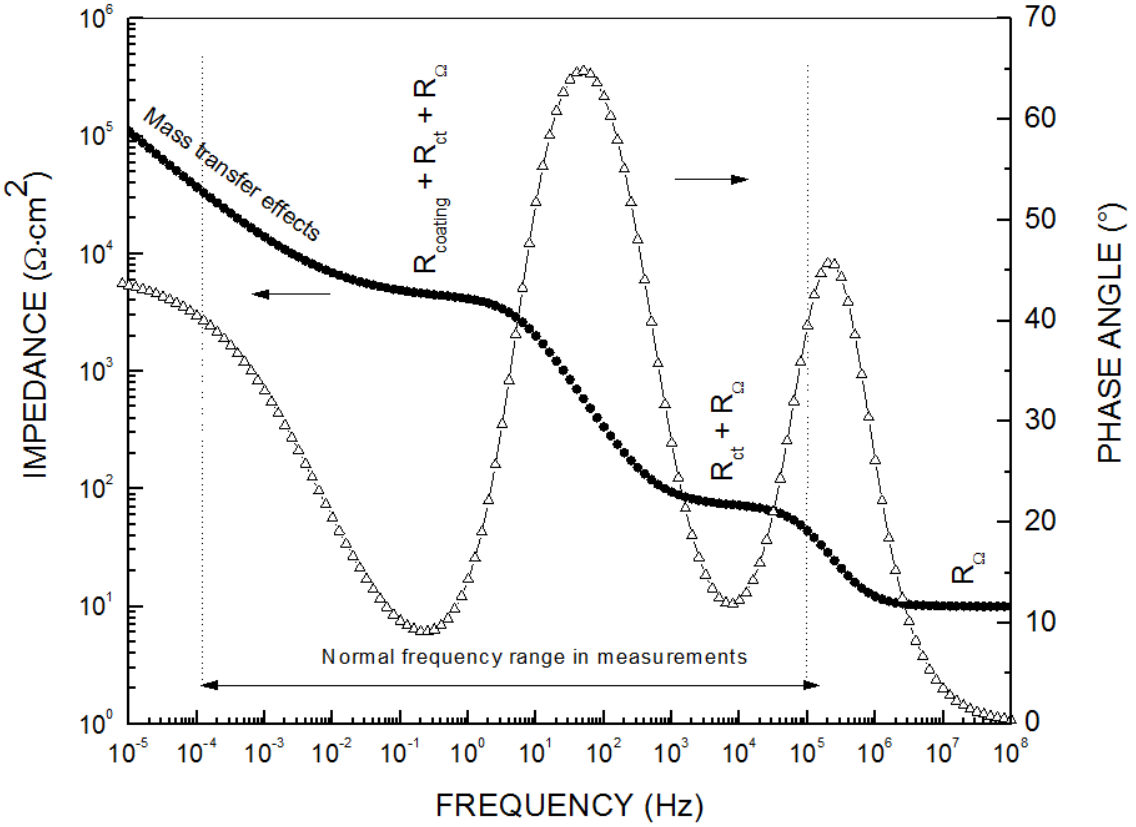

Figure 33. Example of impedance spectrum Bode representation.

Modeling and calculations of EIS results

EIS Bode representation contains not enough information to determine the solution resistance, polarization resistance (R_p) and capacitance (C_{dl}). Therefore EIS results must be modelled for example in Microsoft Excel -program. Solution resistance is determined by calculating the average of the first impedance values in the horizontal region (frequency near 100 000). Polarization resistance is determined by calculating difference between the average of the first impedance values in the horizontal region (frequency near 100 000 Hz) and the last impedance values in the horizontal region (frequency near 0.01 Hz). Capacitance is calculated by determining f and Z from the graph and placing the values into the Formula 20. In addition, the values of polarization resistance and capacitance should be proportional to the surface area of sample. Polarization resistance is multiplied by surface area and capacitance divided by surface area.

$$C_{dl} = 2\pi \cdot f \cdot R_p \cdot Z \qquad (20)$$

where f and Z are determined by drawing a line in the growing area and searching the center point of line. f is a value in the x-axis (frequency Hz) and Z is the value in the y-aisl (impedance Ω·cm^2).

An example of the EIS spectrum in Excel is shown in Figure 34. The impedance before immersion is drawn with blue circles and after immersion with orange triangles.

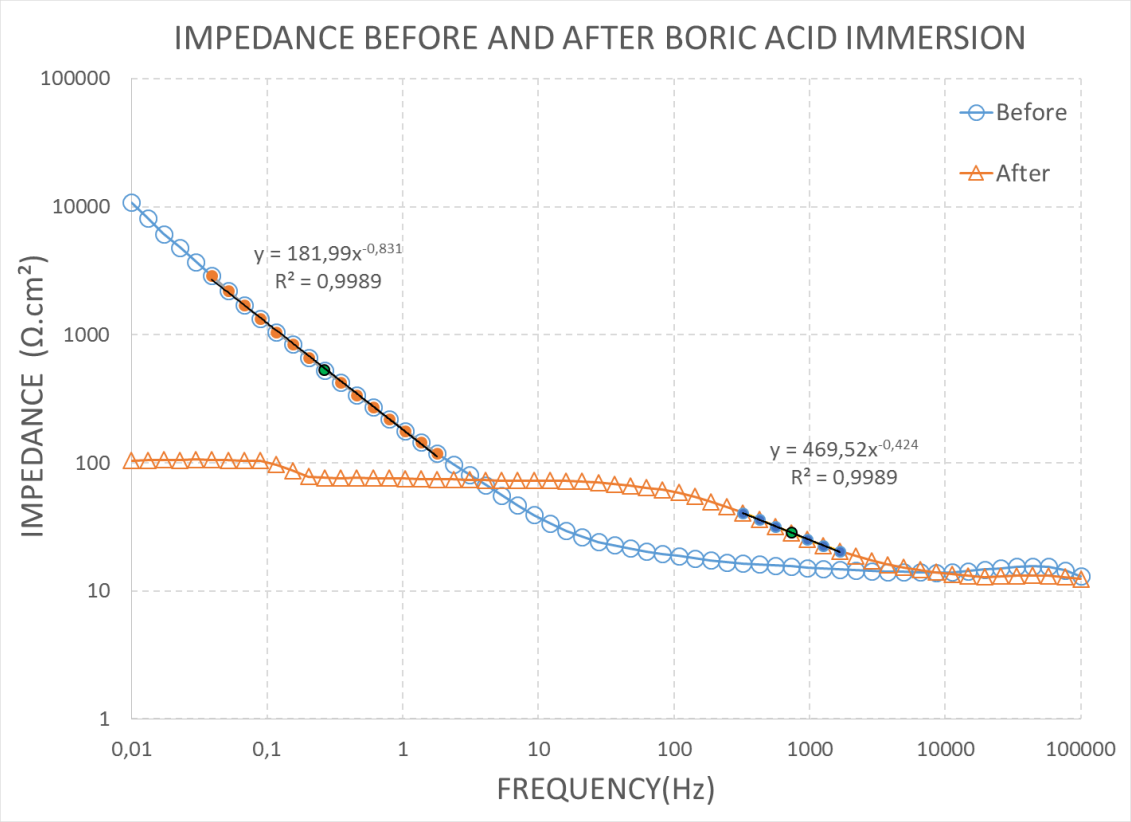

Figure 34. Example of impedance spectrums in Excel.

4.5 Test procedures

The heat treatment tests were carried out in a 300 °C - 400 °C furnace. Treatment times varied between 10 min to 3h. EIS tests for CNT were carried out in copper sulfate bath (bath 1) before and after heat treatment. For Cu/CNT tests, yarn (September 2014), code 26 was electrodeposited with copper and cut into smaller parts (sample codes 26.1, 26.2, 26.3 and 26.4). Samples were treated differently in the furnace and the resistance was measured before and after the heat treatment. A part of Cu/CNT composites were heated with nitrogen gas, when the surface of samples was not oxidized. Oxidation decreases the electrical conductivity. Citric acid was used to remove the oxidation of some of the samples.

The EIS in copper sulfate bath (bath 1) and Watts bath (bath 2) was carried out by measuring EIS at first in copper sulfate bath before treatments, then in Watts bath and finally again in copper sulfate. The sample was rinsed with distilled water between the baths.

In the Watts bath (bath 2), acetone, boric acid (H_3BO_3), sulfuric acid (H_2SO_4) and nitric acid (HNO_3) were used with different immersion times. The samples were immersed completely in the selected solution. Watts bath immersion times varied between 30 min and 72 h, acetone immersion times were 30 min, boric acid (40 g/l) immersion times were 60 min, sulfuric acid (1M) immersion times varied between 30 and 40 min and sulfuric acid + nitric acid immersion times were 15 min. The sulfuric acid + nitric acid solution contained 3 part H_2SO_4 (95 %) and 1 part HNO_3 (65 %). EIS tests were carried out in copper sulfate bath (bath 1) before and after different immersions and the sample was rinsed with distilled water between the solutions.

Ethanol tests were carried out in the base copper sulfate electrolyte (bath 1) with EIS before and after ethanol additions. Ethanol was added into the bath 1. The adding produced 10 % ethanol concentration and after the additions the concentration was 20 %. In addition stirring was used with and without 10 % ethanol addition. Organic ethanol should provide better wetting inside the CNT material and increase the activation in the sample.

In the anodization test, one inert electrode (cathode) was immersed in a 10 wt% H_2SO_4 solution and the CNT sample (anode) was attached to the glass-plate sample holder. Anodization voltage of 2500 mV was used and the anodization time was 49 s (when a sample passes through the solution). EIS tests were carried out in copper sulfate bath (bath 1) before and after anodization, wherein the copper acts as anode and the CNT sample as cathode.

Cell potential tests were carried out in a 1M H_2SO_4 -solution with EIS. The additional DC offset was varying between 0 - 400 mV. A part of tests were made with steps of 50 mV and a part of tests steps of 100 mV. If the sample acts as semiconductor, it can be estimated with differences in the cell potentials in the sample in 1M H_2SO_4.

Galvanostatic series of measurements were carried out with same size fiber samples (A = 0.62 mm^2, l = 20 mm and d = 10 µm). Sample codes G1 and G2 were electrodeposited with -0.1 mA current and 120 s time. Sample codes G3 and G4 were immersed for one hour in Watts bath (bath 2) and then electrodeposited with -0.1 mA current and 120 s time. Sample codes G5 and G6 were immersed only for one hour in Watts bath. After the treatments, the samples were SEM-imaged. In SEM-images secondary electrons (SE) as the back-scattered electrons (BSE) have been used.

Optical microscopy was used to observe the changes of the sample surfaces before and after treatments and electrical depositions. Figure 35 shows a yarn (code yarn1) after depositing (-10 mA, 130 s) and Figure 36 shows a yarn (code yarn1) completely coated

with copper (length of five millimeters). Millimeter paper was used to observe the progress of the deposition.

Figure 35. Optical microscopy image from electrodeposition of sample (code yarn1).

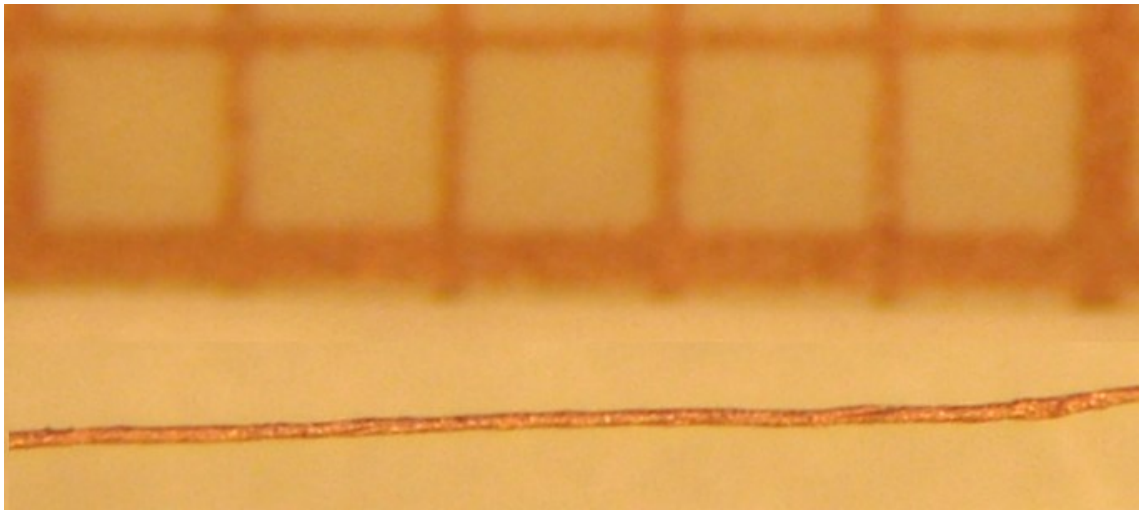

Figure 36. Completely coated sample (code yarn1) and millimeter paper.

Coating rates were carried out with copper depositing values from Pyry-Mikko Hannula's Master thesis and Watts nickel bath (bath 2) immersion results[93]. Coating rates were simulated with current, sample length, depositing time and covering length. On the base of the values were plotted a graph, where X-axis is used current / sample length [mA/cm] and Y-axis is coated length / time [cm/s]. The graph demonstrate that how much treatment affects to, that coated length is as long as possible and used current is as low as possible.

5 RESULTS

5.1 Heat treatment

Table 6. Used samples

Samples (codes)	A (mm^2)	l (mm)	d (µm)	Treatment
Fiber (U2)	0.5	15	10	Before 400 °C, 10 min
Fiber (U2)	0.1	3	10	After 400 °C, 10 min
Fiber (N6)	0.8	25	10	Before 400 °C, 60 min

The EIS before and after furnace (code U2) are shown in Figure 37. The impedance before furnace is drawn with the black circles, the impedance after furnace is drawn with the black triangles, the phase angle before furnace is drawn with the white circles and the phase angles after furnace with the white triangles.

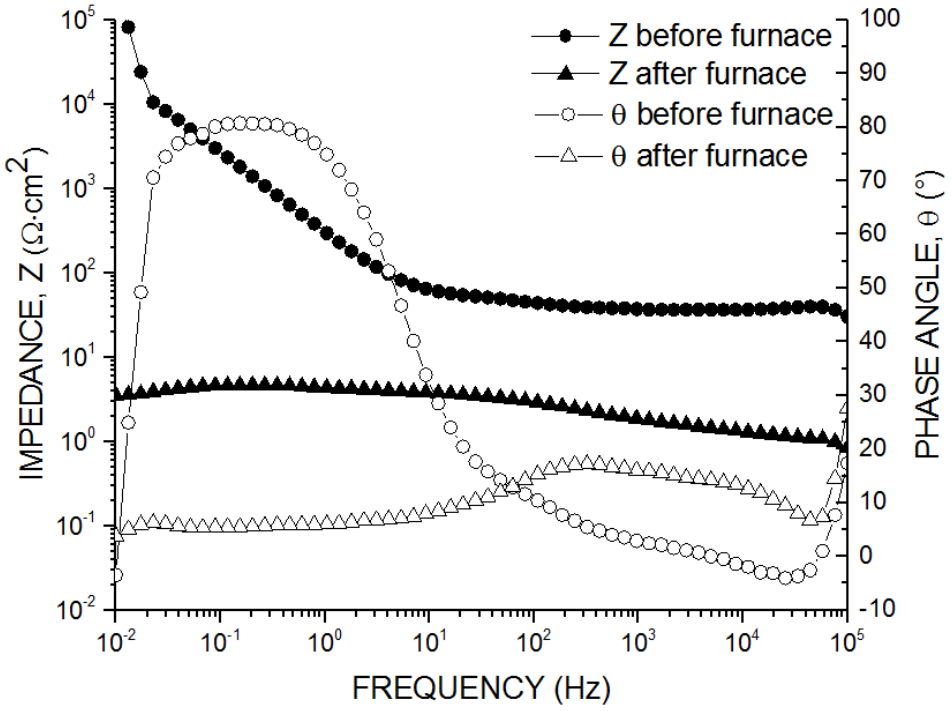

Figure 37. Impedance and phase angle spectrums before and after furnace (code U2).

Table 7. Heat treatment results

Samples (codes)	Polarization resistance (R_p)	Solution resistance (R_Ω)	Capacitance (C_{dl})
Fiber, before furnace (U2)	45200	35	1.2E-08
Fiber, after furnace (U2)	0.4	1.0	3.9E-04
Fiber, after furnace (N6)	15	80	-

From Figure 33 and Table 7 can be seen, that the heat treatment affects strongly to polarization resistance, solution resistance and capacitance of samples (codes U2 and N6). However, heat treatment seems to weaken the structure of the CNT samples, because the samples break after the heating. Heat treatments require more research in optimizing heating times and temperatures before it could be used as the functionalization method for CNT material without weakening the material.

5.2 EIS in bath 1 and bath 2 (Watts bath)

Table 8. Used sample

Samples (codes)	A (mm^2)	l (mm)	d (µm)	Treatment
Fiber (U1)	0.4	13	10	-
Fiber (N7)	0.6	20	10	Immersion time: 3 h 50 min

The impedances in copper sulfate bath (bath 1) and Watts nickel bath (bath 2) (codes U1 and N7) are shown in Figure 38. The impedance in bath 1 before treatment is drawn with the black circles, the impedance in bath 2 is drawn with the black triangles and the impedance in bath 1 after treatment is drawn with the black squares.

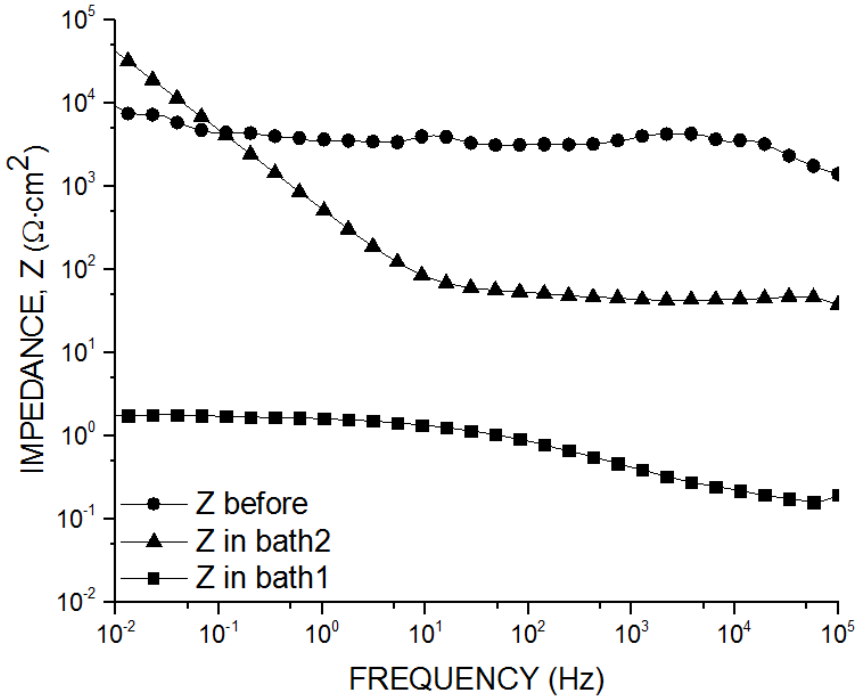

Figure 38. The impedance in copper sulfate bath (bath 1) before treatments, then in Watts bath (bath 2) and finally again in copper sulfate bath (codes U1 and N7).

The phase angles in copper sulfate bath (bath 1) and Watts nickel bath (bath 2) (codes N1 and N7) are shown in Figure 39. The phase angle in bath 1 before treatment is drawn with the white circles, the phase angle in bath 2 is drawn with the white triangles and the phase angle in bath 1 after treatment is drawn with the white squares.

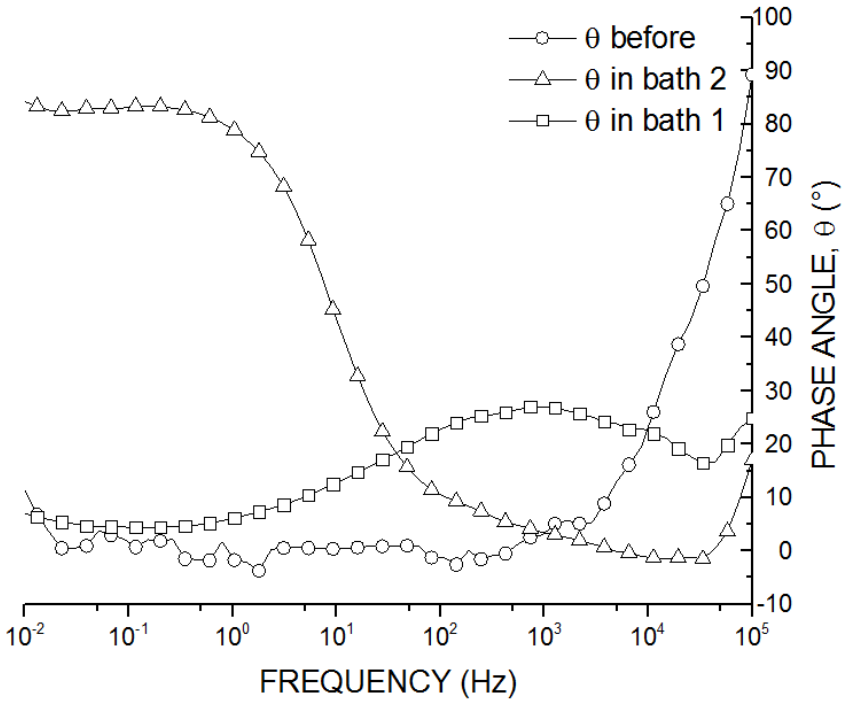

Figure 39. Phase angles at first in copper sulfate bath (bath 1) before treatments, then in Watts bath (bath 2) and finally again in copper sulfate bath (codes U1 and N7).

Table 9. Copper sulfate bath (bath 1) and Watts nickel bath (bath 2) results

Samples (codes)	Polarization resistance (R_p)	Solution resistance (R_Ω)	Capacitance (C_{dl})
Fiber, before (U1)	2600	1560	2.7E-07
Fiber, in bath 2 (N7)	20300	40	1.6E-08
Fiber, in bath 1 (N7)	1.0	0.2	4.0E-04

From Figure 34 and Table 9 can be seen that the immersion in Watts nickel bath (bath 2) affects strongly in polarization resistance, solution resistance and capacitance of sample code N7. Watts bath changes the capacitance and the shape of the curve after immersion indicates a second time constant as impedance value increases below 10 Hz. The value of impedance is much bigger before the immersion to Watts bath than after, and that describes the activation of the surface of the sample.

SEM-imaging was done to the CNT samples to see if there was any changes after the treatment. Figure 40 shows the SEM-images for sample code N7. In figure 40 can observed that there isn't any agglomeration, weakening of the structure or special shape-changes.

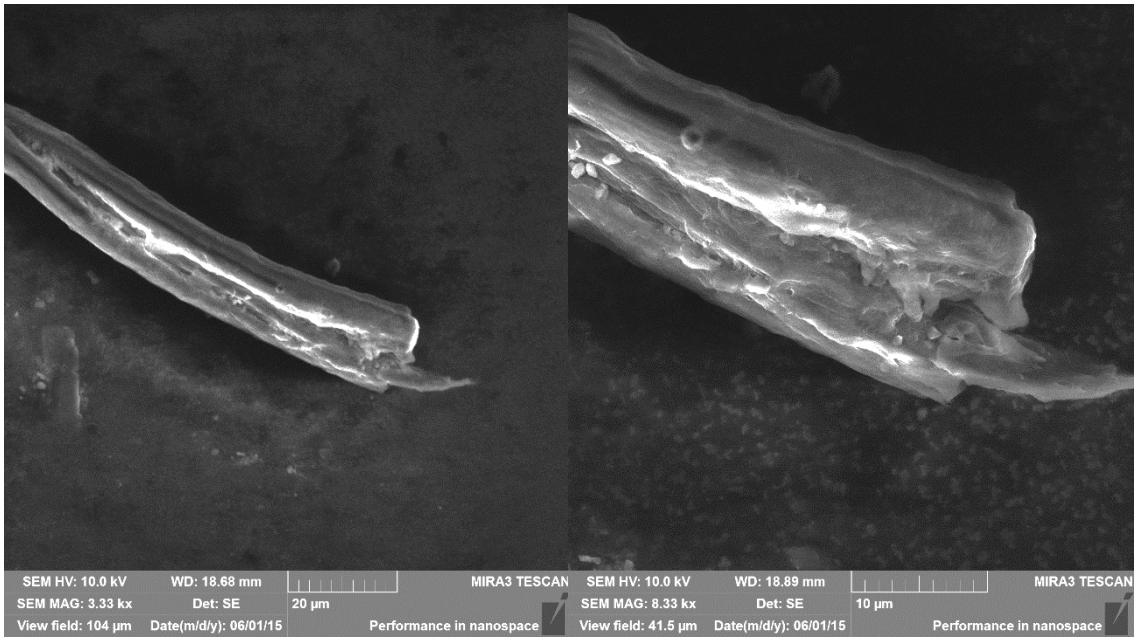

Figure 40. CNT fiber (code N7) after copper sulfate bath (bath 1) and Watts bath (bath 2) treatment.

5.3 Bath 2 (Watts bath) immersion

Table 10. Used samples

Samples (codes)	A (mm2)	l (mm)	d (µm)	Treatment
Fiber (N8)	0.6	20	10	Immersion time: 72 h
Fiber (N9)	0.6	20	10	Immersion time: 30 min
Fiber (N11)	0.9	30	10	Immersion time: 60 min
Yarn (N12)	22	35	200	Immersion time: 40 min
Fiber (P2)	0.8	25	10	Immersion time: 30 min + 1h drying
Yarn (yarn1)	3.3	35	30	Immersion time: 24 h

The EIS after Watts nickel bath (bath 2) immersion, wet and dry (code N9) is shown in Figure 41. The impedance after immersion (wet sample) is drawn with the black circles, the impedance after immersion (dry sample) is drawn with the black triangles, the phase angle before immersion (wet sample) is drawn with the white circles and the phase angles after immersion (dry sample) with the white triangles.

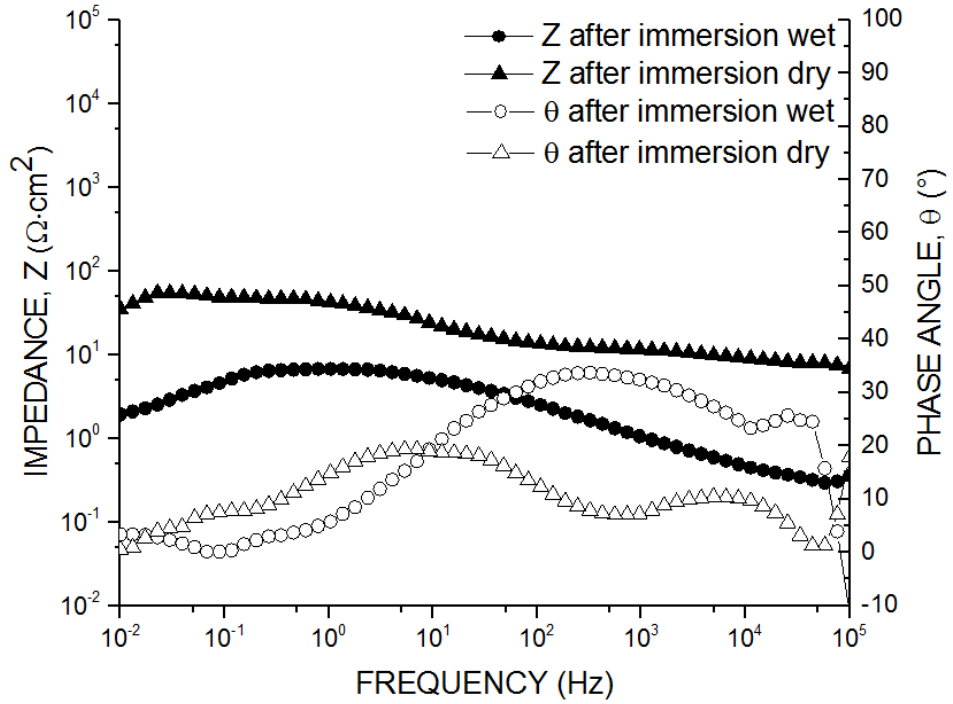

Figure 41. Impedance and phase angle spectrums after Watts bath (bath 2) immersion, wet and dry (code N9).

The EIS before and after Watts nickel bath (bath 2) immersion (code N11) are shown in Figure 42. The impedance before immersion is drawn with the black circles, the impedance after immersion is drawn with the black triangles, the phase angle before immersion is drawn with the white circles and the phase angle after immersion with the white triangles.

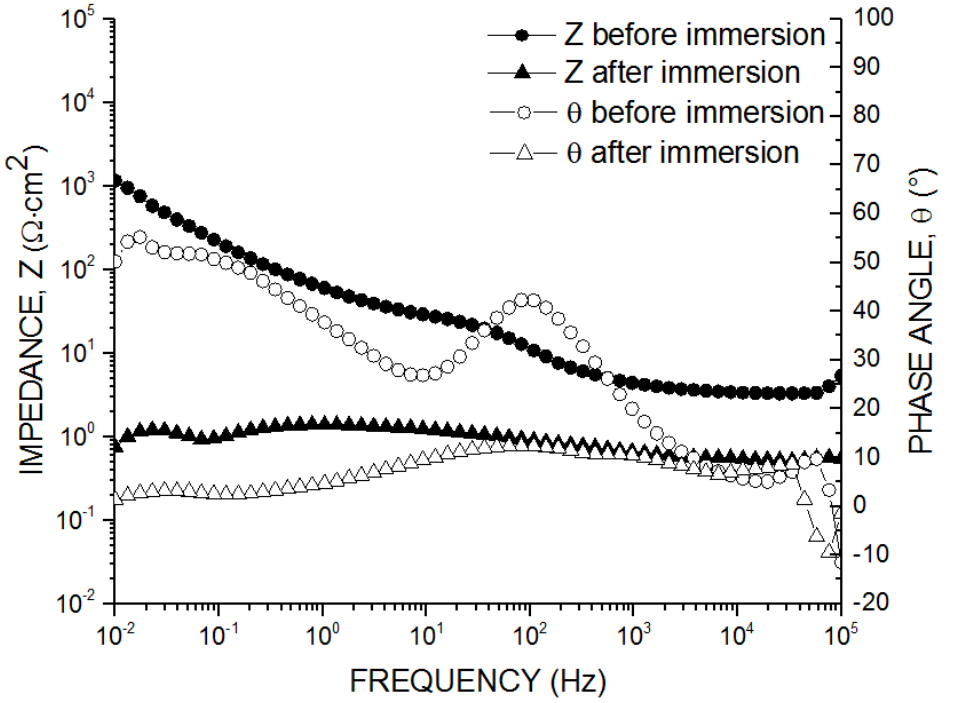

Figure 42. Impedance and phase angle spectrums before and after Watts bath (bath 2) immersion (code N11).

Table 11. Watts bath (bath 2) immersion results

Samples (codes)	Polarization resistance (R_p)	Solution resistance (R_Ω)	Capacitance (C_{dl})
Fiber, before (N8)	3.8	9.8	3.8E-06
Fiber, after (N8)	1.5	1.4	7.9E-05
Fiber, wet (N9)	3.9	0.3	1.1E-04
Fiber, dry (N9)	30	7.4	8.5E-07
Fiber, before (N11)	890	3.3	1.8E-07
Fiber, after (N11)	0.6	0.5	1.2E-03
Yarn, before (N12)	490	0.6	5.6E-06
Yarn, after (N12)	220	0.6	8.3E-05
Fiber, before (P2)	9030	35	4.0E-08
Fiber, after (P2)	270	20	1.1E-04
Yarn, after (yarn1)	1300	0.7	1.1E-05

As can be seen in Figure 41, the impedance of a wet sample is lower than the impedance of a dry sample. This refers to that there could be crystallized residues of electrolyte from the Watts bath (bath 2) on the surface of the sample or inside the sample. The crystallized electrolyte residues does not dissolve back into the copper sulfate bath (bath 1). Due to this, if this activation method would be used on an industrial scale, CNT material should not be allowed to dry after activation i.e. the process should be a continuous. In addition, Table 11 shows that polarization resistance, solution resistance and capacitance of sample code N9 are changing depending on the sample (wet or dry sample).

Figure 42 shows that the effect of Watts bath (bath 2) is significant for the sample code N11. The values of impedance and the phase angle decreased significantly after the immersion in Watts bath. This refers to activation in the CNT fiber surface. In Table 11, the values of polarization resistance, solution resistance and capacitance are changing after immersion in Watts bath with each sample. The differences between the samples R_p, R_Ω and C_{dl} are due to the inhomogeneous nature of CNT material.

Figures 43, 44 and 45 show the SEM-imaging for Watts bath (bath 2) immersed samples (code N9, N11, and yarn1). It can observed from the figures that there is no agglomeration, weakening of the structure or special shape-change. Watts bath immersion do not seem to damage the structure of the sample, but additional research of the effects of the bath is needed. Only in figure 44 sample code N11 in the upper images looks untypical, but the change of sample morphology can caused by inhomogeneous material.

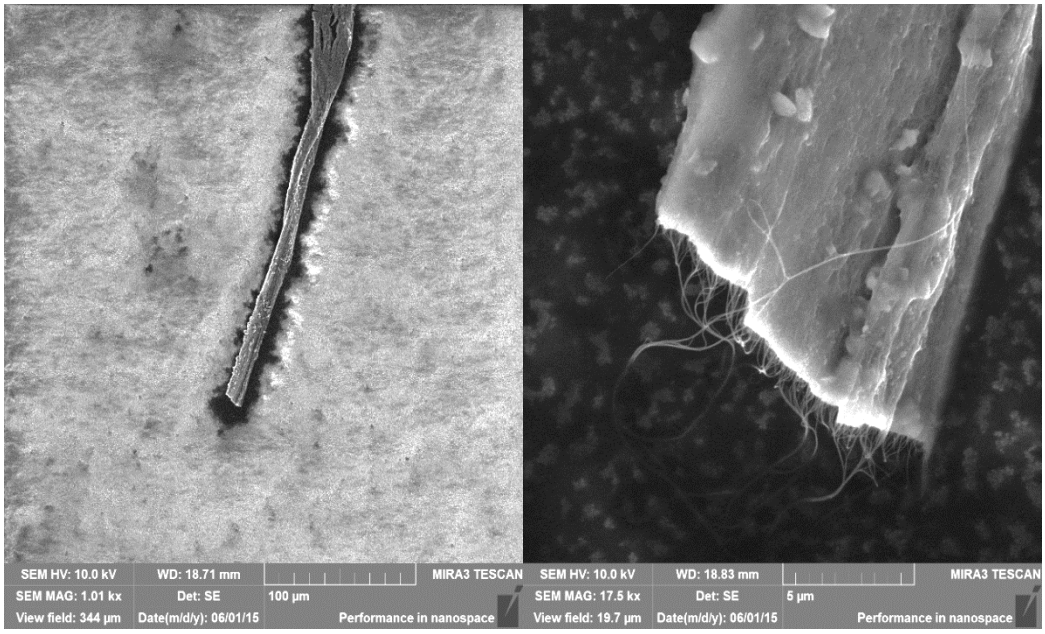

Figure 43. CNT fiber (code N9) after bath 2 (Watts bath) immersion.

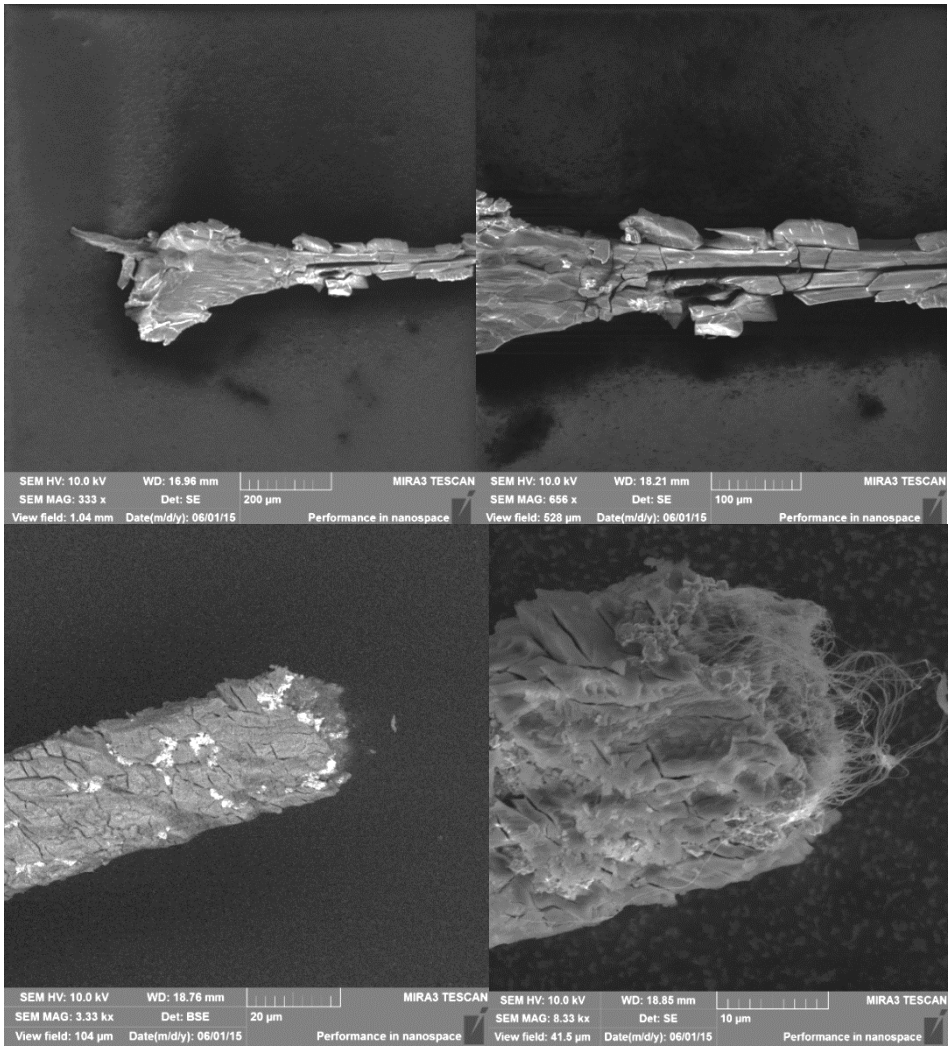

Figure 44. The top and end of CNT fiber (code N11) after Watts bath (bath 2) immersion

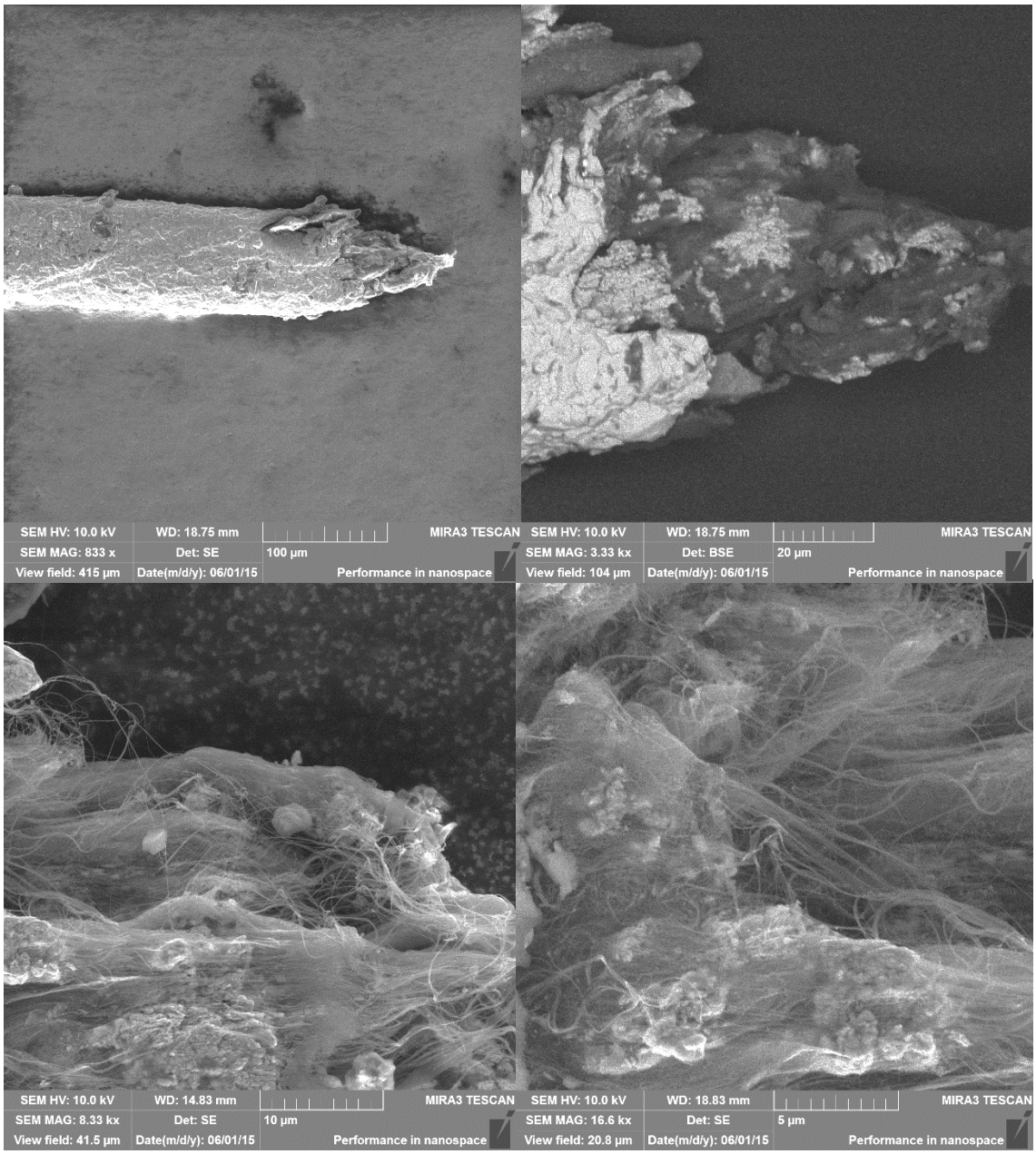

Figure 45. A CNT yarn (code yarn1) after Watts bath (bath 2) immersion.

5.4 Acetone

Table 12. Used samples

Samples (codes)	A (mm^2)	l (mm)	d (µm)	Treatment
Yarn (yarn2)	6.6	70	30	Wetting with acetone, bath 2 immersion time: 30 min
Yarn (yarn3)	6.6	70	30	Bath 2 immersion time: 30 min

The EIS before and after wetting with acetone (code yarn2) are shown in Figure 46. The impedance before treatment is drawn with the black circles, the impedance after treatment is drawn with the black triangles, the phase angle before treatment is drawn with the white circles and the phase angles after treatment with the white triangles.

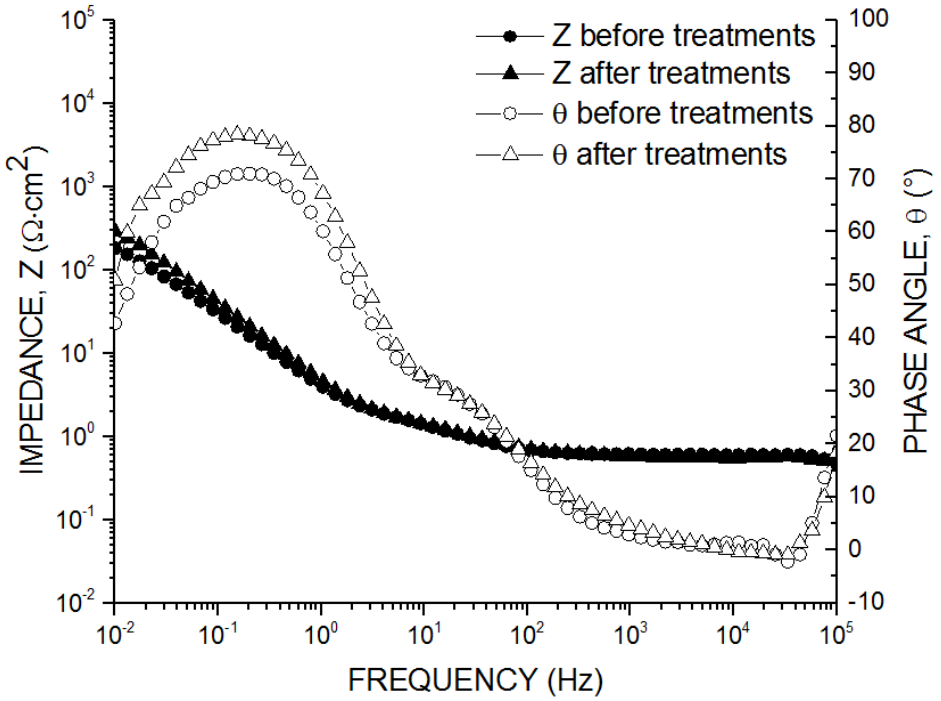

Figure 46. Impedance and phase angle spectrums before and after wetting with acetone and Watts bath (bath 2) immersion (code yarn2).

The EIS before and after Watts bath (bath 2) immersion (code yarn3) are shown in Figure 47. The impedance before immersion is drawn with the black circles, the impedance after immersion is drawn with the black triangles, the phase angle before immersion is drawn with the white circles and the phase angles after immersion with the white triangles.

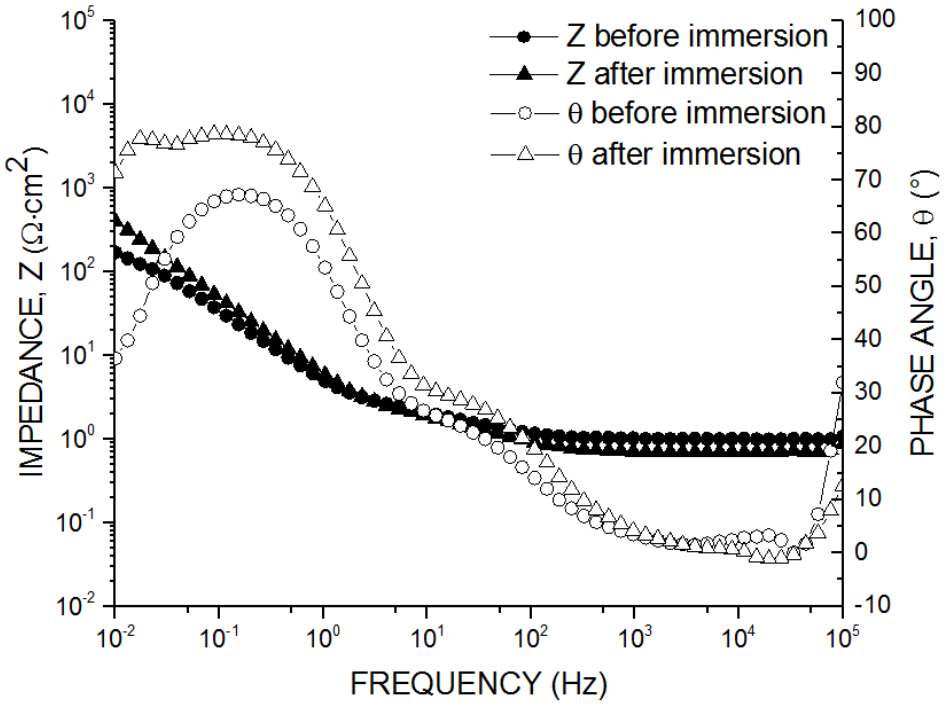

Figure 47. Impedance and phase angle spectrums before and after Watts bath (bath 2) immersion (code yarn3).

Table 13. Wetting with acetone and Watts bath (bath 2) immersion results

Samples (codes)	Polarization resistance (R_p)	Solution resistance (R_Ω)	Capacitance (C_{dl})
Yarn, before (yarn2)	1000	0.5	4.8E-05
Yarn, after (yarn2)	1600	0.5	2.4E-05
Yarn, before (yarn3)	950	1.0	4.5E-05
Yarn, after (yarn3)	2080	0.7	1.6E-05

As Figures 46, 47 and the Table 13 show, acetone has no effect on the electrochemical activity of the sample. Moreover, Watts nickel bath (bath 2) immersion is not as effective for yarn specimens as fibers.

5.5 Anodization

Table 14. Used sample

Samples (codes)	A (mm^2)	l (mm)	d (µm)	Treatment
Fiber (A1)	0.5	15	10	49s, 2500 mV, 10wt-% H_2SO_4

The EIS before and after anodization (code A1) are shown in Figure 48. The impedance before anodization is drawn with the black circles, the impedance after anodization is drawn with the black triangles, the phase angle before anodization is drawn with the white circles and the phase angles after anodization with the white triangles.

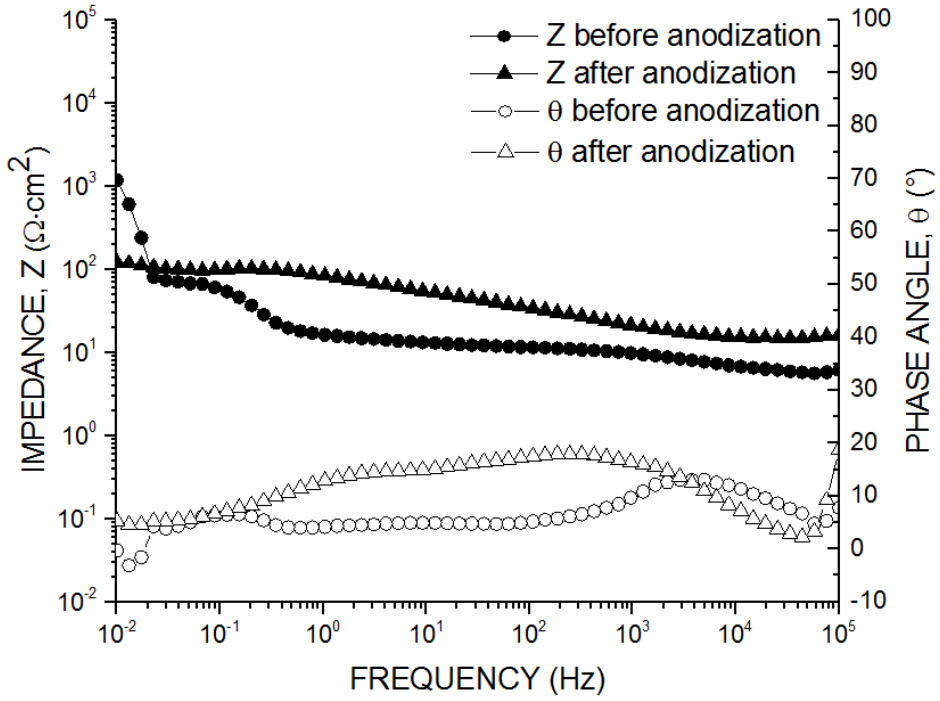

Figure 48. Impedance and phase angle spectrums before and after anodization (code A1).

Table 15. Anodization results

Samples (codes)	Polarization resistance (R_p)	Solution resistance (R_Ω)	Capacitance (C_{dl})
Fiber, before (A1)	315	5.7	1.2E-04
Fiber, after (A1)	50	15	7.2E-07

Figure 44 and table 15 show that anodization affect strongly to electrochemical activity of the sample code A1. If the EIS measurements were made wider frequency area, the graph would have been appear although the size of another time constant. The slight increase in solution resistance and large increase in capacitance could indicate removal of loose material from the surface.

5.6 Ethanol (C_2H_6O)

Table 16. Used sample

Samples (codes)	A (mm^2)	l (mm)	d (µm)	Treatment
Fiber (UN4)	0.9	29	10	C_2H_6O 10 %, 20 %

The impedances before and after addition of ethanol (code UN4) are shown in Figure 49. The impedance before addition of ethanol is drawn with the black circles, the impedance after 10 % ethanol and stirring is drawn with the black triangles, the impedance after 10 % ethanol without stirring is drawn with the white squares and the impedance after 20 % ethanol is drawn with the white stars.

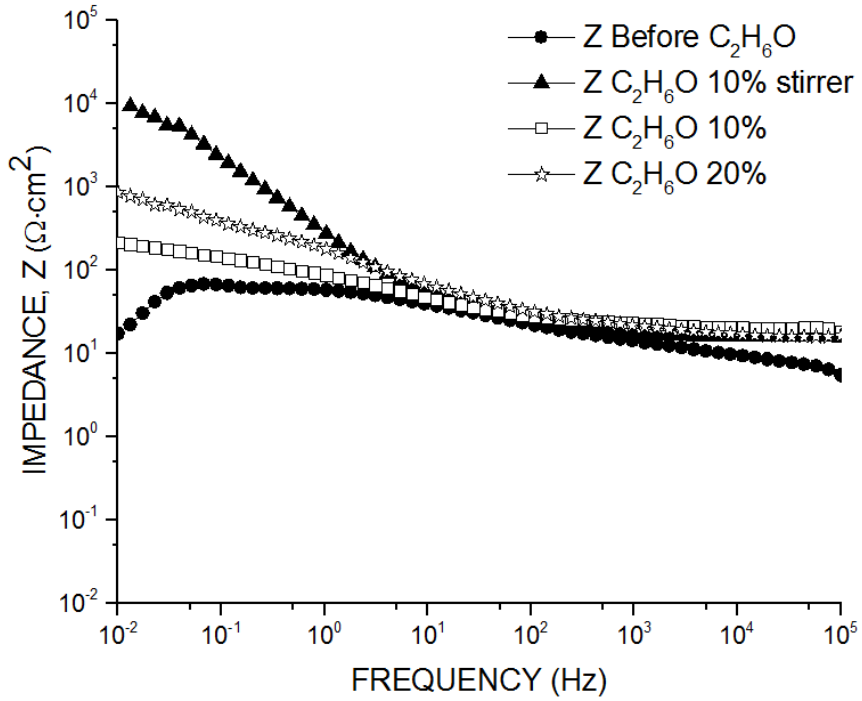

Figure 49. Impedance spectrums before and after addition of ethanol (code UN4).

The phase angles before and after addition of ethanol (code UN4) are shown in Figure 50. The phase angle before addition of ethanol is drawn with the black circles, the phase angle after 10 % ethanol and stirring is drawn with the black triangles, the phase angle after 10 % ethanol without stirring is drawn with the white squares and the phase angle after 20 % ethanol is drawn with the white stars.

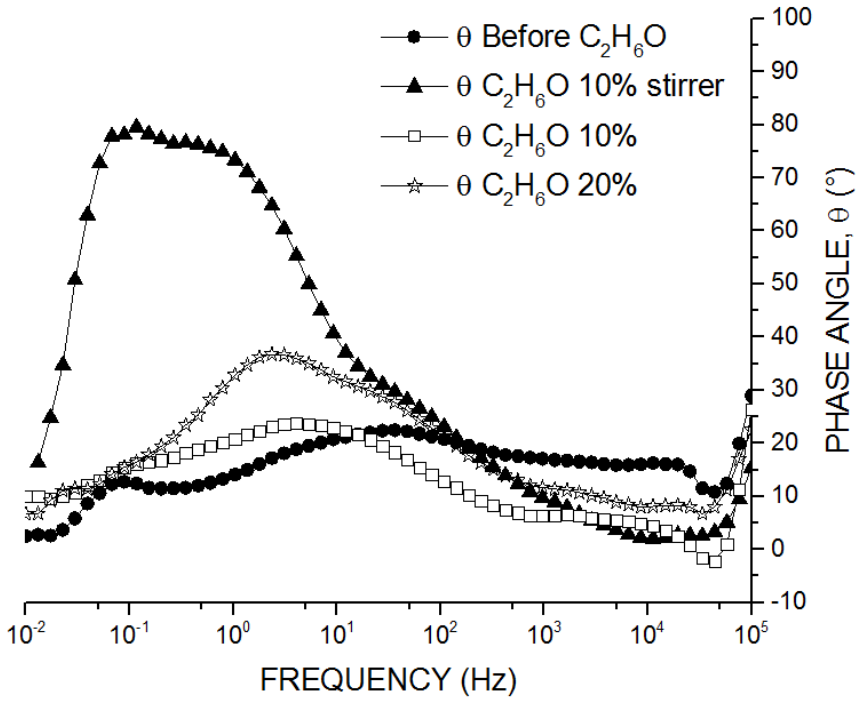

Figure 50. Phase angle spectrums before and after addition of ethanol (code UN4).

Table 17. Addition of ethanol results

Samples (codes)	Polarization resistance (R_p)	Solution resistance (R_Ω)	Capacitance (C_{dl})
Fiber, before, in bath1 (UN4)	50	7.4	2.9E-06
Fiber, C_2H_6O 10% + stirrer (UN4)	7130	20	9.4E-08
Fiber, C_2H_6O 10% (UN4)	170	20	2.6E-06
Fiber, C_2H_6O 20% (UN4)	690	20	4.6E-06

Organic ethanol should provide better wetting of CNT material and activation in the sample. In Figure 49, 50 and Table 17 show that addition of ethanol does not improve the electrochemical activity of sample. Especially the stirring affected undesirably to activity. 20 % ethanol addition caused visible sedimentation of electrolyte. The sediment accumulated into the surface of the sample.

5.7 Acid treatments

Table 18. Used sample in acid solution (3 H_2SO_4 (95 %): 1 HNO_3 (65 %))

Samples (codes)	A (mm^2)	l (mm)	d (µm)	Treatment
Fiber (N1)	0.6	20	10	Immersion time: 15 min

The EIS before and after acid solution immersion (code N1) are shown in Figure 51. The impedance before immersion is drawn with the black circles, the impedance after immersion is drawn with the black triangles, the phase angle before immersion is drawn with the white circles and the phase angles after immersion with the white triangles.

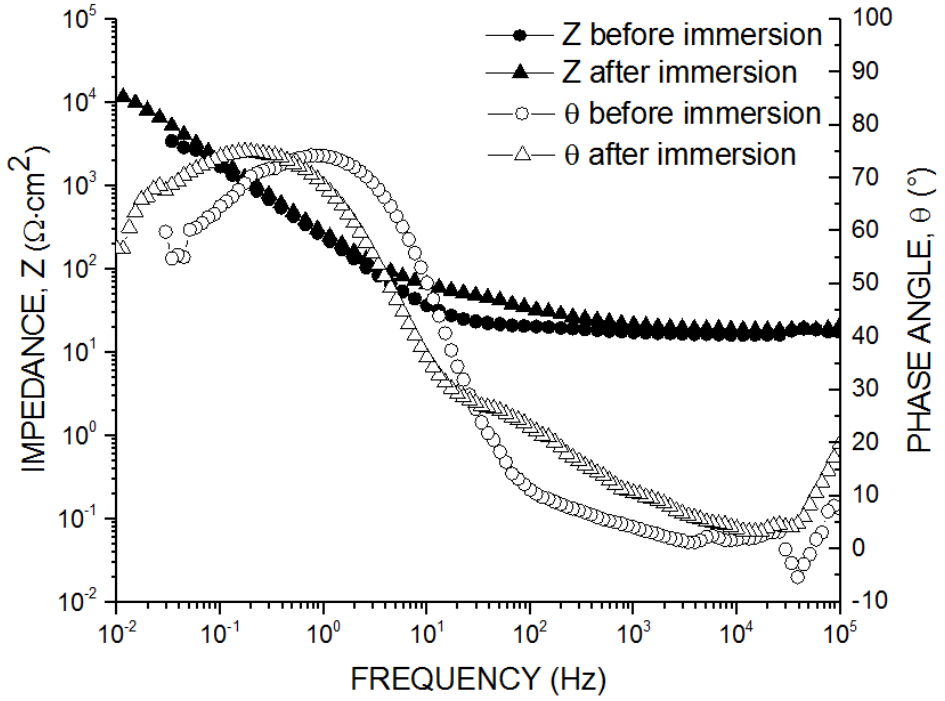

Figure 51. Impedance and phase angle spectrums before and after acid-solution immersion (code N1)

Table 19. Sulfuric acid + nitric acid immersion results

Samples (codes)	Polarization resistance (R_p)	Solution resistance (R_Ω)	Capacitance (C_{dl})
Fiber, before (N1)	2090	20	3.4E-07
Fiber, after (N1)	7080	20	1.1E-07

Figure 51 and Table 19 show that immersion in the solution of 3 H_2SO_4 (95 %): 1 HNO_3 (65 %) did not improve the electrochemical activity. Solution resistance is not changed, capacitance decreased lightly and polarization resistance increased 3.5 times.

Table 20. Used sample in sulfuric acid (1M H_2SO_4)

Samples (codes)	A (mm^2)	l (mm)	d (µm)	Treatment
Fiber (h1)	0.3	10	10	Immersion time: 40min
Fiber (h2)	0.3	10	10	Immersion time: 30min

The EIS before and after sulfuric acid immersion (code h2) are shown in Figure 52. The impedance before immersion is drawn with the black circles, the impedance after immersion is drawn with the black triangles, the phase angle before immersion is drawn with the white circles and the phase angles after immersion with the white triangles.

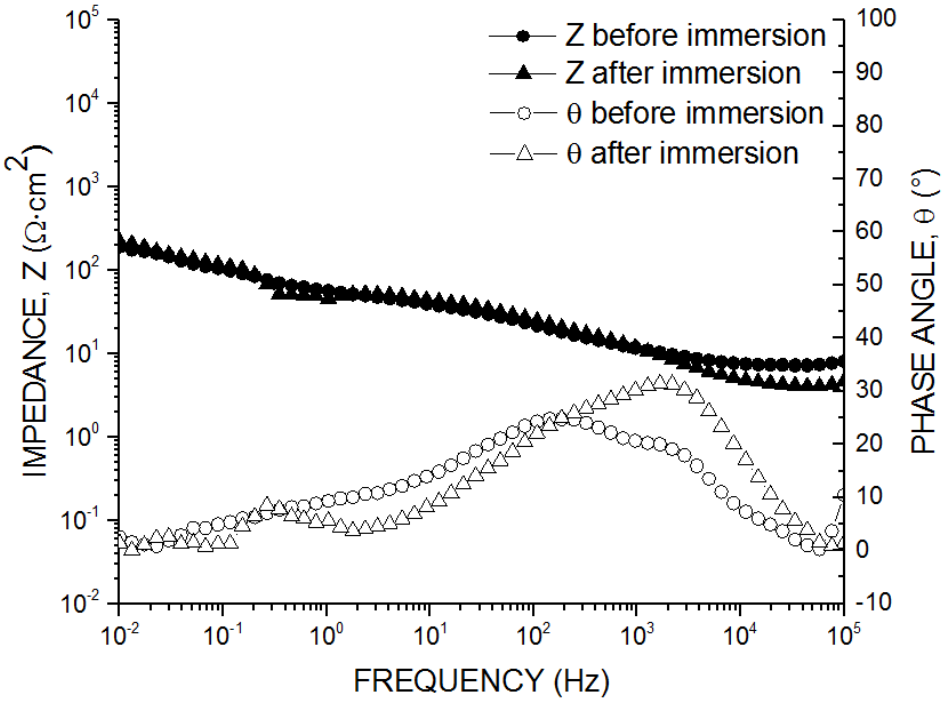

Figure 52. Impedance and phase angle spectrums before and after immersion (code h2)

Table 21. Sulfuric acid immersion results

Samples (codes)	Polarization resistance (R_p)	Solution resistance (R_Ω)	Capacitance (C_{dl})
Fiber, before H_2SO_4 (h1)	550	10	2.8E-05
Fiber, after H_2SO_4 (h1)	2100	1300	1.0E-12
Fiber, before H_2SO_4 (h2)	50	7.2	2.2E-07
Fiber, after H_2SO_4 (h2)	60	4.1	1.6E-07

Figure 52 and Table 21 show that immersion in 1M sulfuric acid provides no observed significant changes in the electrochemical activity. A large solution resistance is comparable to conductivity of the sample. The results suggest that the CNT structure may swell i.e. the nanotubes are separated from each other and the resistance increases.

Table 22. Used sample in boric acid (40 g/l)

Samples (codes)	A (mm^2)	l (mm)	d (µm)	Treatment
Fiber (b1)	0.2	7	10	Immersion time: 60 min

The EIS after acid immersion (code b1) is shown in Figure 53. The impedance before immersion is drawn with the black circles, the impedance after immersion is drawn with the black triangles, the phase angle before immersion is drawn with the white circles and the phase angles after immersion with the white triangles.

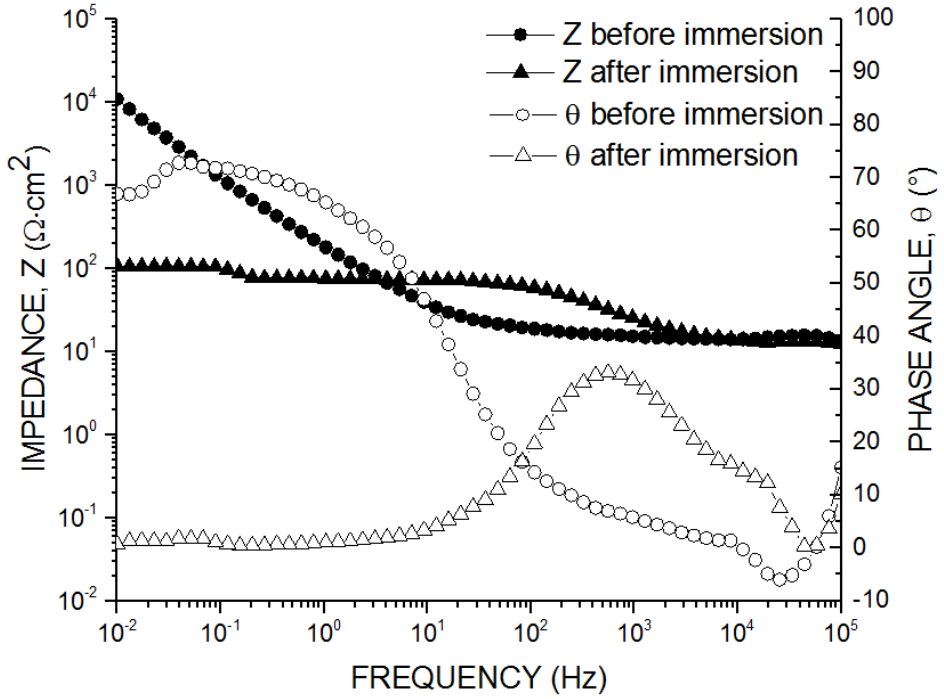

Figure 53. Impedance and phase angle spectrums before and after immersion (code b1)

Table 23. Boric acid immersion results

Samples (codes)	Polarization resistance (R_p)	Solution resistance (R_Ω)	Capacitance (C_{dl})
Fiber, before H_3BO_3 (b1)	1840	15	6.2E-07
Fiber, after H_3BO_3 (b1)	20	10	3.8E-07

Figure 53 and Table 23 show that immersion in 40 g/l boric acid improves the electrochemical activity. Impedance and phase angle reduces and polarization resistance decrease significantly.

5.8 Polarized samples in H_2SO_4

Table 24. Used samples

Samples (codes)	A (mm^2)	l (mm)	d (µm)	Other
Fiber (N14)	0,6	20	10	
Yarn (N13)	1,3	20	20	
Yarn (yarn3)	6,6	70	30	Immersed in Watts -bath

The impedances using polarization potentials 0 - 400 mV in 1M H_2SO_4 (code N14) are shown in Figure 54. The impedance at 0 mV is drawn with the black circles, impedance at 100 mV is drawn with the black triangles, impedance at 200 mV is drawn with the black squares, impedance at 300 mV is drawn with black stars and impedance at 400 mV is drawn with the black diamonds.

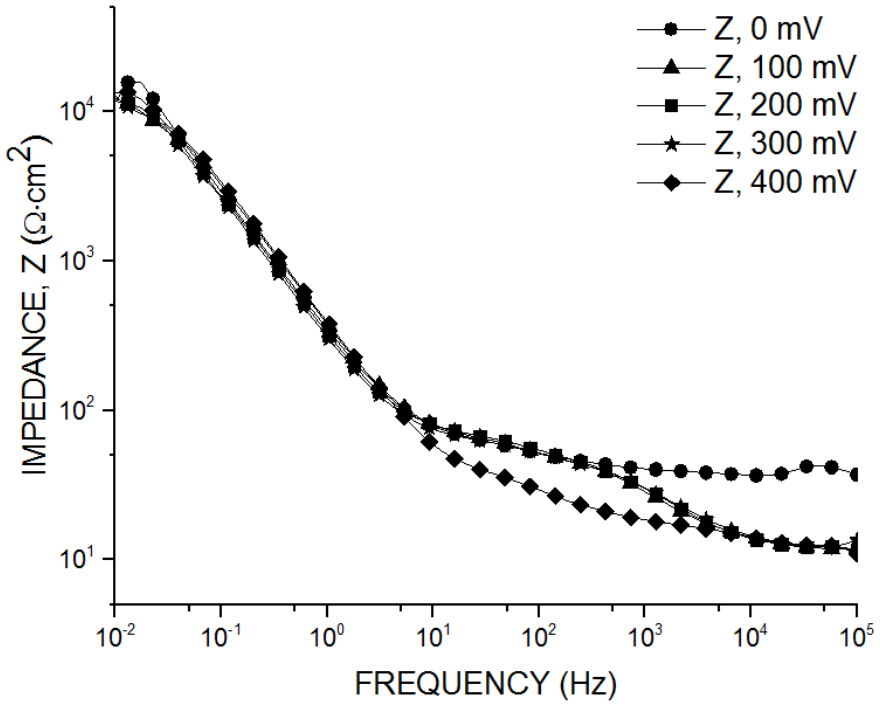

Figure 54. Impedance spectrums: 0 mV - 400 mV in sulfuric acid (code N14).

The phase angles using potentials 0 - 400 mV in 1M H_2SO_4 (code N14) are shown in Figure 55. The phase angle at 0 mV is drawn with the white circles, phase angle at 100 mV is drawn with the white triangles, phase angle at 200 mV is drawn with the white squares, phase angle at 300 mV is drawn with white stars and phase angle at 400 mV is drawn with the white diamonds.

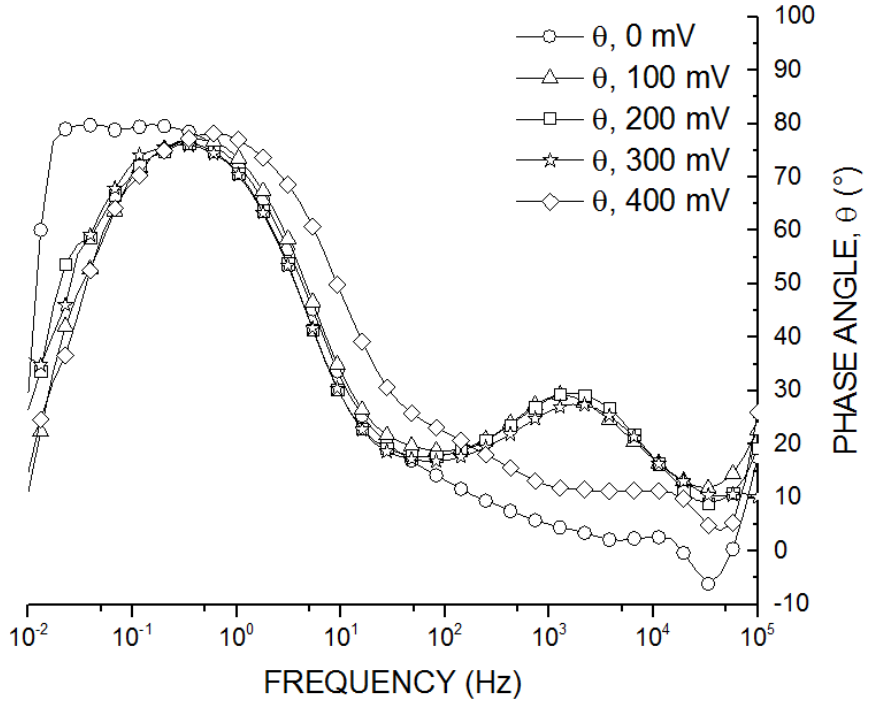

Figure 55. Phase angle spectrums: 0 mV - 400 mV in sulfuric acid (code N14).

The impedances at polarization potentials 0 - 400 mV in 1M H_2SO_4 (code N13) are shown in Figure 56. The impedance at 0 mV is drawn with the black circles, impedance at 100 mV is drawn with the black triangles, impedance at 200 mV is drawn with the black squares, impedance at 300 mV is drawn with black stars and impedance at 400 mV is drawn with the black diamonds.

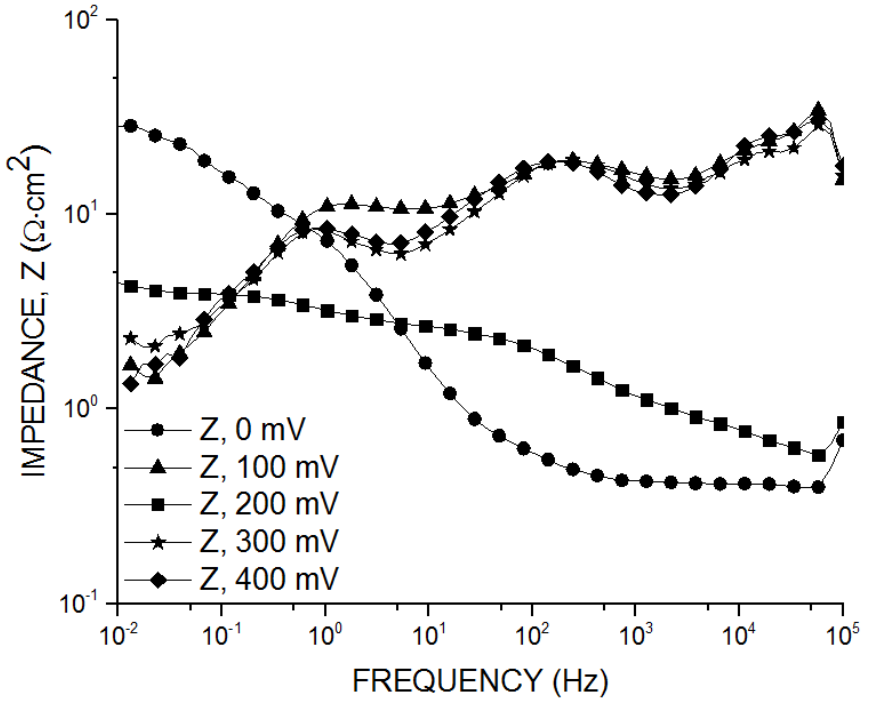

Figure 56. Impedance spectrums: 0 mV - 400 mV in sulfuric acid (code N13).

The phase angles at polarization potentials 0 - 400 mV in 1M H_2SO_4 (code N13) are shown in Figure 57. The phase angle at 0 mV is drawn with the white circles, phase angle at 100 mV is drawn with the white triangles, phase angle at 200 mV is drawn with the white squares, phase angle at 300 mV is drawn with white stars and phase angle at 400 mV is drawn with the white diamonds.

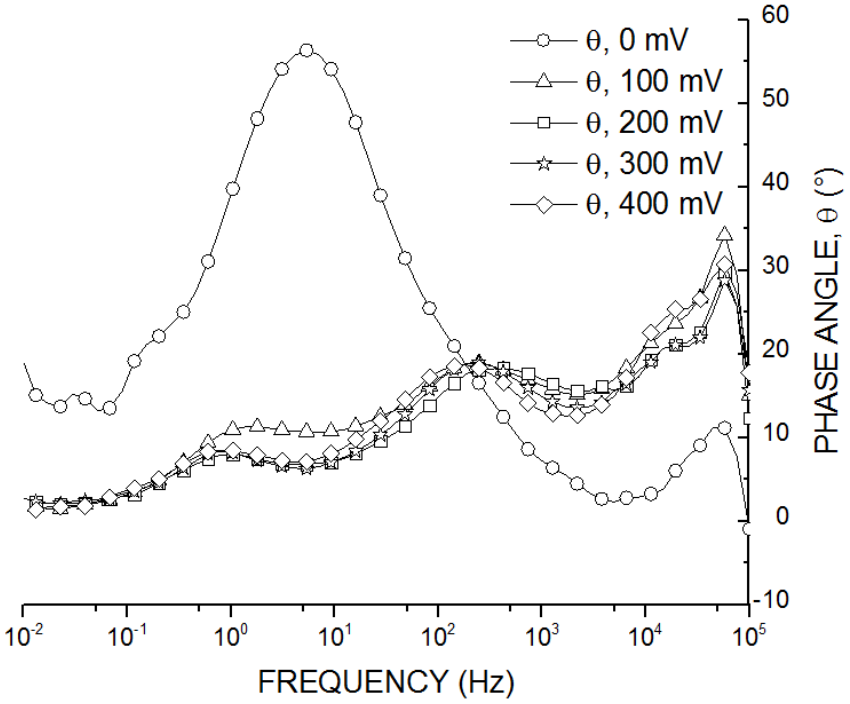

Figure 57. Phase angle spectrums: 0 mV - 400 mV in sulfuric acid (code N13).

The impedances at polarization potentials 0 - 200 mV in 1M H_2SO_4 (code yarn3) are shown in Figure 58. The impedance at 0 mV is drawn with the black circles, impedance at 100 mV is drawn with the black triangles, impedance at 200 mV is drawn with the black squares, impedance at 300 mV is drawn with black stars and impedance at 400 mV is drawn with the black diamonds.

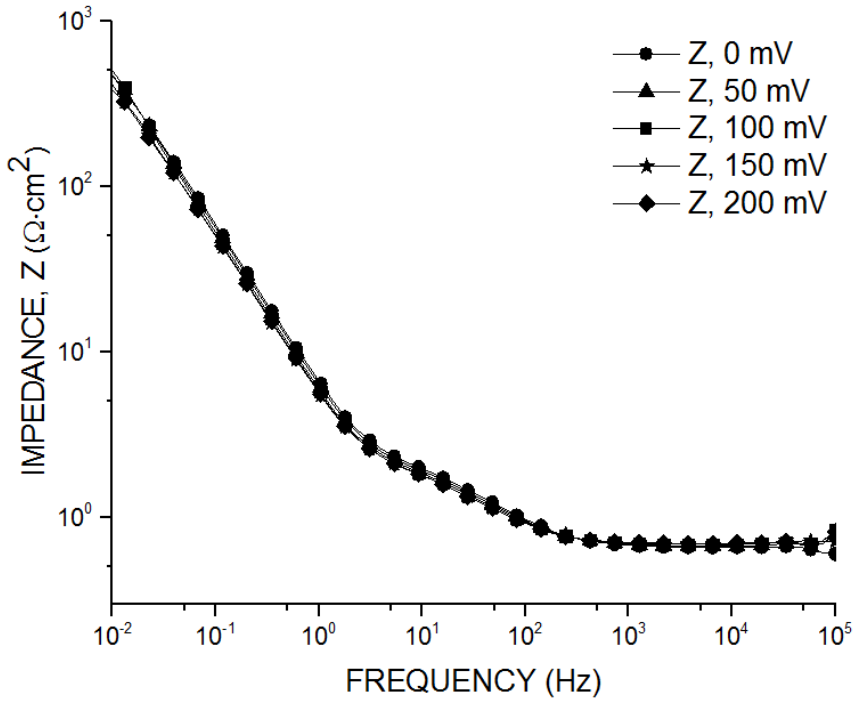

Figure 58. Impedance spectrums: 0 mV - 200 mV in sulfuric acid (code yarn3).

The phase angles at polarization potentials 0 - 200 mV in 1M H_2SO_4 (code yarn3) are shown in Figure 59. The phase angle at 0 mV is drawn with the white circles, phase angle at 100 mV is drawn with the white triangles, phase angle at 200 mV is drawn with the white squares, phase angle at 300 mV is drawn with white stars and phase angle at 400 mV is drawn with the white diamonds.

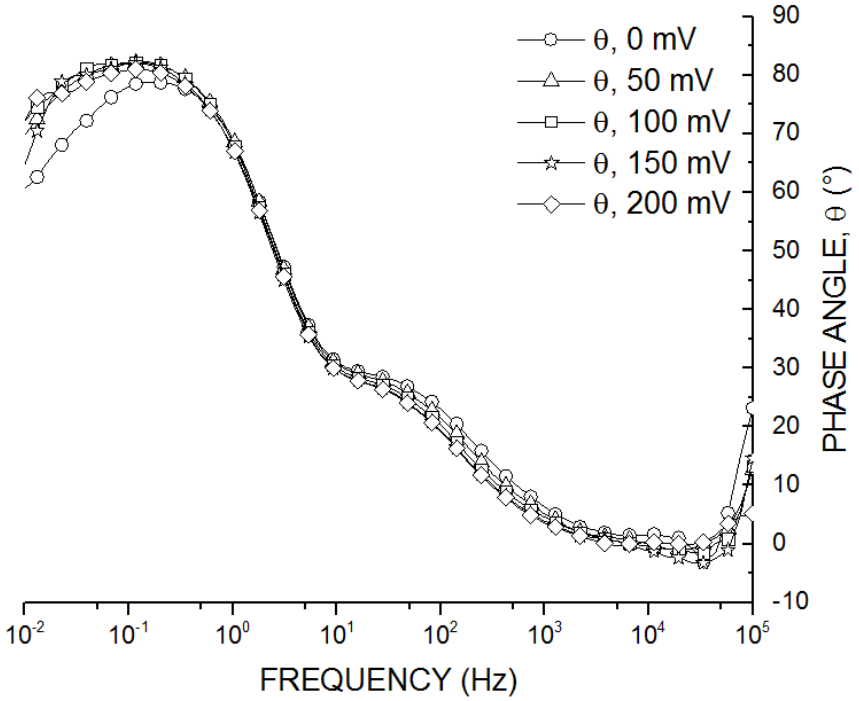

Figure 59. Phase angle spectrums: 0 mV - 200 mV in sulfuric acid (code yarn3).

Table 25. EIS results with different potentials in H_2SO_4

Samples (codes)	Polarization resistance (R_p)	Solution resistance (R_Ω)	Capacitance (C_{dl})
Fiber, 100 mV, in H_2SO_4 (N14)	6700	10	6.6E-08
Yarn, 0 mV, in H_2SO_4 (N13)	35	0.4	3.1E-04
Yarn, 200 mV, in H_2SO_4 (N13)	5	0.6	5.4E-06
Yarn (bath2), 50 mV, in H_2SO_4 (yarn3)	2500	0.7	1.1E-05

The EIS measurements at different potentials in 1M H_2SO_4 were used to estimate if the sample is a semiconductor. Based on Figures 54 - 59 and table 25 can be concluded that semiconductor features are not noticeable. Samples N14, N13 and yarn3 impedances and phase angles stay almost unchangeable at different potentials. Treatment in Watts nickel bath (bath 2) did not have effect on conductive properties.

5.9 Cu/CNT composites

Table 26. Used samples

Samples (codes)	Resistivity	Treatment
Cu/CNT before furnace (26.1)	0.065 Ω	400 °C, 60 min (citric acid 2 h)
Cu/CNT after furnace (26.1)	0.067 Ω	400 °C, 60 min (citric acid 2 h)
Cu/CNT before furnace (26.2)	0.100 Ω	400 °C, 3 h (citric acid 2 h)
Cu/CNT after furnace (26.2)	0.089 Ω	400 °C, 3 h (citric acid 2 h)
Cu/CNT before furnace (26.3)	0.138 Ω	300 °C, 60 min + nitrogen gas
Cu/CNT after furnace (26.3)	0.125 Ω	300 °C, 60 min + nitrogen gas
Cu/CNT before furnace (26.4)	0.133 Ω	300 °C, 3 h + nitrogen gas (extinct)
Cu/CNT after furnace (26.4)	0.130 Ω	300 °C, 3 h + nitrogen gas (extinct)

In table 26 shown that the measured resistances varied most in sample 26.3. The difference is almost 10 %. Other heat treatments did not succeed because oxygen in the furnace oxidized the sample surfaces. Citric acid was used to remove the oxidation of some of the samples but it not affect enough. A part of Cu/CNT composites were heated with nitrogen gas atmosphere like sample code 26.3, when the surface of samples was not oxidized. Oxidation decreases the electrical conductivity. The resistance range without heat treatment varied between 0.065 Ω and 0.138 Ω. Figures 60 and 61 show SEM images of a bent and cut sample code 26.3 and Figures 62 - 65 show SEM images of a bent and cut sample code 26 without treatments.

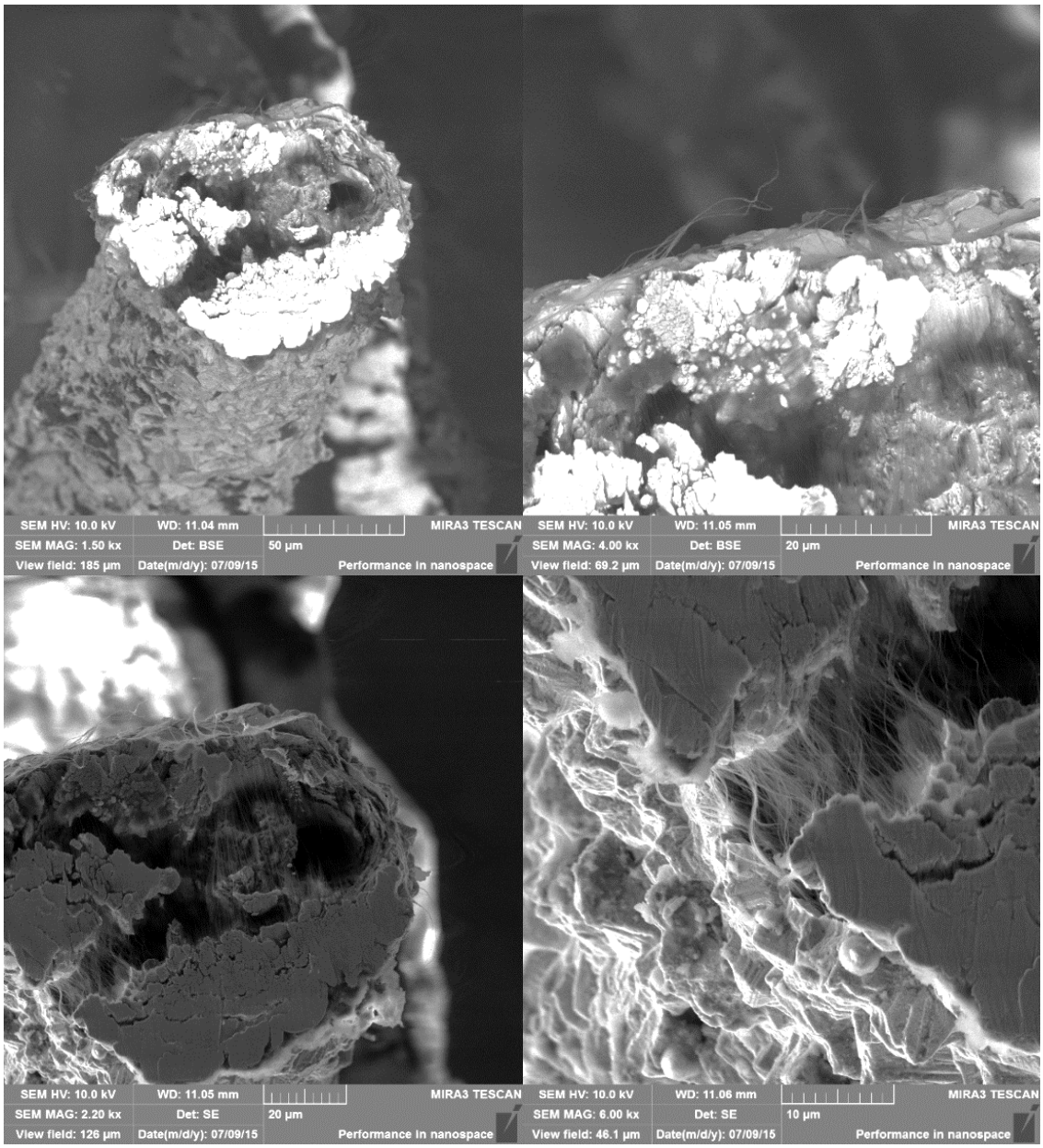

Figure 60. Bent sample code 26.3.

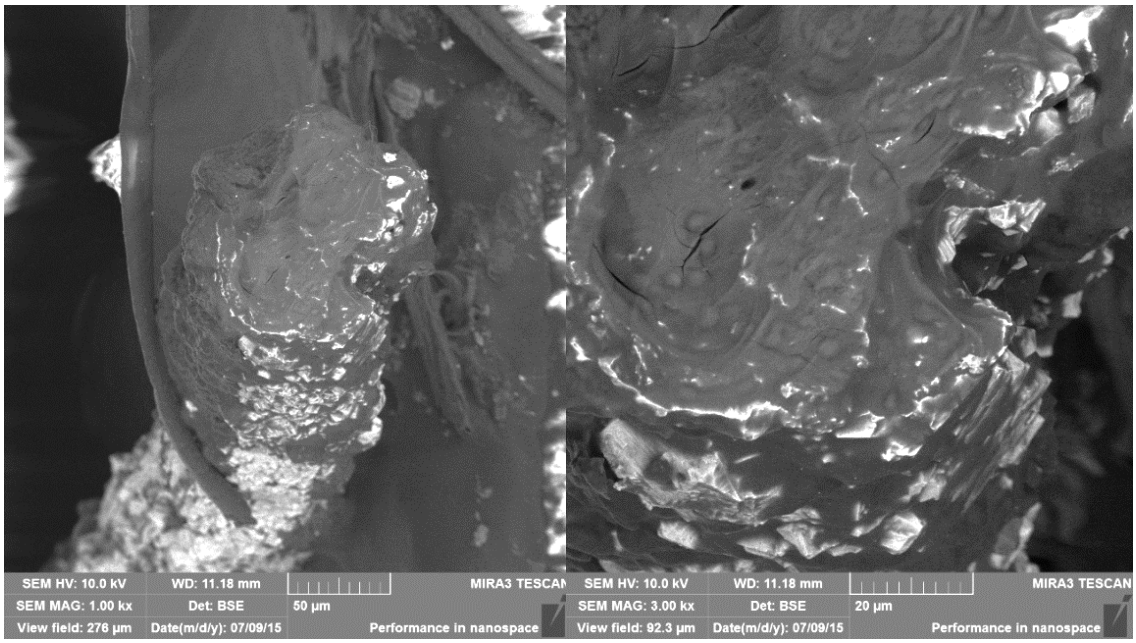

Figure 61. Cut sample code 26.3.

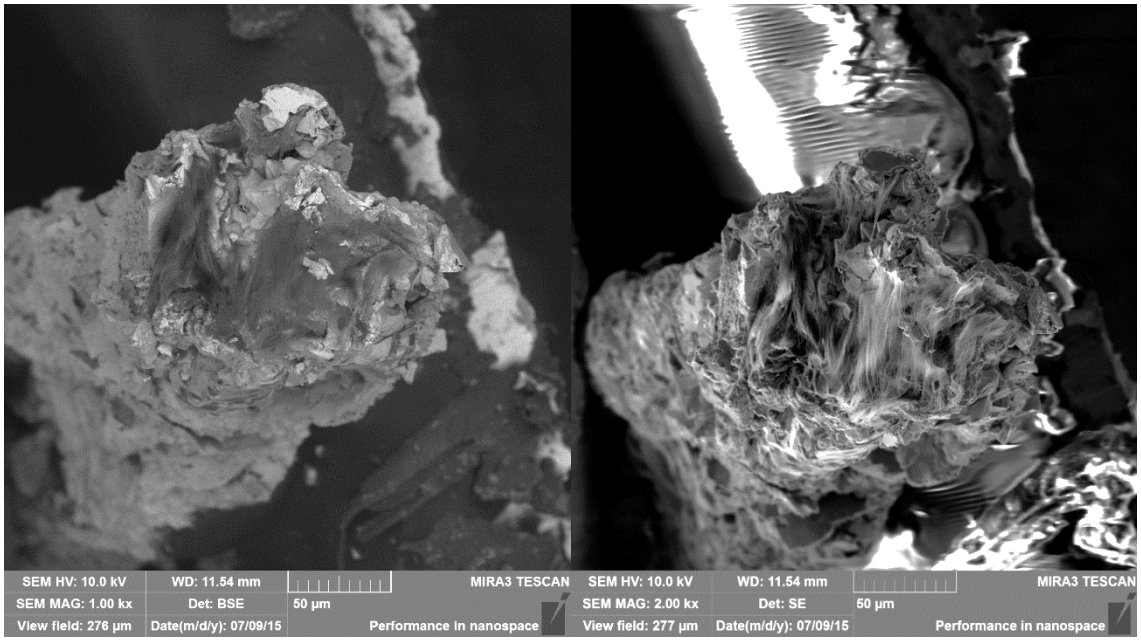

Figure 62. Bent sample code 26 (without treatments).

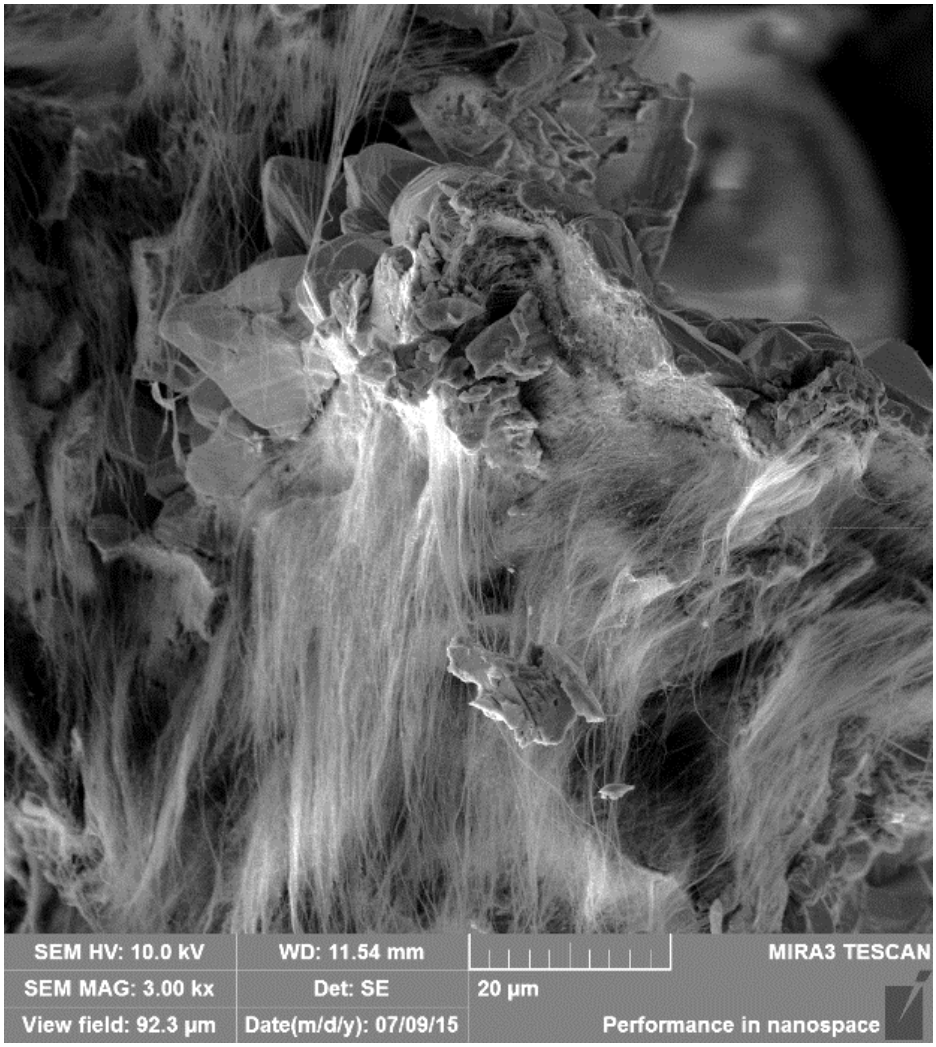

Figure 63. Bent sample code 26 near the end of the sample (without treatments).

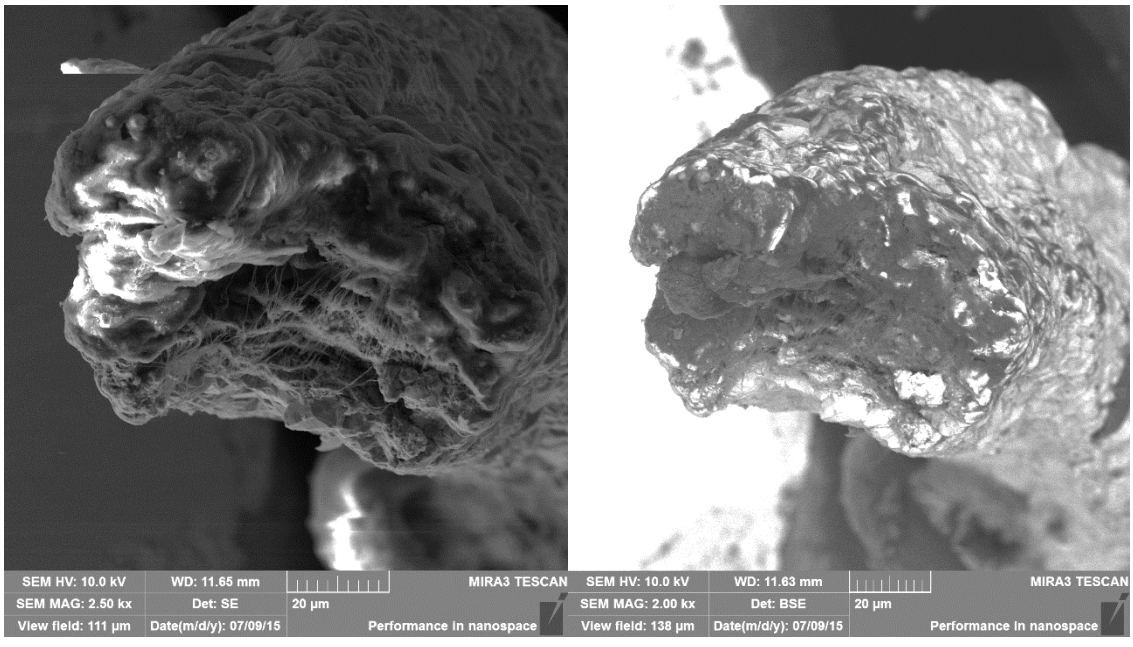

Figure 64. Cut sample code 26 (without treatments).

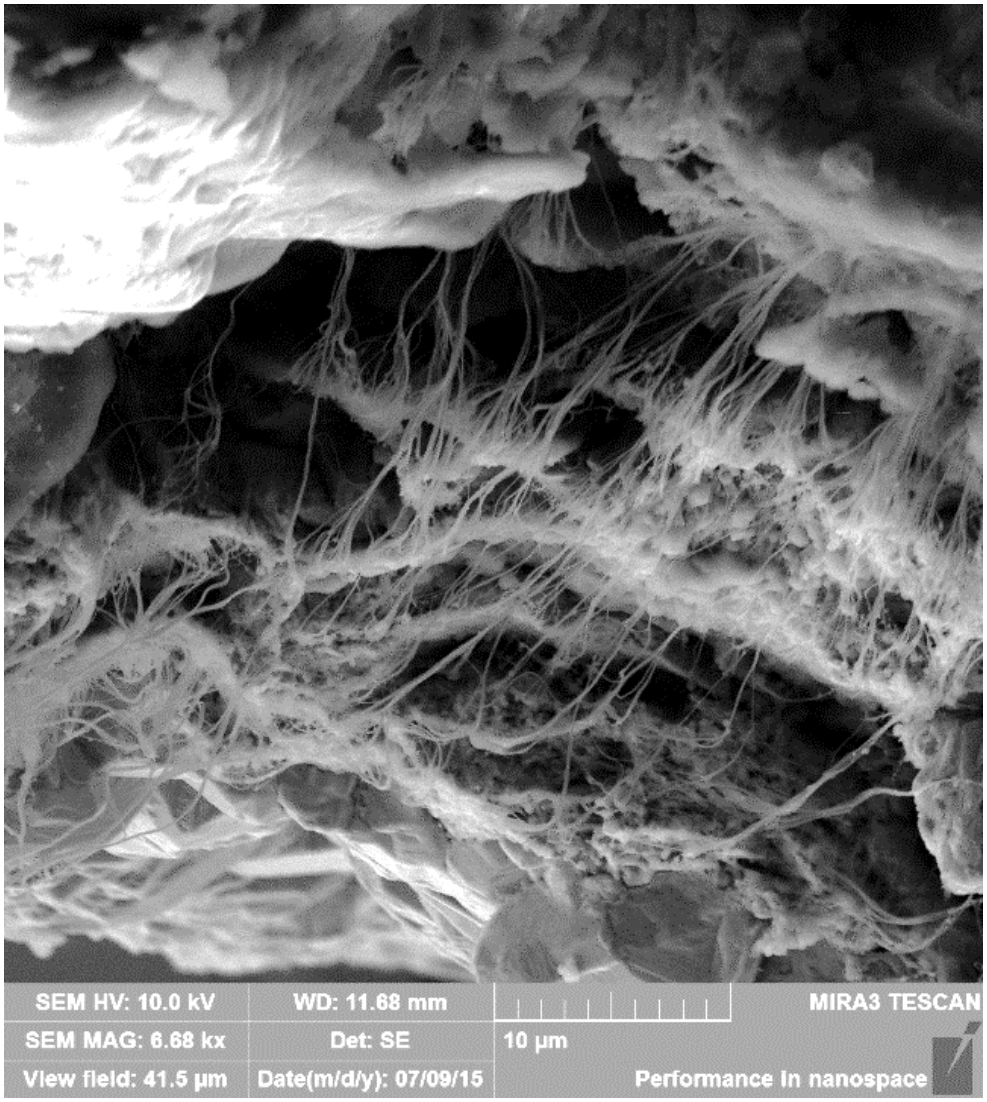

Figure 65. Cut sample code 26 near the end of the sample (without treatments)

In Figures 61 the better conductive and heat treated sample code 26.3 is shown in the SEM images more closely than the untreated sample code 26. It could causes by successful cutting, or then heat treatment with nitrogen gas atmosphere make a more compact structure. However, on the basis of images the changes in properties can't interpreted exactly and more research should be done. The changes in SEM images may also be due to the inhomogeneous material.

5.10 Galvanostatic deposition tests

Table 27. Treatment and deposition information

Samples (codes)	Treatment	Deposition
Fiber (G1)	-	Deposition: -0.1 mA, t=120s
Fiber (G2)	-	Deposition: -0.1 mA, t=120s
Fiber (G3)	Immersion time in Watts-bath: 1h	Deposition: -0.1 mA, t=120s
Fiber (G4)	Immersion time in Watts-bath: 1h	Deposition: -0.1 mA, t=120s
Fiber (G5)	Immersion time in Watts-bath: 1h	-
Fiber (G6)	Immersion time in Watts-bath: 1h	-

Galvanostatic deposition tests were done for selected samples after activation treatments. The purpose was to determine how activation improves nucleation and growth of copper along the sample length. Each sample was a same size fiber (A=0.62 mm^2, l=20 mm and d=10 µm). Figures 66 - 71 show SEM-images from sample codes G1, G2, G3, G5 and G6 after treatments and depositions.

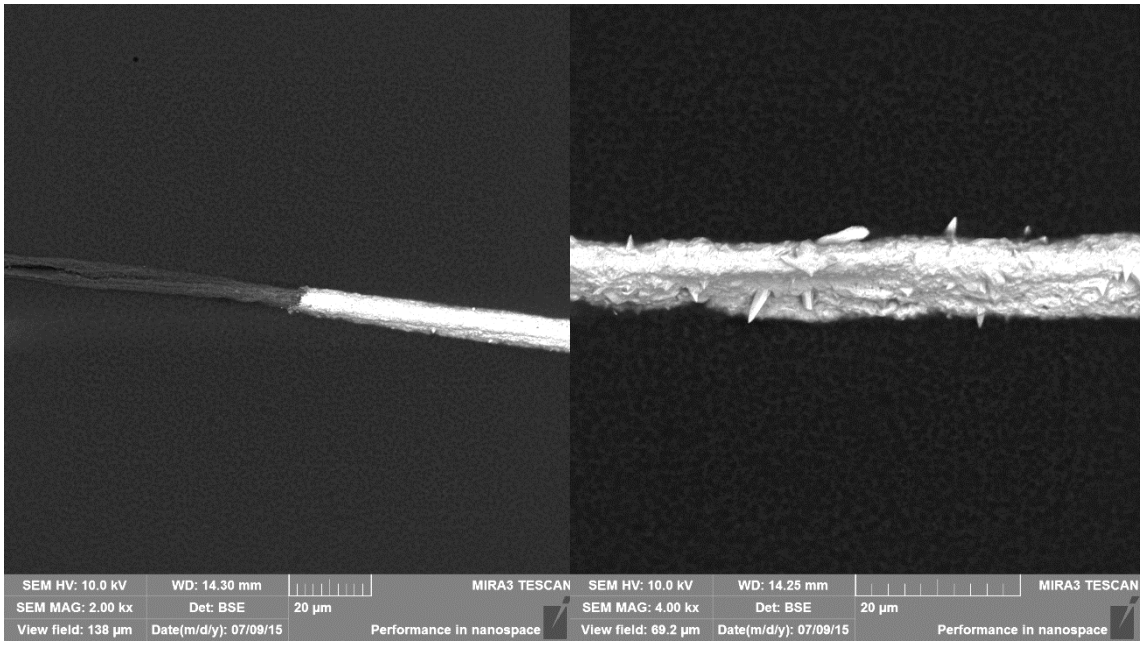

Figure 66. The border of coated and uncoated carbon sample (code G1) and a close up of a coated area.

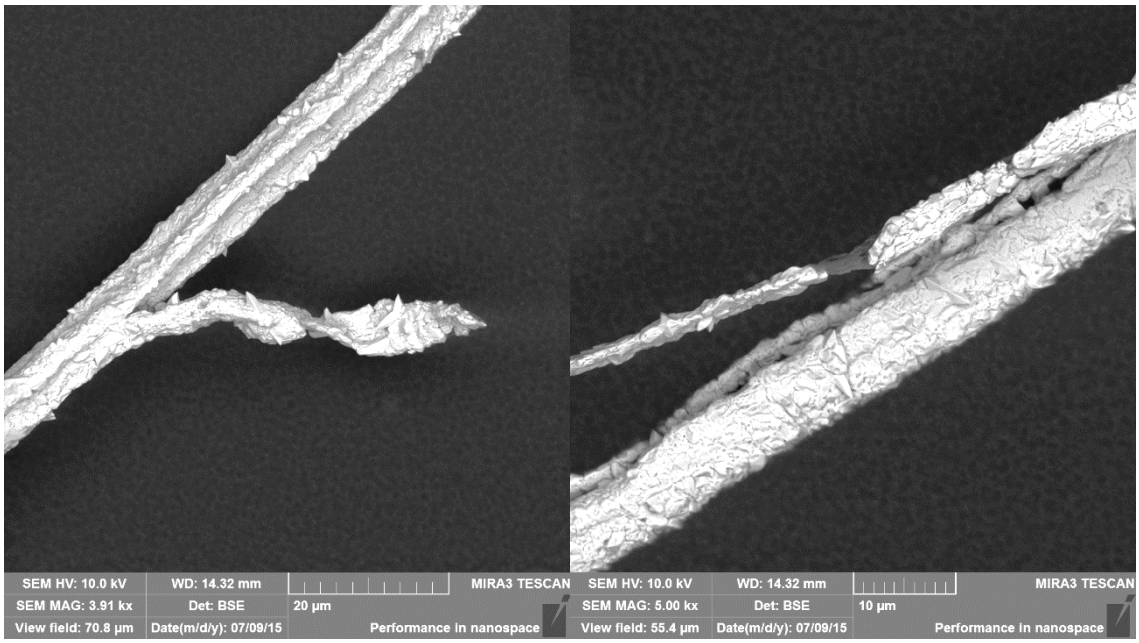

Figure 67. Protrusions in middle of the sample code G2. The copper does not cover the whole surface.

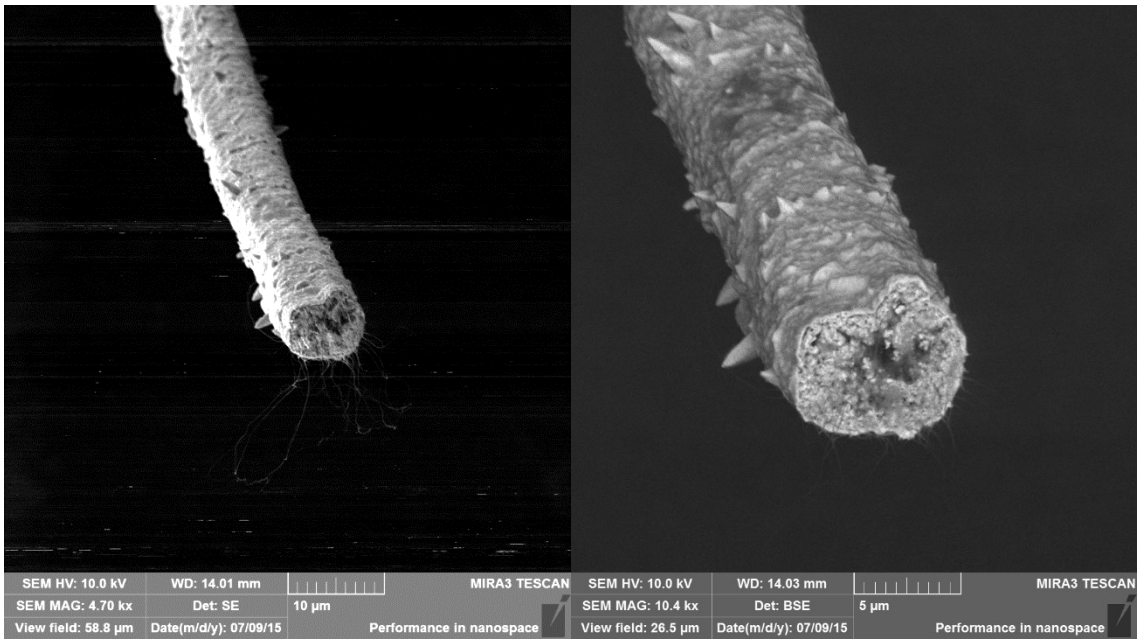

Figure 68. The end of the sample code G3.

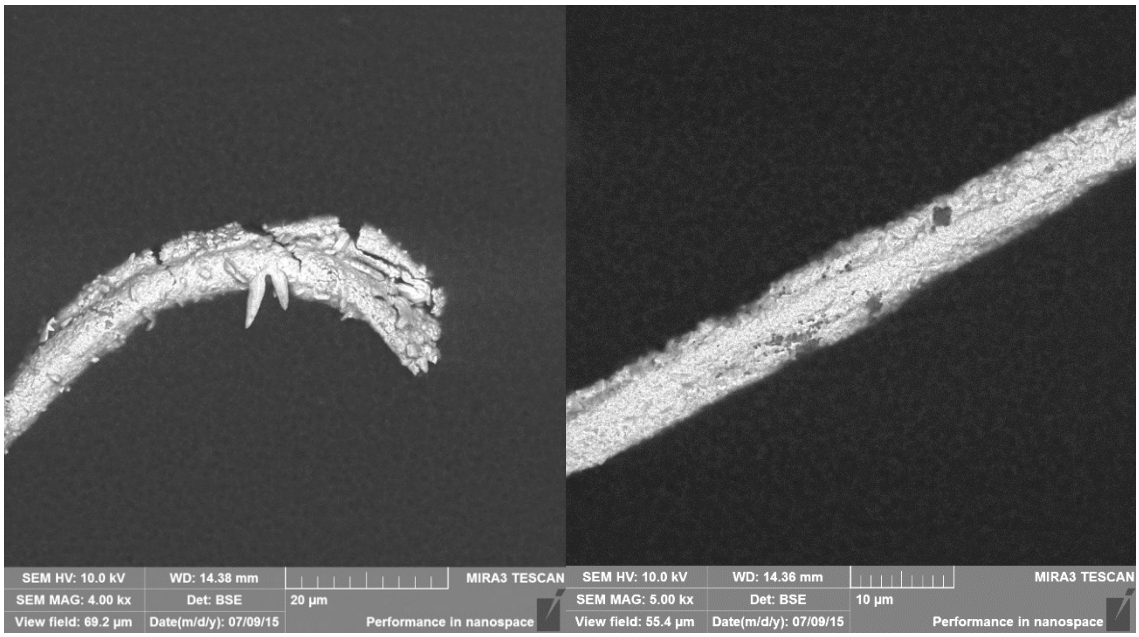

Figure 69. The other end of the sample code G3. The copper does not cover the whole surface.

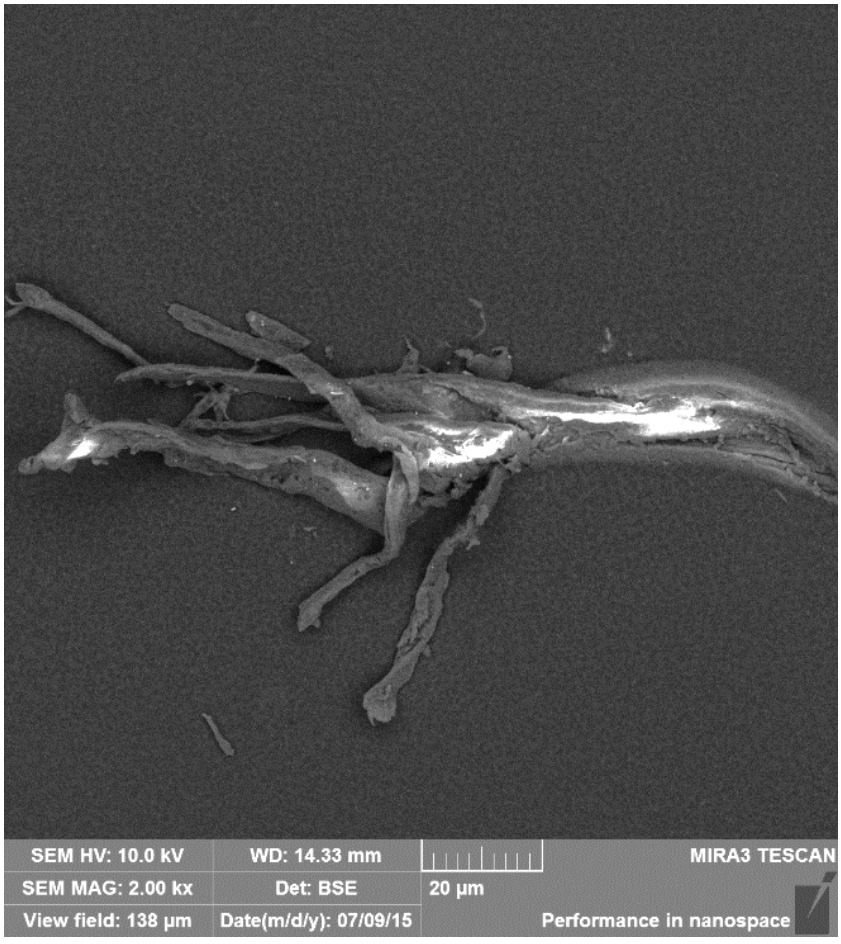

Figure 70. Branched end of the sample code G5.

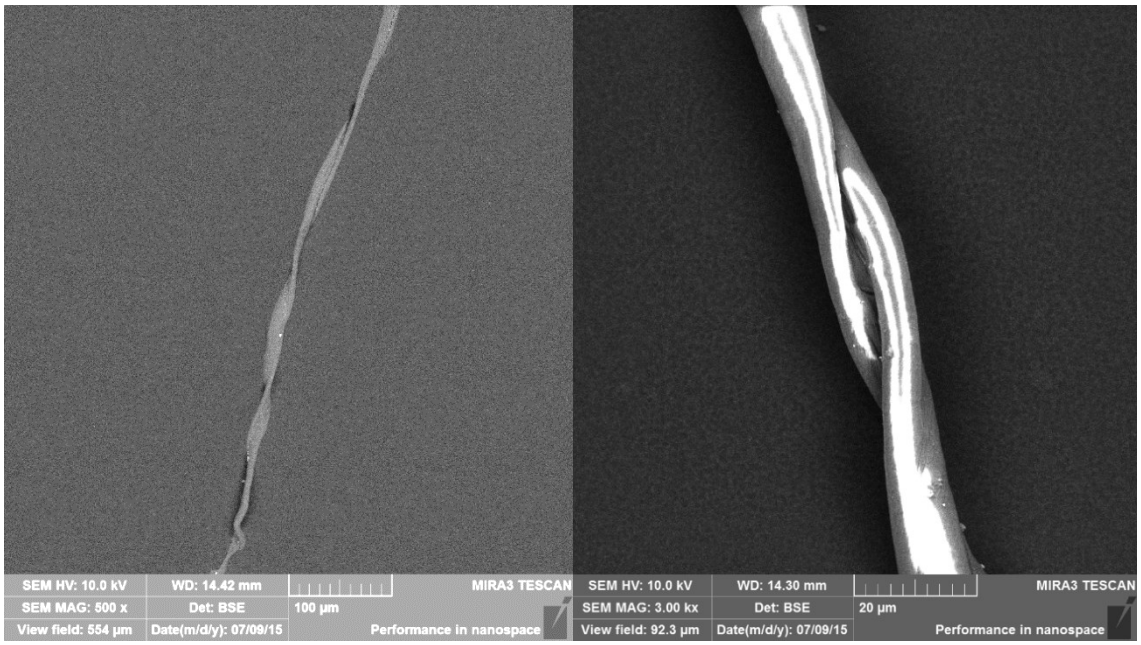

Figure 71. The curly structure of sample code G5.

Figures 66 - 71 show that the immersion in Watts nickel bath (bath 2) has hardly been affecting the surface of the samples. The coatings are almost similar despite the used treatment. This can be seen when comparing Figures 66 - 69 with the copper coated samples (codes G1 and G2), and the Watts bath immersed and the copper coated samples (codes G3 and G4). In either case, the coating was not completely covering every point in the sample as shown in Figures 67 and 69. In addition, the copper coating was uneven for an unknown reason. The uneven surface is due to inhomogeneous nature of CNT material, because the electrolyte composition and used current are typical for producing smooth copper deposits. From the Figure 68 can be estimated, that the electrolyte has wetted the sample quite well because it can be seen from BSE image that there is copper nucleation also in the middle section of the sample. However, on the innermost point copper has not deposited at all. In Figures 70 and 71 can be seen, that the sample material is very branched and threaded without electrodeposition. In this case, it does not allow good electrical conductivity. Otherwise, in the uncoated samples (codes G5 and G6) there are no observed residues from Watts bath.

5.11 Coating rate

Copper depositing values are from Pyry-Mikko Hannula's Master thesis (sample codes 47, 49.1, 49.1.5, 50.1, 50.1.2, 52, 53 and 54) and Watts nickel bath (bath 2) immersion results are the results from this Master thesis (sample codes G3 and G4)[93]. The used samples and electrodepositing parameters are shown in Table 28. The Figure 72 are drawn on the basis of the values from Table 28.

Table 28. Used samples

Sample code	Treatment	Current [mA]	Sample length [cm]	Time [s]	Coated length [cm]
47	-	-0.006	1.1	7200	0.5
49.1	-	-0.18	3.5	180	1.0
49.1.5	-	-0.18	3.5	1500	3.5
50.1	-	-1.8	3.5	180	2.5
50.1.2	-	-1.8	3.5	300	3.5
52	-	-0.5	3.5	600	3.5
53	-	-0.5	3.5	600	3.5
54	-	-0.5	3.5	600	1.3
G3	Immersion in bath 2	-0.1	2.0	120	2.0
G4	Immersion in bath 2	-0.1	2.0	120	2.0

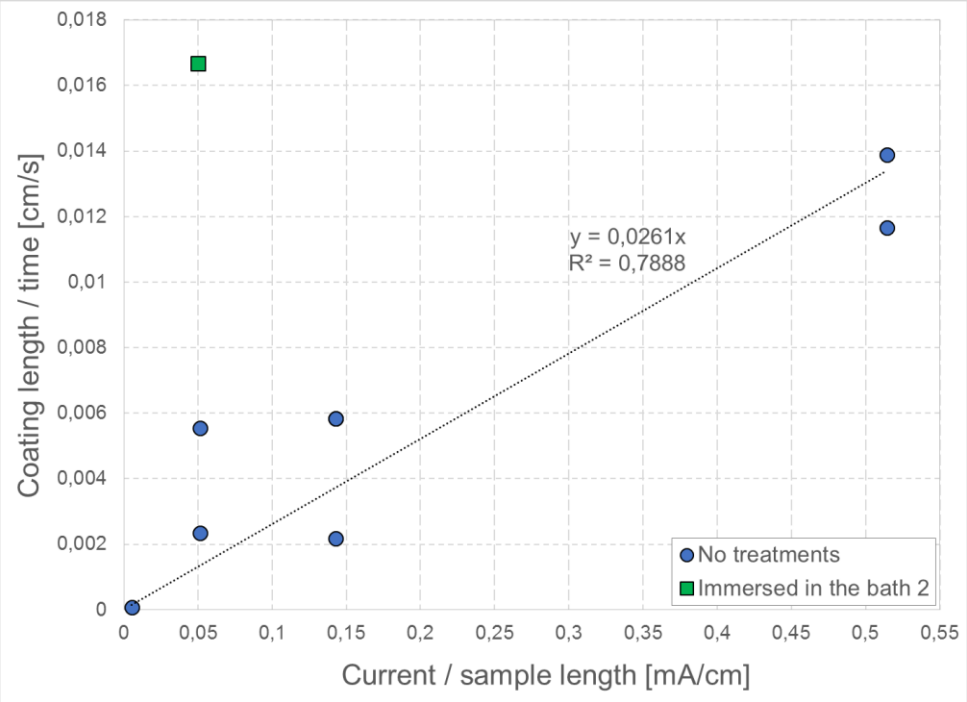

Figure 72. Coating rate with lowest current per surface area of sample.

Figure 72 shows the coating rate as a function of current. Coating rate is calculated from visual inspection after deposition test. The current is given with respect to sample length. Because all of these fiber samples had approximately same thickness, it can be assumed that the current delivered per surface area of samples was identical. The highest coating rates with lowest current are clearly those in Watts bath (bath 2) immersed samples G3 and G4. This means that Watts bath treatment affects the coating rate, and this is probably due to more active surface of sample than without immersion in Watts bath. However, more results are needed to confirm the effect.

6 DISCUSSION

The production of Cu/CNT composites require a lot of research, because none of produced Cu/CNT composites reach better electrical conductivity than copper. Today's research shows that the manufactured CNTs contain too many impurities and different oriented wall structures causing poor conductivity with CNT substrates. In addition the interface between copper and CNTs is not sufficient for substantial transfer of electrons over the boundary at typical applied potentials. The conductivity and activity of CNT-materials may be improved by functionalizing and modifying the CNT structure. The purpose of this Master's thesis was to investigate methods, which can be used to improve the conductivity and electrochemical activity of carbon nanotube substrates. The focus was on the modification of surface properties of CNTs and in the growth of nucleation. Surface properties of CNT substrates were measured and characterized by different methods such as electro-chemical impedance spectroscopy (EIS). The nucleation was estimated with galvanostatic deposition tests, scanning electron microscope (SEM) and optical microscopy. The experiments aimed to find correlations between surface modification and nucleation and growth of copper. The surface properties of CNT substrates were modified with heat treatment, Watts nickel bath, acetone, anodization, ethanol and different acid treatments. On some of the successfully treated samples copper was deposited to produce Cu/CNT composites, which were characterized by resistance measurements. The deposition rates in copper deposition were compared before and after modification treatments. Some of Cu/CNT composite samples were heat treated in nitrogen gas atmosphere.

The results show that heat treatment, Watts nickel bath (bath 2), anodization and boric acid are the most effective methods in the electrical conductivity and electrochemical activity of CNT material. The heat treatment affects strongly the electrochemical activity, but it seems to weaken the structure of the CNT samples. Heat treatments require more research in optimizing heating times and temperatures before they can be used as a reliable functionalization method for CNT materials without weakening the material. Immersion in Watts bath affects strongly the electrochemical activity and based on SEM-images, there isn't any agglomeration, weakening of the structure or special shape-changes. The value of impedance is much bigger before the immersion to Watts bath than after indicating the sample being activated. However, Watts bath immersion was not as effective for yarn specimens as fibers. The impedance of a sample still wet is lower than the impedance of a dried and wetted sample after immersion in Watts bath. This refers to that there would be remaining residues of electrolyte from the Watts bath

on the surface of the sample or inside the sample. The crystallized electrolyte residues do not dissolve back. Due to this, if this activation method would be used on an industrial scale, CNT material should not be allowed to dry after activation i.e. the process should be a continuous. In addition, Watts bath immersion significantly affect the coating rates with lowest current, and this is probably due to more active surface, but more results are needed to confirm the effect. Immersion in 40 g/l boric acid affects the electrochemical activity, and the impedance and phase angle are reduced and polarization resistance decreases significantly. The effect of boric acid might be related to electroless deposition. Unconfirmed hints in the literature indicate that boric acid could act as reductant for metal ions. Anodization affects the electrochemical activity of the tested sample. The polarization resistance decreases but ohmic resistance increases. This might be a combination of removal of some conductive impurities by forced dissolution while at the same time producing new functionalized groups.

Acetone, sulfuric acid or nitric acid improve the electrochemical activity only slightly and addition of ethanol provides no observed significant changes in the electrochemical activity. Immersion in the solution of 3:1 H_2SO_4 (95 %) and HNO_3 (65 %) decreased lightly capacitance, increased polarization resistance 3.5 times but did not change solution resistance. The results of immersion in 1M sulfuric acid suggest that the CNT structure may be affected i.e. the nanotubes are separated from each other and the resistance increases. Organic ethanol should provide better wetting of CNT material and activation in the sample, but based on the tests, the addition of ethanol does not improve the electrochemical activity of tested samples. Especially the stirring affected undesirably to activity, but there is no research data in the literature about its effect. 20 % ethanol addition causes sedimentation of electrolyte and the sediment is accumulated into the surface of the sample.

The best reproducibility of measured resistances of Cu/CNT composites varied almost by 10 %. The heat treatment affected resistance only when using nitrogen gas because oxygen in the furnace oxidized the sample surfaces. Oxidation decreased the electrical conductivity. On the basis of images the change in properties can’t be interpreted exactly, and more research should be done. Variation in SEM images may also be due to the inhomogeneous material.

SEM-imaging was done on samples undergone the galvanostatic series of measurements (sample codes G1 - G6) to see if there was any changes after the treatment. SEM-images clarified that the immersion in Watts nickel bath (bath 2) had hardly been affect-

ing the surface of the samples. The coatings were almost similar despite the used treatment. In either case, the coating was not completely covering at every point on the tested samples. In addition, the copper coating was uneven be due to inhomogeneous nature of CNT material. In results it can be seen, that the CNT material is very branched and threaded without electrodeposition. In this case, it does not allow good electrical conductivity. Otherwise, in the Watts nickel bath immersed but uncoated samples there are no observed residues from the bath. Immersion in the Watts bath does not seem to damage the structure of the sample, but additional research on the effects of the bath is needed.

The mechanism of the Watts bath immersion for CNT's activation is not yet entirely clear. The immersion in Watts bath might be an autocatalytic spontaneous reaction that lowers the necessary binding energy. In this case it would explain the fact that some of the samples were activated in immersion to Watts bath so strongly that they were coated with copper in immersion to copper plating bath without electricity. Based on the results, it can be assumed that the immersion in Watts bath affects only the activity of the sample. It doesn´t modify the morphology of the sample like the functionalization methods which create functional groups to improve on the sample surface to be coated. After noticing that Watts bath clearly affects the EIS results with CNT samples, the effect of boric acid was studied. The results revealed that boric acid was clearly influencing the activity in the CNTs, but not as much as immersion to the Watts bath. Therefore as activation method the Watts bath immersion requires more research to find out about the mechanism and effect of nickel.

Even a lot of research has been conducted about CNT materials, the EIS method used as main tool for electrochemical characterization in this thesis has not been used in the CNT activity estimations according to literature. Various researchers have studied the CNT functionalization and documented effective methods like heat treatment, anodization, sulfuric acid and nitric acid. However, the results are not comparable since the CNT samples and their uses vary so much that the benefit of one method may not be suitable for another development path. In particular, Watts bath and boric acid effect on the coating rate was promising, but the exact mechanism is not known. The beneficial effect might be due to smaller work function difference between nickel and carbon than copper and carbon. The effect of the activation treatments may also depend on the semiconductive properties of the substrate. It is known that p-type semiconductors that have positive charge carriers are resistive to cathodic currents, that is resistive to electrodeposition

To estimate the semiconductive properties the CNT material was analyzed using different polarization potentials in 1M H_2SO_4. With this method it can estimated if the CNT

sample is a semiconductor. It was concluded from the results that semiconductor features are not noticeable. Impedances and phase angles of every sample stayed almost unchangeable at different potentials.

The measurement of conductivity before and after different treatments would have been useful to do for every sample, but was impossible due to the limitations of the test procedures. The resistance measurements were tested with a 4-wire circuit board. The method is suited only to the Cu/CNT composites with sufficient length and strength, as the circuit board determines the length of sample (20 mm minimum). As resistance measurements of treated samples was not possible the alternative solution was to use EIS. The results were interpreted using the idea of potential variation along the wire as discussed in Chapter 3.6. A decrease in the ohmic resistance was taken as improvement in sample conductivity. Several activation treatments resulted in decrease of ohmic resistance measured by EIS, but correlation between ohmic resistance and sample resistance could not be done. More homogeneous and stronger substrate materials are needed to continue in this research direction.

The effects of different activation methods were in some cases beneficial whereas some treatments did not improve sample properties at all and therefore more investigation is needed. Especially comparison of the functionalization methods would be useful in development of CNT treatments, because the as produced CNTs of today do not reach consistently high electrical conductivity. More research should be done for example with comparisons of wetting, conductivity and adhesion before and after functionalization and bond strength between copper and CNTs. Almost every sample tested was a fiber, but also more yarn tests should be done. In addition, the nucleation in copper deposition and possible effects of surface diffusion on porous CNT substrates requires more research. The development of CNTs to highly conductive Ultrawire composite with conductivity of more than 140 % IACS (International Annealed Copper Standard) has still a lot of research to do.

7 CONCLUSIONS

Theoretical estimations indicate that carbon nanotubes have exceptional properties, such as low density, high mechanical strength and particularly excellent electrical and thermal conductivity. Therefore CNT-based conductor materials could have a major impact on both technology and economy. The manufacturing and processing methods of CNTs require still a lot of research, before industrially obtained CNT-based conductor materials and completely working Cu/CNT composites can be published. None of the produced Cu/CNT composites, reach better electrical conductivity than copper. Earlier research shows that the manufactured CNTs contain too much impurities and different wall structures, which decrease the electrical conductivity. Metallic SWCNTs would have best properties as conductors, but they are the most difficult to manufacture and all production methods produce inhomogeneous CNT material. In addition the bond between copper and CNT is too weak to conduct electricity. The conductivity and activity of CNT-materials may be improved by functionalizing and modifying the CNT structure. Functionalizing and modifying the interface contributes to the bond between copper and CNTs and affect the activity of the CNT.

Surface properties of CNT substrates were measured and characterized by different methods like electrochemical impedance spectroscopy (EIS) and nucleation was estimated with galvanostatic deposition tests, scanning electron microscope *(*SEM) and optical microscope. The surface properties of CNT substrates were modified with heat treatment, Watts bath immersion, acetone, anodization, ethanol and different acid treatments. In addition secondary treatments such as copper deposition to Cu/CNT composite and resistance measurements were done to some samples. In copper deposition, the deposition rates before and after the modification treatments were compared. Part of Cu/CNT composites were post-treated with heat treatment using nitrogen gas atmosphere. The results show that heat treatment, Watts bath immersion, anodization and boric acid immersion are the most effective methods for improved the electrical conductivity and electrochemical activity of CNT. The heat treatment affected strongly to electrochemical activity, but it may weaken the structure of the CNT samples. Immersion in Watts bath affects strongly in electrochemical activity and based on SEM-images, there isn't any agglomeration, weakening of the structure or special shape-changes. Acetone, sulfuric acid or nitric acid improved the electrochemical activity only slightly and ethanol addition provided no changes in the electrochemical activity. Watts bath immersion significantly affected the coating rate with lowest current, but more research is needed to confirm the effect.

REFERENCES

1 Rochefort, A., Avouris, P., Lesage, F., Salahub, D.R. 1999. Electrical and mechanical properties of distorted carbon nanotubes. Physical review B, vol. 60(19).

2 Li, C., Thostenson, E.T., Chou, T. 2008. Effect of nanotube waviness on the electrical conductivity of carbon nanotube-based composites. Composites Science and Technology, vol. 68(6), pp. 1445-1452.

3 Miao, M. 2011. Electrical conductivity of pure carbon nanotube yarns. Carbon, vol. 49(12), pp. 3755-3761.

4 Datsyuk, V., Kalyva, M., Papagelis, K., Parthenios, J., Tasis, D., Siokou, A. 2008. Chemical oxidation of multiwalled carbon nanotubes. Carbon, vol. 46(6), pp. 833-840.

5 Randeniya, L.K., Bendavid, A., Martin, P.J., Tran, C. 2010. Composite yarns of multiwalled carbon nanotubes with metallic electrical conductivity. Small, vol. 6(16), pp. 1806-1811.

6 Lekawa-Raus, A., Kurzepa, L., Peng, X., Koziol. K. 2014. Towards the development of carbon nanotube based wires. Carbon, vol. 68(0), pp. 597-609.

7 Hjortstam, O., Isberg, P., Soderholm, P., Dai, H. 2004. Can we achieve ultra-low resistivity in carbon nanotube-based metal composites? Applied physics, vol. 78(8), pp. 1175-1179.

8 Li, C., Thostenson, E.T., Chou, T. 2007. Dominant role of tunneling resistance in the electrical conductivity of carbon nanotube–based composites. Applied Physics Letters, vol. 91(22).

9 Park, J., Lee, K. 2012. Carbon nanotube yarns. Korean Journal of Chemical Engineering, vol. 29(3), pp. 277-287.

10 Hirviniemi, L. 2006. Hiilinanoputket elektrodeina dielektroforeesissa. University of Jyväskylä. pp. 10-30.

11 Lekawa-Raus, A., Patmore, J., Kurzepa, L., Bulmer, J., Koziol, K. 2014. Electrical properties of carbon nanotube based fibers and their future use in electrical wiring. Advanced Functional Materials, vol. 24(24), pp. 3661-3682.

12 Allaoui, A., Bai, S., Cheng, HM., Bai, JB. 2002. Mechanical and electrical properties of a MWNT/epoxy composite. Composites Sci Technol 11, vol. 62(15), pp. 1993-1998.

13 Lievonen, J. 2006. Moniseinäisten nanohiiliputkien elastisuus atomivoimamikroskoopilla mitattuna. University of Jyväskylä. pp. 5-14.

14 Keronen, J. 2015. Hiilinanoputkimusteen valmistaminen. Metropolia University of Applied Sciences. pp. 1-6.

15 Saito, R., Dresselhaus, G., Dresselhaus, M. 1998. Physical properties of carbon nanotubes. Imperial College, London.

16 Wong, H.P., Akinwande, D. 2011. Carbon nanotube and graphene device physics. Cambridge University Press.

17 Collins, PG., Arnold, MS., Avouris, P. 2001. Engineering carbon nanotubes and nanotube circuits using electrical breakdown. Science (New York, N.Y.), vol. 292(5517), pp. 706-709.

18 Xu, F., Sadrzadeh, A., Xu, Z., Yakobson, B.I. 2013. Can carbon nanotube fibers achieve the ultimate conductivity? Coupled-mode analysis for electron transport through the carbon nanotube contact. Journal of Applied Physics, vol. 114(6).

19 Nousiainen, P. 2008. High technology fibres. Structure, manufacture, properties and applications.

20 Palanne, S. 2008. Nanomanipulaatioon ja elektronimikroskopiaan perustuva hiilinanoputkien käsittelymenetelmä. University of Jyväskylä. pp. 3-17.

21 Sharma, R., Rez, P., Brown, M., Du, G., Treacy, M. 2007. Dynamic observations of the effect of pressure and temperature conditions on the selective synthesis of carbon nanotubes. Nanotechnology, vol. 18(12).

22 Eklund, P., Pradhan, B., Kim, U., Xiong, Q., Fischer, J., Friedman, A. 2002. Large-scale production of single-walled carbon nanotubes using ultrafast pulses from a free electron laser. Nano Letters vol. 2(6), pp. 561-566.

23 Cantoro, M., Hofmann, S., Pisana, S., Scardaci, V., Parvez, A., Ducati, C. 2006. Catalytic chemical vapor deposition of single-wall carbon nanotubes at low temperatures. Nano Letters, vol. 6(6), pp. 1107-1112.

24 José-Yacamán, M., Miki-Yoshida, M., Rendon, L., Santiesteban, J. 1993. Catalytic growth of carbon microtubules with fullerene structure. Applied Physics Letters, vol. 62(2), pp. 202-204.

25 Hokkanen, M. 2011. Hiilinanoputkien käyttö transistorikomponenteissa: hiilinanoputkinäytteiden laadun parantaminen, transistorikomponenttien valmistus sekä niiden sähköiset ominaisuudet. University of Jyväskylä. pp. 1-18.

26 Takagi, D., Homma, Y., Hibino, H., Suzuki, S., Kobayashi, Y. 2006. Single-walled carbon nanotube growth from highly activated metal nanoparticles. Nano Letters, vol. 6(12), pp. 2642-2645.

27 Führer, MS., Nygard, J., Shih, L., Forero, M., Yoon, YG., Mazzoni, MS. 2000. Crossed nanotube junctions. Science (New York, N.Y.), vol. 288(5465), pp. 494-7.

28 Jakubinek, M.B., Johnson, MB., White, MA., Jayasinghe, C., Li, G., Cho, W. 2012. Thermal and electrical conductivity of array-spun multi-walled carbon nanotube yarns. Carbon, vol. 50(1), pp. 244-248.

29 Bourlon, B., Miko, C., Forro, L., Glattli, D., Bachtold, A. 2004. Determination of the intershell conductance in multiwalled carbon nanotubes. Physical Review Letters, vol. 93(17).

30 Sun, Y., Onwona-Agyeman, B., Miyasato, T. 2011. Controlling the resistivity of multi-walled carbon nanotube networks by copper encapsulation. Materials Letters, vol. 65(19–20), pp. 3187-3190.

31 Choi, H.J., Ihm, J., Louie, S.G., Cohen, M.L. 2000. Defects, quasibound states, and quantum conductance in metallic carbon nanotubes. Physical Review Letters, vol. 84(13).

32 Ojapalo M. 2008. Hiilinanoputket. Kemian laitos. Kemian opettajankoulutusyksikkö Kandidaatintutkielma.pp. 2-12.

33 Deng, F., Zheng, Q. 2009. Interaction models for effective thermal and electric conductivities of carbon nanotube composites. Acta Mechanica Solida Sinica, vol. 22(1), pp. 1-17.

34 Poole, C.P., Owens, FJ. 2003. Introduction to nanotechnology. John Wiley & Sons.

35 Berber, S., Kwon, Y., Tománek, D. 2000. Unusually high thermal conductivity of carbon nanotubes. Physical Review Letters, vol. 84(20).

36 Kim, P., Shi, L., Majumdar, A., McEuen, P. 2001. Thermal transport measurements of individual multiwalled nanotubes. Physical Review Letters, vol. 87(21).

37 Hone, J., Llaguno, M., Nemes, N., Johnson, A., Fischer, J., Walters, D., Casavant, M., Schmidt, J., Smalley, R. 2000. Electrical and thermal transport properties of magnetically aligned single wall carbon nanotube films. Applied Physics Letters, vol. 77(5), pp. 666-668.

38 Zhang, W. 2004. Influence of the electron mean free path on the resistivity of thin metal films. Microelectronic engineering, vol. 76(1), pp. 146-152.

39 Purewal, M.S., Hong, B.H., Ravi, A., Chandra, B., Hone, J., Kim, P. 2007. Scaling of resistance and electron mean free path of single-walled carbon nanotubes. Physical Review Letters, vol. 98(18).

40 Chai, Y., Xiao, Z., Chan, P.C. 2010. Horizontally aligned carbon nanotube bundles for interconnect application: diameter-dependent contact resistance and mean free path. Nanotechnology, vol. 21(23).

41 Chico, L., Benedict, L.X., Louie, S.G., Cohen, M.L. 1996. Quantum conductance of carbon nanotubes with defects. Physical Review B, vol. 54(4).

42 Frank, S., Poncharal, P., Wang, Z.L., Heer, W.A. 1998. Carbon nanotube quantum resistors. Science, vol. 280(5370), pp. 1744-1746.

43 Yao, Z., Kane, C.L., Dekker, C. 2000. High-field electrical transport in single-wall carbon nanotubes. Physical Review Letters, vol. 84(13).

44 Wei, B., Vajtai, R., Ajayan, P. 2001. Reliability and current carrying capacity of carbon nanotubes. Applied Physics Letters, vol. 79(8), pp. 1172-1174.

45 Mantena, K.V. 2009. Electrical and mechanical properties of MWCNT filled conductive adhesives on lead free surface finished pcb's.

46 Walters, D., Ericson, L., Casavant, M., Liu, J., Colbert, D., Smith, K. 1999. Elastic strain of freely suspended single-wall carbon nanotube ropes. Applied Physics Letters, vol. 74(25), pp. 3803-3805.

47 Kim, K.T., Cha, S.I., Hong, S.H., Hong, S.H. 2006. Microstructures and tensile behavior of carbon nanotube reinforced Cu matrix nanocomposites. Materials Science and Engineering, vol. 430(1), pp. 27-33.

48 Daoush, W.M., Lim, B.K., Mo, C.B., Nam, D.H., Hong, S.H. 2009. Electrical and mechanical properties of carbon nanotube reinforced copper nanocomposites fabricated by electroless deposition process. Materials Science and Engineering, vol. 513, pp. 247-253.

49 Koziol, K., Vilatela, J., Moisala, A., Motta, M., Cunniff, P., Sennett, M. 2007. High-performance carbon nanotube fiber. Science (New York, N.Y.), vol. 318(5858), pp. 1892-1895.

50 Harris, P.J.F. 2001. Carbon nanotubes and related structures: new materials for the twenty-first century. Cambridge university press.

51 Schulz, M., Shanov, V., Yin, Z. 2013. Nanotube Superfiber Materials: Changing Engineering Design. William Andrew.

52 Eder, D. 2010. Carbon nanotube−inorganic hybrids. Chemical Review, vol. 110(3), pp. 1348-1385.

53 Titus, E., Ali, N., Cabral, G., Gracio, J., Babu, P.R., Jackson, M. 2006. Chemically functionalized carbon nanotubes and their characterization using thermogravimetric analysis, fourier transform infrared, and raman spectroscopy. Journal of Materials Engineering and Performance, vol. 15(2), pp. 182-186.

54 Hirsch, A. 2002. Functionalization of single-walled carbon nanotubes. Angewandte Chemie International Edition, vol. 41(11), pp. 1853-1859.

55 Virtanen, T. 2014. Grafeenioksidin funktionalisointi. University of Jyväskylä. pp. 3-50.

56 Xu, G., Zhao, J., Li, S., Zhang, X., Yong, Z., Li, Q. 2011. Continuous electrodeposition for lightweight, highly conducting and strong carbon nanotube-copper composite fibers. Nanoscale, vol. 3(10), pp. 4215-4219.

57 Aromaa, J. 2007. Electrochemical Engineering. In: Encyclopedia of Electrochemistry, Wiley-VCH Verlag GmbH & Co. KGaA, pp. 161-196.

58 Schlesinger, M., Paunovic, M. 2006. Fundamentals of electrochemical deposition. 2nd edition. New Jersey. Wiley. ISBN: 978-0-471-71221-3.

59 Aromaa, J. 2000. Materiaalien sähkökemia. Helsinki University of Technology Publications in Materials Science and Metallurgy, Teknillisen korkeakoulun materiaalitekniikan ja matallurgian julkaisuja, TKK-MK-102, Espoo.

60 Yhdistys SG. 2000. Kemiallinen ja Sähkökemiallinen pintakäsittely osa II. Jyväskylä. Gummerus kirjapaino Oy.

61 Subbaiah, T., Das, S. 1989. Physico-chemical properties of copper electrolytes. Metallurgical Transactions B, vol. 20(3), pp. 375-380.

62 Förch, R., Schönherr, H., Jenkins, A.T.A. 2009. Surface design: applications in bioscience and nanotechnology. John Wiley & Sons.

63 Ketelson, H.A., Perry, S.S., Sawyer, W.G., Jacob, J.T. 2011. Exploring the Science and Technology of Contact Lens Comfort. Contact Lens Spectrum. Supplement.

64 Ranade, M. 1987. Adhesion and removal of fine particles on surfaces. Aerosol Science and Technology, vol. 7(2), pp. 161-176.

65 Bhattacharya, S., Mittal, K.L. 1978. Mechanics of removing glass particulates from a solid surface. Surface Technology 11, vol. 7(5), pp. 413-425.

66 Grujicic, D., Pesic, B. 2002. Electrodeposition of copper: the nucleation mechanisms. Electrochim Acta, vol. 47(18), pp. 2901-2912.

67 Fischer, H. 1954. Elektrolytische Abscheidung und Elektrokristallisation von Metallen. Berlin, Springer-Verlag.

68 Winand, R. 1998. Contribution to the study of copper electrocrystallization in view of industrial applications-submicroscopic and macroscopic considerations. Electrochim Acta, vol. 43(19), pp. 2925-2932.

69 Schlesinger, M., Paunovic, M. 2011. Modern electroplating. John Wiley & Sons.

70 Alkire, R., Varjisn, R. 1974. Resistive wire electrodes. Journal of the Electrochemical Society, vol. 121(5), pp. 622-631.

71 Matlosz M, Vallotton P, West A, Landolt D. 1992. Nonuniform current distri-bution and thickness during electrodeposition onto resistive substrates. Journal of the Electrochemical Society, vol. 139(3), pp. 752-761.

72 Gamburg, YD., Zangari, G. 2011. Theory and practice of metal electrodeposition. Springer Science & Business Media. ISBN 978-1-4419-9669-5.

73 Bard, AJ., Stratmann, M., McDonald, D., Schmuki, P. 2007. Encyclopedia of Electrochemistry, vol. 5, Electrochemical Engineering.

74 Armini, S., Vereecken, P.M. 2010. Impact of" Terminal Effect" on Cu Plating: Theory and Experimental Evidence. ECS Transactions, vol. 25(27), pp. 185-194.

75 Durney, L.J. 2005. Electrochemical and chemical deposition. In: Ullmann's Encyclopedia of Industrial Chemistry, Wiley-VCH Verlag GmbH & Co. KGaA, pp. 13-14.

76 Seah, C., Mridha, S., Chan, L. 2001. Adhesive strength of electroplated copper films. Journal of Materials Processing Technology, vol. 114(3), pp. 252-256.

77 Prentice, G., Chen, K. 1998. Effects of current density on adhesion of copper electrodeposits to polyimide substrates. Journal of Applied Electrochemistry, vol. 28(9), pp. 971-977.

78 Baumgarnter, C.E., Scott, L.R. 1995. Adhesion Science, vol. 9.

79 Baumgarnter, C.E. 1992. Plating Surface Finishing, vol. 79.

80 Krause, L.J., Speckhard, T.A. 1991. An Electrochemical Method of Polyimide Metallization. Metallized Plastics 2: Springer, pp. 3-14.

81 Rosa, J.L., Robin, A., Silva, M., Baldan, C.A., Peres, M.P. 2009. Electrodeposition of copper on titanium wires: Taguchi experimental design approach. Journal of Materials Processing Technology, vol. 209(3), pp. 1181-1188.

82 Sun, H., Delplancke, J., Winand, R., O'Keefe, T. 1991. Nucleation and growth of copper electrodeposits on titanium substrates. Copper (Cobre 1991), pp, 405-417.

83 Weil, R. 1989. The structures of electrodeposits and the properties that depend on them. Annual Review of Materials Science, vol. 19(1), pp. 165-182.

84 Lahiri, I., Seelaboyina, R., Hwang, J.Y., Banerjee, R., Choi, W. 2010. Enhanced field emission from multi-walled carbon nanotubes grown on pure copper substrate. Carbon, vol. 48(5), pp. 1531-1538.

85 Calderón-Colón, X., Geng, H., Gao, B., An, L., Cao, G., Zhou, O. 2009. A carbon nanotube field emission cathode with high current density and long-term stability. Nanotechnology, vol. 20(32).

86 Suntio, A. 2009. Characterization of stainless steel cathode blanks. Helsinki University of Technology. pp. 3-21.

87 Wei, C. 2006. Adhesion and reinforcement in carbon nanotube polymer composite. Applied Physics Letters, vol. 88(9).

88 Moon, J., Alegaonkar, P., Han, J., Lee, T., Yoo, J., Kim, J. 2006. Enhanced field emission properties of thin-multiwalled carbon nanotubes: role of SiOx coating. Journal of Applied Physics, vol. 100(10).

89 Yang, Y., Wang, Y., Ren, Y., He, C., Deng, J., Nan, J. 2008. Single-walled carbon nanotube-reinforced copper composite coatings prepared by electrodeposition under ultrasonic field. Material Letters, vol. 62(1), pp. 47-50.

90 Aromaa, J. 2003. Sähkökemialliset tutkimusmenetelmät. Otamedia Oy. Espoo.

91 Xu, L., Zhu, J., Lu, M., Zhang, L., Chang, W. 2015. Electrochemical impedance spectroscopy study on the corrosion of the weld zone of 3Cr steel welded joints in CO2 environments. International Journal of Minerals, Metallurgy, and Materials, vol. 22(5), pp. 500-508.

92 Holm, T. 2014. Litiumioniakuston matalat lämpötilat huomioiva impedanssimalli. Tampere University Of Technology. pp. 15.

93 Hannula, P. 2014. Electrodeposition of copper on a carbon nanotube fiber. Aalto university School of Chemical Technology. pp. 46-49.

APPENDIX

Used samples and treatments

Samples (codes)	A (mm^2)	l (mm)	d (µm)	Treatment
Fiber (U2)	0.5	15	10	Furnace: Before 400 °C, 10 min
Fiber (U2)	0.1	3	10	Furnace: After 400 °C, 10 min
Fiber (N6)	0.8	25	10	Furnace: Before 400 °C, 60 min
Fiber (U1)	0.4	13	10	Without treatments
Fiber (N7)	0.6	20	10	Immersion time: 3 h 50 min in Watts bath
Fiber (N8)	0.6	20	10	Immersion time: 72 h in Watts bath
Fiber (N9)	0.6	20	10	Immersion time: 30 min in Watts bath
Fiber (N11)	0.9	30	10	Immersion time: 60 min in Watts bath
Yarn (N12)	22	35	200	Immersion time: 40 min in Watts bath
Fiber (P2)	0.8	25	10	Immersion time: 30 min in Watts bath + 1h drying
Yarn (yarn1)	3.3	35	30	Immersion time: 24 h in Watts bath
Yarn (yarn2)	6.6	70	30	Wetting with acetone, immersion time: 30 min in Watts bath
Yarn (yarn3)	6.6	70	30	Immersion time: 30 min in Watts bath
Fiber (A1)	0.5	15	10	Anodization: 49s, 2500 mV, 10wt-% H_2SO_4
Fiber (UN4)	0.9	29	10	C_2H_6O add (10 % and 20 %)
Fiber (N1)	0.6	20	10	Immersion time: 15 min in 3:1 H_2SO_4 (95 %) and HNO_3 (65 %)
Fiber (h1)	0.3	10	10	Immersion time: 40min in H_2SO_4 (1M)
Fiber (h2)	0.3	10	10	Immersion time: 30min in H_2SO_4 (1M)
Fiber (b1)	0.2	7	10	Immersion time: 60 min in H_3BO_3 (40 g/l)
Fiber (N14)	0.6	20	10	Without treatments
Yarn (N13)	1.3	20	20	Without treatments
Fiber (G1)	0.63	20	10	Without treatment, deposition: -0.1 mA, t=120s
Fiber (G2)	0.63	20	10	Without treatment, deposition: -0.1 mA, t=120s
Fiber (G3)	0.63	20	10	Immersion time: 1h in Watts bath, deposition: -0.1 mA, t=120s
Fiber (G4)	0.63	20	10	Immersion time: 1h in Watts bath, deposition: -0.1 mA, t=120s
Fiber (G5)	0.63	20	10	Immersion time: 1h in Watts bath
Fiber (G6)	0.63	20	10	Immersion time: 1h in Watts bath

Samples (codes)	Resistance	Treatment
Cu/CNT (26.1)	0.065 Ω	Furnace: Before 400 °C, 60 min (citric acid 2 h)
Cu/CNT (26.1)	0.067 Ω	Furnace: After 400 °C, 60 min (citric acid 2 h)
Cu/CNT (26.2)	0.100 Ω	Furnace: Before 400 °C, 3 h (citric acid 2 h)
Cu/CNT (26.2)	0.089 Ω	Furnace: After 400 °C, 3 h (citric acid 2 h)
Cu/CNT (26.3)	0.138 Ω	Furnace: Before 300 °C, 60 min + nitrogen gas
Cu/CNT (26.3)	0.125 Ω	Furnace: After 300 °C, 60 min + nitrogen gas
Cu/CNT (26.4)	0.133 Ω	Furnace: Before 300 °C, 3 h + nitrogen gas (extinct)
Cu/CNT (26.4)	0.130 Ω	Furnace: After 300 °C, 3 h + nitrogen gas (extinct)